EFFICIENT, FLEXIBLE, AND RESILIENT CONTROL FOR OPTIMAL OPERATION OF HYBRID-ELECTRIC SHIPBOARD MICROGRIDS

A Dissertation
Submitted to
the Temple University Graduate Board

In Partial Fulfillment
of the Requirements for the Degree
DOCTOR OF PHILOSOPHY
in ELECTRICAL ENGINEERING

By
Kaitlyn R. Sitch
April 2023

Examining Committee Members:
Liang Du, Advisory Chair, Department of Electrical and Computer Engineering
Saroj Biswas, Department of Electrical and Computer Engineering
Iyad Obeid, Department of Electrical and Computer Engineering
Chris Dafis, Naval Surface Warfare Center Philadelphia Devision
Haijun Liu, Department of Mechanical Engineering

ABSTRACT

Electric transportation has been a well-studied research topic with electric ships gaining momentum. Ships can have a wide range in size from small cargo ships to military vessels. The benefits of electrification include meeting environmental sustainability goals and operational benefits in terms of flexibility and renewed operation. The power systems onboard a ship can be considered a microgrid, which is called a shipboard microgrid. This system poses unique challenges compared to land-based microgrids due to the resiliency requirements of being at sea. A control system for a hybrid- electric ship is proposed with both an energy storage system (ESS) and traditional diesel generators and gas turbines. This system balances economics with resilient control by calculating a baseline load distribution using the cost of operating each unit for the expected load profile. Additionally, the control system ensures that the generation capacity is available if the load does not follow the expected profile. To maintain flexibility, the system will redispatch the units as needed based on the actual load applied, while reducing the control efforts and maintaining the generation contingency. Therefore, the proposed shipboard microgrid control offers a control method that considers the cost of operation while maintaining the required standards of shipboard microgrid control.

ACKNOWLEDGMENTS

I'm very grateful to my advisor, Dr. Liang Du whose support and guidance was invaluable throughout this program. He made me feel welcome to Temple University from my acceptance to the program. My first visit to Temple was during a nor'easter snowstorm and he did not rush me and ensured I had all of the required information to make my decision to attend. This eased the transition from my small city undergraduate university, Wilkes University, to the larger Philadelphia area.

I would like to extend my sincerest thanks to my committee members, Dr. Saroj Biswas, Dr. Iyad Obeid, Dr. Chris Dafis, and Dr. Haijun Liu. They were able to provide their knowledge and expertise with patience.

Additionally, this work would not have been possible without being awarded the SMART Scholarship. I would like to give a special thanks to my mentors for this program, Steve Kolesar and Dr. Chris Dafis. Their support has not only assisted me throughout my Ph.D. program but has set me up for success following the completion of my degree.

Words cannot express my gratitude to my family who supported me through this process. Their belief in me kept me motivated throughout my Ph.D. journey.

TABLE OF CONTENTS

ABSTRACT ii

ACKNOWLEDGMENTS iii

LIST OF TABLES vii

LIST OF FIGURES ix

CHAPTER 1: INTRODUCTION 1

1.1 Background 1

1.2 Motivation 2

1.3 Problem Statement 7

1.4 Outline of Dissertation 9

1.5 Contributions 11

CHAPTER 2: ECONOMIC CONTROL CONSIDERING BATTERY CYCLING LIFE COSTS 14

2.1 Droop Control 14

2.1.1 Droop Control Background 15

2.2 Economic Droop Control 20

2.2.1 Battery Cost Function 23

2.2.2 Proposed Cycle Life Cost 25

2.2.3 Battery Incremental Cost 28

2.2.4 Case Study and Optimization 30

2.3 Conclusion 33
2.3.1 Summary of Contributions 33

CHAPTER 3: FUEL EFFICIENCY OF DIESEL GENERATORS AND GAS TURBINES 35

3.1 Fuel Efficiency Curve for Diesel Generators 35
3.2 Fuel Efficiency Curve for Gas Turbines 42
3.3 Test Case and Simulation Results 46
3.4 Time Horizon Optimization 51
3.5 Simulation Results 56
3.5.1 Battery Price Reduction with Short Load Profile 57
3.5.2 Load Profile 1 - Center Load Peak 60
3.5.3 Load Profile 2 - Early Load Peak 65
3.5.4 Load Profile 3 - Two Load Peaks 69
3.6 Summary of Contributions 73

CHAPTER 4: SOURCE REDISPATCH WITH CONTROL EFFORT REDUCTION 79

4.1 Optimization Formulation 80
4.1.1 Modes of Operations 85
4.2 Case Study 86
4.3 Simulation Results 86
4.3.1 Redispatch of Load Profile 1 - Center Load Peak 87
4.3.2 Redispatch of Load Profile 2 - Early Load Peak 92
4.3.3 Redispatch of Load Profile 3 - Two Load Peaks 99
4.4 Conclusion 107
4.5 Summary of Contributions 109

CHAPTER 5: SUMMARY OF CONTRIBUTIONS 111

5.1 Publications 115

CHAPTER 6: FUTURE WORK 117

BIBLIOGRAPHY 119

APPENDICES 125

A. CHAPTER 3 CODE 125

B. CHAPTER 4 CODE 133

LIST OF TABLES

Page

2.1 Data for a $LiFePO_4$ battery displaying the DoD, cycles until failure, and full cycles until failure [50] 28

2.2 Simulation results displaying the applied load, generator load, P_{G1}, battery load P_{B1}, and the cost, which is the sum of the IC of the generator and the cost of the battery. 32

3.1 Simulation results of the fuel efficiency load distribution for two diesel generators and two gas turbines. The total load, load applied to the two diesel generators, P_{D1} and P_{D2}, and two gas turbines, P_{G1} and P_{G2}, and the total fuel used. 48

3.2 Fuel usage of two diesel generators and two gas turbines with equal loading conditions for comparison to unequal split loading. The total load, load applied to the two diesel generators, P_{D1} and P_{D2}, and two gas turbines, P_{G1} and P_{G2}, and the total fuel used. 49

3.3 Cost breakdown of load profile shown in Figure 3.5 without a battery implemented. 59

3.4 Cost breakdown of load shown in Figure 3.5 with a battery implemented. . . 62

3.5 Preset values for the time horizon optimization of the control of shipboard microgrid resources. 65

3.6 Cost of each diesel generator, gas turbine, and battery, the total cost, and the reserve power allocation at each time step for 24 Load Profile shown in Figure 3.8. 75

3.7 Cost of each diesel generator, gas turbine, and battery, the total cost, and the reserve power allocation at each time step for 24 hour load profile 2. . . 76

3.8 Cost of each diesel generator, gas turbine, and battery, the total cost, and the reserve power allocation at each time step for the 24 hour load profile 3 shown in Figure 3.14. 77

3.9 Available power based on the number of units turned on at each time step for Load Profiles 1, 2, and 3. 78

4.1 Change in load applied to each unit including the two diesel generators, two gas turbines, and change in charge and discharge power of the batteries. These results were obtained from the redispatch optimization of Load Profile 1, shown in Figure 4.2 for the reserve increase section. 91

4.2 Change in load applied to each unit including the two diesel generators, two gas turbines, and change in charge and discharge power of the batteries. These results were obtained from the redispatch optimization of Load Profile 1, shown in Figure 4.2 for the operation mode change section. 94

4.3 Change in load applied to each unit including the two diesel generators, two gas turbines, and change in charge and discharge power of the batteries. These results were obtained from the redispatch optimization of Load Profile 1, shown in Figure 4.5 for the reserve increase section. 98

4.4 Change in load applied to each unit including the two diesel generators, two gas turbines, and change in charge and discharge power of the batteries. These results were obtained from the redispatch optimization of Load Profile 1, shown in Figure 4.5 for the operation mode change section. 101

4.5 Change in load applied to each unit including the two diesel generators, two gas turbines, and change in charge and discharge power of the batteries. These results were obtained from the redispatch optimization of Load Profile 3, shown in Figure 4.8 for the reserve increase section. 105

4.6 Change in load applied to each unit including the two diesel generators, two gas turbines, and change in charge and discharge power of the batteries. These results were obtained from the redispatch optimization of Load Profile 1, shown in Figure 4.8 for the operation mode change section. 108

LIST OF FIGURES

Page

1.1 Notional model of an electrified shipboard microgrid with a hybrid storage system featuring distributed energy storage systems (ESS). This shipboard microgrid is designed a DC microgrid with distributed ESS in different zones. Main movers such as generators provide AC power that is rectified via AC/DC rectifiers. 3

1.2 Notional ship power system model used for the robust combat power and energy controls (RCPC) demonstrations [25]. 5

2.1 The cycles until failure versus the DoD for a $LiFePO_4$ battery [50] 26

2.2 The full cycles until failure versus the DoD for a $LiFePO_4$ battery [50] . . . 27

3.1 The top graph is the fuel usage from 10-100MW using the fuel efficiency curve and the bottom graph is the derivative of the top graph. 41

3.2 The top graph is the fuel usage from 10-100MW of the gas turbine using the fuel efficiency equation and the bottom graph is the derivative of the top graph. 43

3.3 The optimization results are displayed for the total load on the shipboard microgrid with the load distribution across the generating units, the two diesel generators, P_{D1} and P_{D2}, and the gas turbines, P_{G1} and P_{G2}, where the y-axis represents the power applied to each unit. 50

3.4 Sample load profile with the predicted load profile, P_t, the load change accommodation, P_t^+, P_t^- shown to develop the economic baseline load distribution. 52

3.5 Load profile with 7 time steps to test cost difference between using only traditional generators and implementing a battery. 58

3.6 Generator distribution for load profile shown in Figure 3.5 without a battery implemented. 59

3.7 Load distribution across diesel generators, gas turbines, and battery for load profile shown in Figure 3.5. 61

3.8 A sample predicted 24 hour load profile with the reserve requirement. . . . 62

3.9 Load distribution across the two diesel generators and two gas turbines for the load profile shown in Figure 3.8. 63

3.10 Charging and Discharging power of the two batteries across the load profile shown in Figure 3.8. 64

3.11 The second sample predicted 24 hour load profile with the reserve requirement. This profile peaks early in the time horizon. 66

3.12 Load distribution across two diesel generators and two gas turbines for the predicted load profile shown in Figure 3.11. 67

3.13 Charging and discharging power of the two batteries for the predicted load profile shown in Figure 3.11. 68

3.14 The third sample predicted 24 hour load profile with the reserve requirement. This profile has two peaks within the time horizon. 70

3.15 Load distribution across two diesel generators and two gas turbines for the predicted load profile shown in Figure 3.14. 71

3.16 Charging and discharging power of the two batteries for the predicted load profile shown in Figure 3.14. 72

4.1 Redispatch load profile with the predicted load profile, P_t, the load change accommodation, P_t^+, P_t^-, and the actual load profile $\Delta P_t^+, \Delta P_t^-$ shown. . . 84

4.2 The predicted load profile and reserve requirement from Figure 3.8 with the actual load and minimum allowable load based on ramp-down of the units at each time step. 88

4.3 Load distribution across diesel generators, gas turbines, and batteries. 90

4.4 Load distribution across diesel generators, gas turbines, and batteries. 93

4.5 The predicted load profile and reserve requirement from Figure 3.11 with the actual load and minimum allowable load based on ramp-down of the units at each time step. 95

4.6 Load distribution across diesel generators, gas turbines, and batteries for load profile shown in Figure 4.5. 97

4.7 Load distribution across diesel generators, gas turbines, and batteries for load profile shown in Figure 4.5. 100

4.8 The predicted load profile and reserve requirement from Figure 3.14 with the actual load and minimum allowable load based on ramp-down of the units at each time step. 102

4.9 Load distribution across diesel generators, gas turbines, and batteries for load profile shown in Figure 4.8. 104

4.10 Load distribution across diesel generators, gas turbines, and batteries for load profile shown in Figure 4.8. 106

CHAPTER 1

INTRODUCTION

1.1 Background

Transportation electrification has become widely studied across academia and industry sectors, ranging from electrifying vehicles to ensuring adequate infrastructure to charge electric vehicles, with a particular interest in the grid capability. Microgrids have played a role in this effort to provide power in areas with congestion or reliability issues, as well as being a fully operational system for larger types of electrified transportation. A microgrid is a relatively small-scale, low-voltage electric power system that manages various distributed energy resources, such as renewable generations, microturbine, full cells, controllable loads, and energy storage systems (ESS), in a physically close location. The microgrids can operate in two modes, islanded and grid connected, and may switch between them if capable [1, 2]. Islanded microgrids are not connected to the grid and are self-sufficient at supporting the attached loads. Grid connected microgrids can connect to the grid to support the load and/or feedback excess power. Another classification for microgrids is based on the bus voltage type, AC, DC, or hybrid AC/DC [3, 4]. AC microgrids have an AC bus, DC microgrids have a DC bus, and hybrid microgrids have both an AC and DC bus [5, 6]. As discussed above, these systems can be used to support the electrified vehicles or power the system, such as on electric ships.

Microgrids supply the loads applied with the available sources within the small system. This is similar to the operation of shipboard power systems when at sea, which handle

the sources with prime movers and potentially ESS without support from a stiff grid [7]. These power systems are referred to as *shipboard microgrids* [8, 9]. A notional model of a shipboard microgrid with a zonal configuration, ESS and traditional generators, and two control levels is shown in Figure 1.1. Ships range in size, varying from small cargo ferries to large cruise ships and military vessels. These ships provide a large benefit to societal functions, such as transporting 80% of consumer goods, providing transportation for people, and freedom of the seas [10, 11]. With this large societal benefit, the negative environmental effects of the on-board generators have prompted a paradigm shift to electrification. Specifically, these electrification efforts have been seen on transit ferries [12], naval vessels [13], and maritime ships [14]. However, electrifying ships has posed a unique problem due to the high reliability standards and required self-sufficiency when at sea. Therefore, hybrid-electrification has been proposed to provide sufficient and reliable voyage distances to address the needs of the maritime sector. Hybrid energy resources utilized include traditional thermal engines, as well as energy storage systems (ESSs) and flywheels [12, 15]. Fully electric ships are possible, such as the e-ferry *Ellen*, widely acknowledged as the world's most powerful fully electric ferry with 4.3 MWh capability by Li-ion battery cells with no emergency back-up generator [10]. However, the traditional generation sources onboard provide a transition for larger ships or ships that require high reliability standard. Therefore, effective, economic, and reliable operations of on-board ESSs are critical for electrified ships.

1.2 Motivation

The interest with electrifying ships has been motivated by both environmental concerns and handling increasing power demands on ships [16]. The first factor is environmental

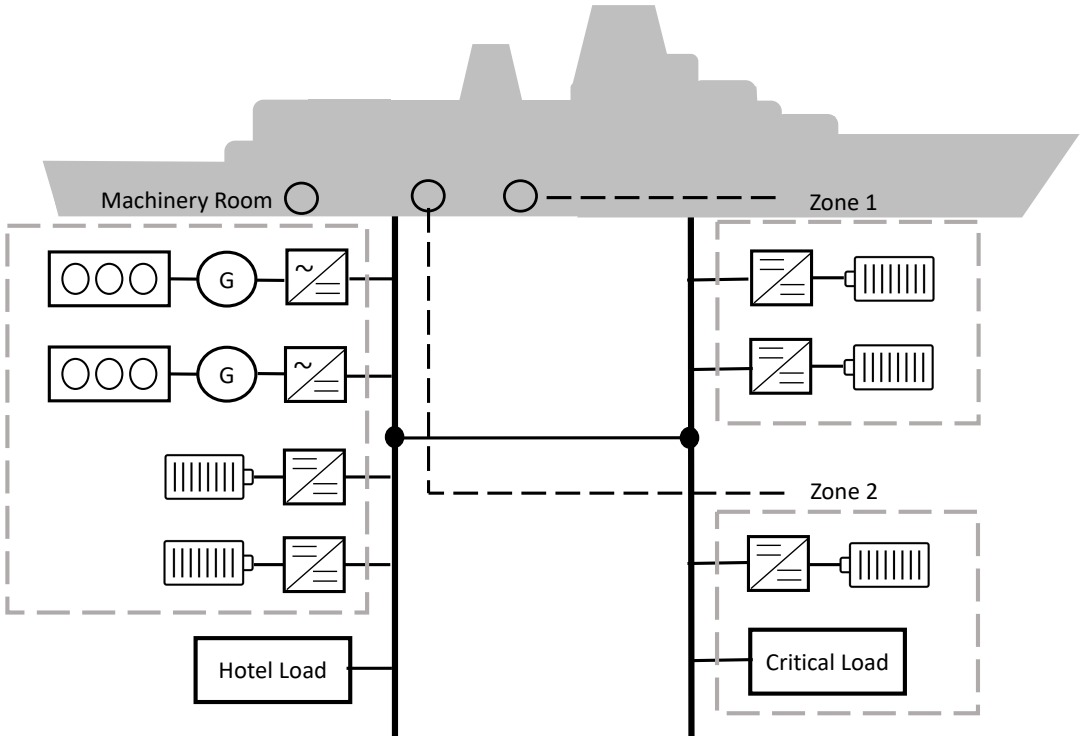

Figure 1.1: Notional model of an electrified shipboard microgrid with a hybrid storage system featuring distributed energy storage systems (ESS). This shipboard microgrid is designed a DC microgrid with distributed ESS in different zones. Main movers such as generators provide AC power that is rectified via AC/DC rectifiers.

concerns, which has been highly motivating the shift away from traditional prime movers [17]. The emissions caused by ships are of particular interest to communities near the shore and ports, where the effect of traditional prime movers on air quality has had a negative impact [10]. Additionally, the higher power availability of ESS and super capacitors is expected to be able to meet increasing power demands on board ships [12].

The power demands on the ships are typically classified as hotel loads or propulsion loads. Hotel loads are considered anything unrelated to the prime movers of the ship. The hotel loads can include lighting, air conditioning, appliances, etc. These loads can be estimated based upon past trips with similar condition, but may change due to unforeseen circumstances such as route and weather conditions [18]. This discrepancy between the predicted and actual load must be accommodated in real time to ensure the system remains operational [19, 20]. These load changes are similar to other renewable resource uncertainties, such as solar panels which change based on the weather conditions [21]. These loads can be further classified into pulsed loads depending on the type of ship and equipment onboard [16, 22]. These allow for the ships load to be predicted, although the pulsed loads present unique challenges with regard to reliability constraints.

One method to manage these additional constraints is by adding batteries and supercapacitors, which have a faster response time, but lower power density compared to the traditional prime movers. Therefore, batteries have been investigated for both a fully electric and hybrid approach. The largest fully electric ferry has a 4.3 MWh Li-ion battery with no back-up generation on-board [10]. However, some ship applications may have high power demands that require the prime mover to meet reliability standards. A hybrid-electric power system allows for the increased reliability of the traditional generators while taking advantage of the benefits of ESS.

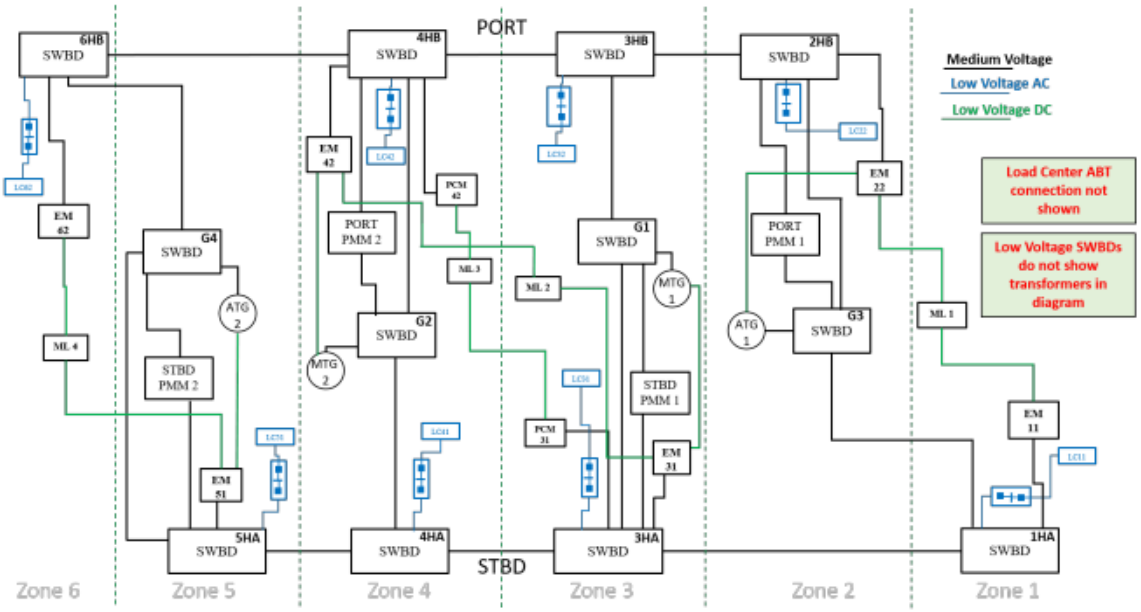

Figure 1.2: Notional ship power system model used for the robust combat power and energy controls (RCPC) demonstrations [25].

The control of microgrids has had renewed interest to solve the problems that occur as electrification grows. The popular method to separate the control problem was to create zones within the system. The zonal configuration of hybrid microgrids has not solely been studied for shipboard microgrids. In [23], an economic control was developed by separating the microgrid into "nanogrids" to control the system, while considering the cost of each unit. This also appears in the form of microgrid clusters, which coordinate the transfer of power between the microgrids while minimizing the costs and transmission losses [24]. In order to prevent a single point of failure, a distributed system was developed. An example of a six-zone shipboard microgrid is shown in Figure 1.2 [25].

As shown in Figure 1.2, the system is distributed with connection to two buses, representing the port and starboard sides with ESS throughout. This displays the direction that the ships will be following to achieve the resilient control and power management

required while implementing ESS. Therefore, the control of a hybrid power system onboard ships will continue to develop unique problems that will influence research efforts.

The problems investigated with the shipboard microgrids include zone configuration options, as shown in Figure 1.2 [26], preventing a single point of failure [27], balancing the load between traditional generators and ESS [28], and coordinating the transition from an islanded microgrid to grid-connected when at port [12]. In [26], the zones are set initially but may be reconfigured via a state space model. The state space model considers any failures that may occur, such as disconnections, and reconfigures the zones to keep as many loads online as possible. If all the loads cannot be accommodated, then non-critical loads were shed. The reconfiguration typically also requires that the critical loads have two separate paths to power the units, which provides further assurance that those loads will be sustained in case of a fault [29]. Additionally, the power sharing between the zones has been studied for hybrid shipboard microgrids as these constraints may cause issues if they are not addressed [30]. These methods require knowledge of the entire system to determine the reconfiguration strategy. Therefore, if any new loads or sources were added, the model and control must be adjusted accordingly. Therefore, [27] uses a fuzzy logic control that does not require full knowledge of the system to distribute the load. This also works to prevent a single point of failure to increase reliability.

As these efforts continue, including the higher efficiency and environmental goals, the balance between the traditional generating units and the ESS has become more important. Therefore, rather than using traditional droop control, an inverse droop control may be used to leverage both types of units onboard [28]. This type of control takes advantage of both the high-power output of the generators and the direct DC power of the ESS. As these resources are used at sea, the hybrid system may also be balanced based on the use of the

ESS and generators. This method uses the pure electric mode for trips where the ESS is sufficient. Meanwhile a coordinated control between the generators and ESS extends the possible range. Finally, when the ship was at port, the ESS were charged to prepare for the next trip [12]. There have also been control methods that do not focus solely on the overarching control but look specifically at the solid-state devices used [31]. This method allowed the system to remain flexible and leverage the system by efficiently switching the sources. The control of shipboard microgrids has been multi-faceted with pros and cons to each solution.

1.3 Problem Statement

The control of the shipboard microgrid considers two economic factors and two control factors. The economic factors include the cost of the ESS onboard and the fuel efficiency of the generator. A common control method for generators is droop control, which determines the load distribution based on a droop coefficient. Although ships do not follow the same financial market competing for lowest cost and highest payoff considering the operation and management costs, the economics of using each unit may be considered [32]. The droop control method distributes the load across the units based on the physical factors, such as the maximum load. However, distributing the units based on the economic cost would save operation costs of the units. This can be implemented using an economic droop control using the quadratic cost function of the unit. The quadratic cost function can be easily fit to traditional sources of generation, such as diesel generators and gas turbines. However, the battery degradation does not fit as well into this method since it does not inherently have the same function as a generator. Therefore, the battery was either excluded from this type of control or fit to the quadratic cost function as best as possible. Therefore, a cost

function that was comparable to the generator was developed using the cycle life aging of the battery to fit into this economic droop control scheme. Furthermore, it was found that the quadratic missed an opportunity for an uneven load distribution across generators when the fuel efficiency curve was considered. For example, if the quadratic cost function was used for two identical generating sources, the most efficient method was calculated to be an equal split between the two units. However, when the fuel efficiency curve of the generator was used, which was formulated as a fourth order equation, a solution for an unequal split was provided. This offered an opportunity to save fuel that was not represented in the quadratic cost function. Therefore, the proposed formulation developed a baseline economic function using the predicted load on-board the ship.

Meanwhile, the control factors considered were discrepancy in load applied and the predicted load in terms of ensuring the online generating sources can handle the change and redispatch when differences inevitably occurs. As mentioned, the baseline function was developed based on the best economic distribution for the predicted load. However, to remain reliable, the system must be prepared for fluctuations between the predicted loads. Therefore, the predicted load also considers a set percentage that the online units can handle above and below the predicted load. Furthermore, when these fluctuations occur, the system remains flexible and may deviate from the most economic state. During this redispatch process, the control efforts are reduced rather than the cost of using the units. Therefore, the change in load redistribution across the units was minimized. This scheme develops an efficient, flexible, and resilient control in terms of both economic and control efforts for the hybrid-electric shipboard microgrid.

1.4 Outline of Dissertation

This dissertation investigates the control of hybrid-electric ships from an economic control perspective. This dissertation has 7 chapters, Chapter 1 is the Introduction, Chapter 2 covers the Economic Control Considering Cycling Life Costs, Chapter 3 discusses the Fuel Efficiency of Diesel Generators and Gas Turbines, Chapter 4 investigates the Source Redispatch with Control Effort Reduction, Chapter 5 summarizes the Summary of Contributions, Chapter 6 is Future Work that will be performed, and Chapter 7 is the Appendix.

The Introduction covered the background information including microgrid types and how they translate to shipboard power systems i.e. shipboard microgrids. The motivation covers the inspiration for this work including the current usage of generators and batteries onboard ships and the improvements that are intended as a part of this work. The problem statement covers the specific issues that will be tackled. This includes the control scheme that was implemented for the hybrid electric microgrid and an introduction to the formulations.

The Economic Control Considering Cycling Life Costs develops a versatile cost function for batteries. On most battery manufacturer data sheets, the cycles until failure are given. This data was used to develop a cost function in terms of the cycle life lost as a result of the discharge of the battery. This was then used to compare with the incremental cost of a traditional generator. As a result of this, the battery was able to be used as a main power source onboard the shipboard microgrid.

The Fuel Efficiency of Diesel Generators and Gas Turbines improves the formulation of the generators by distributing the load based on the fuel consumption using the fuel

efficiency curves. The fuel efficiency curves provides the gallons of fuel needed for the power output in terms of MW. Using this information rather than a quadratic cost curve, the efficiency of the distribution was improved. This was then formulated into a cost function to be compared with the cost of batteries onboard. This allowed the load demand, given by a predicted load curve, to be met while minimizing the cost using the batteries and generators. This was demonstrated for three predicted load curves.

The Source Redispatch with Control Effort Reduction considers the occurrences when the load does not follow the predicted load curve. In this case, the load must be redispatched across the sources to meet the new load demand. In this case, the goal was no longer to minimize the cost, but instead to reduce the control effort. This was achieved by minimizing the change applied to each of the sources while meeting the new load demand and other constraints. Two operation modes were developed to provide further flexibility, a reserve increase and a required number of on-line generators. Two load deviations were considered for each of the three load profiles where one deviation was handled with a reserve increase and the second was handled with a required number of generators turned on.

The Summary of Contributions discusses the culmination of the work discussed in this dissertation. The contributions of each of the chapters was discussed in this section. This includes the versatile battery cycling cost, the versatile cost function developed for the battery, which allows the to be used as a main power source. The efficiency improvements as a result of implementing the fuel efficiency equations into the control scheme rather than the quadratic cost function was explained. Flexibility and resiliency improvements were concluded as a result of the redispatch formulation with the control effort reduction.

The Future Work discusses what can be improved upon from the work discussed in this dissertation. The improvements mainly revolve around the zonal control, which is the state

of practice as discussed in the introduction. Each of these control schemes were inspired by the zonal control but do not directly implement constraints involving zones.

The Appendix provides the Python code used to simulated the predicted load distribution and the redispatched load distribution.

1.5 Contributions

The contributions of the dissertation follow the work that was completed over the course of the Ph.D. program. The publications that contributed to the contributions of this work include:

- The battery cycling life costs were formulated using data that is included on most battery data sheets, which provides versatility. When the cost function was formulated in this manner, the battery was able to be used a main power source with an economic component included.
  - The publication that discussed this contribution is: **K. Sitch** and L. Du, "Economic Control for Hybrid-Electric Shipboard Microgrids Considering Battery Degradation and Cycling Life Costs," 2022 IEEE Transportation Electrification Conference & Expo (ITEC), 2022, pp. 647-651, doi: 10.1109/ITEC53557.2022.9813757 [33].
- The efficiency of the load distribution across generators was improved by implementing the fuel efficiency equations, which are typically a fourth order or greater equation, rather than a quadratic equation.
  - The publication that discussed this contribution is: **K. Sitch** and L. Du, "Efficient, Resilient Control of Hybrid Shipboard Microgrids Considering Fuel

Efficiency and Battery Cycle Life," 2023 IEEE Transportation Electrification Conf. & Expo., Detroit, MI [34]

- The efficiency of the generator was formulated as a cost function and compared with the battery cost function to minimize the cost of the load distribution across all of the available sources. A reserve requirement was also included to ensure that when the load demand could be met when the predicted load profile was not followed.
  - The publication that discussed this contribution is: **K. Sitch** and L. Du, "Efficient, Resilient Control of Hybrid Shipboard Microgrids Considering Fuel Efficiency and Battery Cycle Life," 2023 IEEE Transportation Electrification Conf. & Expo., Detroit, MI [34]
- When the load does not follow the predicted load demand, the sources must be redistributed based on the deviations that occur. This was achieved via a redispatch optimization.
  - The publication that discussed this contribution is: **K. Sitch** and L. Du, "Flexible Load Uncertainty Management on Shipboard Microgrids Through Redispatch with Control Effort Reduction," 2023 IEEE Transportation Electrification Conf. & Expo., Detroit, MI [35]
- The redispatch provided additional flexibility with two mode changes, a reserve increase and a required number of units to be on throughout the redispatched period.
  - The publications that discussed this contribution is: **K. Sitch** and L. Du, "Flexible Load Uncertainty Management on Shipboard Microgrids

Through Redispatch with Control Effort Reduction," 2023 IEEE Transportation Electrification Conf. & Expo., Detroit, MI [35]

– **K. Sitch**, D. Sun, L. Du and H. Yang, "Pulsed Electric Bus Charging Management Considering Charge Redistribution Effect," 2020 IEEE Transportation Electrification Conference & Expo (ITEC), 2020, pp. 1088-1092, doi: 10.1109/ITEC48692.2020.9161717 [36].

CHAPTER 2

ECONOMIC CONTROL CONSIDERING BATTERY CYCLING LIFE COSTS

Shipboard microgrids have been gaining popularity, particularly regarding electric ships. The electric ships require batteries onboard regardless of if the system is fully electric or hybrid. The implementation of batteries creates unique control problems, but the economic consideration of batteries has not been well studied. Typically, batteries are either considered to be free, as in they are added to the load when being charged or subtracted from the load when being discharged. This does not consider the timing of the batteries being charged or ensuring an acceptable lifetime. If the battery's cost is considered, it is typically modeled as a quadratic cost function, which does not fit well with the battery aging dynamics. As discussed in the background section of this paper, droop control has been studied for shipboard microgrid control. This section discusses considering the battery aging costs in terms of its cycle life within an economic droop control scheme. The following work was presented at IEEE Transportation Electrification Conference in June 2022 [33].

2.1 Droop Control

A popular method to control sources within microgrids is droop control due to the versatility, ease of implementation, and power sharing capabilities. This method was adjusted for all types of microgrids and can be used in both islanded and grid-connected modes. The sources were controlled by using the droop coefficient, power, and bus voltage and/or frequency to meet the requirements. Whether the frequency or voltage was used

to adjust the values is based on the type of microgrid considered. AC microgrids use the frequency and DC microgrids use the bus voltage to control the bus and provide the required load. Meanwhile hybrid AC/DC microgrids use both frequency and voltage with a normalization between the two values to control each bus and allow power sharing.

2.1.1 Droop Control Background

Droop control operates by distributing the loads among the sources by setting the droop coefficient. The droop control was set based on the type of microgrid to meet the load demand. This method may be communication-less or include communication. This is mainly determined by the control levels that were included in the control scheme. These levels were considered a hierarchical control, which includes primary, secondary, and tertiary control [37]. The primary control level is typically communication-less, which increases reliability, but suffers from drifting from the set value [5]. Meanwhile the secondary level corrects the drifting that occurs but requires communication. It is possible to remain communication-less within the secondary droop control layer but is not typical [38]. The tertiary control level allows for the microgrid to interact with the power grid in terms of receiving support for the applied loads or feedback of excess power [37].

The type of microgrid determines the droop control relationship that was used, such as $P-f$, which controls the frequency based on the real power, and $Q-V$, which controls the voltage based on the active power for AC microgrids. These relationships were set using the equations below [5].

$$f_i = f_{max} - m_i P_i = f_{max} - \frac{f_{max} - f_{min}}{P_{i,max}} P_i \tag{2.1}$$

$$V_i = V_{max} - n_i Q_i = V_{max} - \frac{V_{max} - V_{min}}{Q_{i,max}} Q_i \tag{2.2}$$

where f_{max} and f_{min} were the maximum and minimum frequencies, m_i and n_i were the droop coefficients, which were set based on the maximum possible deviations of the active power, $P_{i,max}$, and reactive power, $Q_{i,max}$ as shown. Since the frequency at steady state, f must be equal across the units' power, P_i, was calculated as:

$$P_i = \frac{f_{max} - f}{m_i} \tag{2.3}$$

Therefore, this sets the power for the units within AC microgrids while maintaining the frequency and DC bus voltage. Furthermore, this configuration is both distributed and communication-less, which increases the system reliability [5].

DC microgrids follow a similar scheme except that the frequency was not involved in the formulation. Therefore, the DC bus voltage was controlled with the active power using the following relationship.

$$V_{DC}^* = V_{DCmax} - d_j P_j = V_{DCmax} - \frac{V_{DCmax} - V_{DCmin}}{P_{j,max}} P_j \tag{2.4}$$

where V_{DCmax} and V_{DCmin} was the maximum and minimum allowable DC bus voltages, d_j was the droop coefficient, which was again based on the maximum power, $P_{j,max}$. Then the power generated, P_j was calculated using the steady state bus voltage, V_{DC}.

$$P_j = \frac{V_{DCmax} - V_{DC}}{d_j} \tag{2.5}$$

Hybrid AC/DC microgrids use a combination of these two functions by developing a per-unit basis to compare the two buses and allow power sharing [5].

Furthermore, this droop control scheme was further developed to include an economic factor. This was based on a quadratic cost function where derivative is an incremental cost (IC) function. Therefore, this IC is equivalent to a Lagrangian multiplier, which can be used to determine the most economic state across generation sources. Therefore, the droop control finds a solution to meet the load demand, while ensuring it is operating in the most economic state. This was performed by using a quadratic cost function, $C_i(P_i)$.

$$C_i(P_i) = a_i + a_{i1}P_i + a_{i2}P_i^2 \tag{2.6}$$

where a_i, a_{i1}, and a_{i2} were the coefficients. The IC was developed by taking the derivative of this equation.

$$IC_i(P_i) = \frac{\partial C_i(P_i)}{\partial P_i} = a_{i1} + 2a_{i2}P_i \tag{2.7}$$

The main goal of the control was to minimize the cost of the generating units while meeting the load demand and operating within the units' limits. Therefore, economic dispatch problem is represented as follows:

$$C_{\text{total}} = \sum_{i=1}^{n} C_i\left(P_i\right) \tag{2.8}$$

$$\sum_{i=1}^{n} P_i = P_D \tag{2.9}$$

$$P_{i\,\min} \leq P_i \leq P_{i\,\max}, i = 1, \ldots, n \tag{2.10}$$

where P_D was the load demand. As mentioned above, the IC was found by taking the derivative of the cost function, which is the objective of the economic dispatch problem.

Therefore, the economic droop control equation for an AC microgrid became:

$$f_i = f_{\max} - m_{IC} \cdot IC_i\left(P_i\right) = f_{\max} - \frac{f_{\max} - f_{\min}}{IC_{\max}} IC_i(P_i) \tag{2.11}$$

where m_{IC} was the droop coefficient, which was based on the maximum IC, IC_{max}. Therefore, two equivalent droop control curves were developed where the IC was matched between the units and set to the equivalent power based on the IC function. In other words, the IC of each unit was mapped to the frequency, which was set equal to the units. This contrasted with directly setting the frequency to the equivalent power output, where each unit outputs the given ratio of power without considering the cost of operating the units. This was similarly performed for the DC microgrid.

$$V_j = V_{dc,max} - d_{IC} IC_j(P_j) = V_{dc,max} - \frac{V_{dc,max} - V_o}{IC_{max}} IC_j(P_j) \tag{2.12}$$

Again, with this formulation, the IC of all the units were matched to ensure the units were operating optimally [5]. However, this formulation still suffers from the drifting effect since it only includes primary control.

To correct this drifting effect, a secondary control level was added in [39] to correct the drifting effect. The primary control in this scheme operated the same as the above formulation except that the maximum terms in the droop coefficients were removed.

$$d_{ac} = f_{ac\max} - f_{ac\min}, d_{dc} = V_{dc\max} - V_{dc\min} \tag{2.13}$$

As shown above, the droop coefficients simply consider the difference between the minimum and maximum frequency, f_{acmin} and f_{acmax} for AC microgrids and the difference between the minimum and maximum bus voltage, $V_{dc\min}$ and $V_{dc\max}$. The drift caused by

the droop control must be corrected without affecting the best economic state. First, the curve was shifted upward by δx to meet the nominal x_n, which was the set value for the frequency or voltage. This same value of δx would occur across all the DGs, which were communicated via communication with neighbors to maintain a distributed system. Next, a relative loading index (RLI), normalized the maximum and minimum to be between 1 and 0 based on the difference it was shifted to.

$$\mathrm{RLI}(x) = \frac{x - x'_n}{\delta x}, x'_n = x_n + \Delta x \tag{2.14}$$

where $x_n = 0.5(x_{max} + x_{min})$ and $\sigma x = 0.5(x_{max} - x_{min})$. This RLI not only adjusts the drift, but also allows knowledge of the loading conditions. Since the change in x is known, although the voltage and frequency were set to the nominal value, the δx provides visibility to calculate the loading conditions. To implement this into the control system, the new droop equations with the RLI became as follows:

$$f_{ac} = f_{ac\max} - d_{ac} IC_i + \Delta f_{ac} \tag{2.15}$$

$$V_{dc} = V_{dc\max} - d_{dc} IC_j + \Delta V_{dc} \tag{2.16}$$

The RLI was applied to the above droop equations as follows:

$$\mathrm{RLI}\left(f_{ac}\right) = \frac{f_{ac\max} - d_{ac} IC_i + \Delta f_{ac} - \left(f_{acn} + \Delta f_{ac}\right)}{0.5\left(f_{ac\max} - f_{ac}\min\right)} \tag{2.17}$$

$$\mathrm{RLI}\left(V_{dc}\right) = \frac{V_{dc\max} - d_{dc} IC_j + \Delta V_{dc} - \left(V_{dcn} + \Delta V_{dc}\right)}{0.5\left(V_{dc\max} - V_{dc\min}\right)}. \tag{2.18}$$

where the RLI equates to IC values IC_i and IC_j respectively. Therefore, this system corrected the drift caused by droop control while maintaining a distributed system [39].

This would be best used on ship where a drop in power quality may be detrimental to the equipment on board.

This shows the versatility of the droop control scheme on how it may be used on general microgrids, as well as on a ship. This method can apply simply to the power distribution or considered with an economic consideration. These papers inspired the work that will be discussed in the following chapter, which implements this economic droop control scheme in a shipboard microgrids. As shown in these schemes, they are heavily reliant on the quadratic cost function. However, the batteries that are being implemented into the hybrid power system do not fit well into this scheme.

2.2 Economic Droop Control

As mentioned previously, traditional droop control provided equations to control the available sources by setting a droop coefficient and correlating the power and DC bus voltage for DC microgrids. This control method was adapted to consider an economic factor by considering the cost function for each unit to produce the output power. Specifically, a quadratic cost function was used to determine the cost of the power produced. The quadratic cost function within a droop control scheme can be implemented with many considerations. For example, a versatile, distributed method can be implemented by only using a primary control level [5]. However, this suffers the typical droop control drift from the set value. Adding a secondary control level can correct this but requires communication [39]. A penalty factor is another method that has been used to correct this issue [40]. Therefore, the quadratic cost function has been a widely used method to develop an economic droop control scheme.

The derivative of quadratic cost function is considered the IC. The Lagrangian relaxation technique was used to determine the optimized result. The Lagrangian relaxation technique states that the Lagrange multiplier, λ, was calculated based on the derivative of the function being optimized. The function was most efficient when each of the Lagrange multipliers were equal [5, 39]. Therefore, since the function being optimized is the cost function of each unit, the IC of the units were set to be equal to achieve the optimal result. Therefore, the cost functions of the units were minimized, and the ICs of the units were set to be equal. The Lagrangian function was defined as follows:

$$\mathcal{L}(x, \lambda) = f(x) - \lambda g(x) \tag{2.19}$$

where $f(x)$ is the function being investigated, λ is the Lagrangian multiplier, and $g(x)$ is a constraint. The first order necessary condition for optimality gives:

$$0 = \frac{\partial \mathcal{L}}{\partial x} = \frac{\partial f(x)}{\partial x} - \lambda \frac{\partial g(x)}{\partial x} \tag{2.20}$$

As mentioned previously, the cost functions of the units are a quadratic cost function, as shown below denoted as C_i.

$$C_i(P_i) = a_{i2} P_i^2 + a_{i1} P_i + a_i \tag{2.21}$$

where P_i is the power generated, and $a_i, a_{i1},$ and a_{i2} are the cost function coefficients. Using the Lagrangian relaxation technique, an economic dispatch problem was developed.

The economic dispatch problem operates by minimizing the total cost across all units while meeting the load demand and operating within the units' power limits. This problem was formulated as follows.

$$C_{\text{total}} = \sum_{i=1}^{n} C_i\left(P_i\right) \tag{2.22}$$

$$\sum_{i=1}^{n} P_i = P_D \tag{2.23}$$

$$P_{i\,\min} \leq P_i \leq P_{i\,\max}, i = 1, \ldots, n \tag{2.24}$$

where C_{total} was the total cost across the sum of units where the individual units cost in terms of power output were represented as $C_i(P_i)$. The total power demand is indicated as P_D. As shown the IC is equivalent to the Lagrangian multiplier, λ. If any of the units are operating at their limits, therefore, activating the inequality constraints, the IC would not be able to meet the ideal equal IC metric. Instead, the IC would be:

$$IC_i = \begin{cases} \frac{\partial C_i(P_i)}{\partial P_i} = \lambda^*, \quad P_i^{\min} < P_i < P_i^{\max} \\ \frac{\partial C_i(P_i)}{\partial P_i} \leq \lambda^* \quad P_i = P_i^{\max} \\ \frac{\partial C_i(P_i)}{\partial P_i} \geq \lambda^* \quad P_i = P_i^{\min} \end{cases} \tag{2.25}$$

Therefore, ideally the IC would be equal to the calculated IC, λ^*, but may be greater or less if the constraint is active. To fit within the droop control scheme, the DC droop control equation was adjusted to include the IC. This was implemented by replacing the power with the IC of the units. The original droop control equation was formulated as:

$$V_i = V_{dc,max} - \frac{V_{DCmax} - V_{DCmin}}{P_{imax}} P_i \tag{2.26}$$

where $V_{dc,max}$ is the maximum DC bus voltage, $V_{dc,min}$ is the minimum DC bus voltage, P_{imax} is the maximum power output, and P_i is the output power for source i. The IC was replaced as follows:

$$V_i = V_{dc,max} - \frac{V_{dc,max} - V_o}{IC_{max}} IC_i(P_i) \tag{2.27}$$

where the new droop coefficient was adjusted to use the IC and IC_{max} is the maximum IC [5]. Otherwise, the droop control operated as normal but worked to operate the units economically. This function can be applied to any unit estimated as quadratic cost function.

2.2.1 Battery Cost Function

The typical assumption used when batteries were implemented into systems was that the battery lifetime cost was fixed. If the battery degradation was considered, it was typically in terms of sizing the battery to ensure the predicted lifetime [41]. Although this may meet the requirement, it may lead to errors since the degradation caused by its use was not considered. The degradation does not always need to be considered, such as when the battery was used as a back-up service where it is not being charged and discharged multiple times per day. A quadratic cost function has been applied in the past but may not represent the degradation change as the DoD varies properly [42]. However, when the battery is an integral part of the system, this assumption does not accurately represent the stress caused. There are multiple methods to estimate the cost of the battery.

One method that can calculate the degradation of the battery based on the loss of life of the battery [43]. This method determines the loss of life of the battery in terms of percentage depth of discharge (DoD) and pro-rates the degradation cost based on the replacement cost of the battery. However, this method requires that the stress function, which determines the loss of life of the battery, is known. This is not readily available for all batteries and would make it difficult to implement in any system. Similarly, the chemical properties of the batteries can be used to determine what capacity of the battery was lost,

such as in [44]. However, this again requires in depth knowledge of the particular battery that is being used. These methods would require choosing a battery that already had these tests done or performing tests on them prior to implementation. However, one metric that is typically given on data sheets is the number of cycles until failure at fixed DoD levels.

Batteries are tested by the manufacturer to determine when the lifetime of the battery and reported on the data sheet. This test is typically performed by consistently discharging the battery to a certain DoD, until the battery has 70% of the original capacity [41, 45]. This data is given for a few points and may not be useful to determine the cost of discharge on its own. Testing can be performed to fill this gap in the data as well as add other factors including various discharge currents and temperature [46]. This again requires additional testing to obtain the full picture of the cycling life. However, the data can be fit across all DoD levels of interest using the following equation [47].

$$L = \mu_2 DoD^{-\mu_0} e^{\mu_1(1-DoD)} \tag{2.28}$$

where L is the number of cycles until failure and μ_0, μ_1, μ_2 are the values that were fit based on the manufacturer's data. This function was then used to determine how the DoD affects the lifetime of the battery. This was applied to an economic droop control of various batteries in [48]. This method was limited in that it was only used to apply across various battery systems but showed the versatility of the application across battery modules. This method based on the manufactuer's cycling life data has been proven to be versatile acorss technologies including both lithium-ion and lead acid batteries [49] Additionally, the life was based solely on a consistent discharge level, which is not how batteries are operated in typical control schemes, including economic droop control. Therefore, the lifetime of the battery may be overestimated if this function is used directly to estimate the cost of

discharging the battery. This can lead to overestimating the size of the battery and further increasing costs rather than reducing them [47]. The main appeal of the function is that readily accessible data was and there is valuable information in determining the cycle life of the battery. Therefore, rather than directly using the fixed cycle life data, the number of full cycles per DoD was determined.

2.2.2 Proposed Cycle Life Cost

The previous method of the battery cycling at a fixed DoD may be deceiving if it is looked at individually. As mentioned, during this test the battery is discharged to a fixed DoD, which could range from 10% to 100%. The power or energy output at each DoD is equivalent. Therefore, although there may be more cycles at 10% versus 30%, the output should be used to determine which is the ideal discharge. Therefore, the proposed cycle life consideration used the above cycle life data but considered the number of 100% discharges, or full cycles until failure. This was calculated using the following equation:

$$FC(DoD) = DoD * (\mu_2 DoD^{-\mu_0} e^{\mu_1(1-DoD)}) \tag{2.29}$$

where FC is the number of full cycles and is a function of DoD. To show the discrepancy that can occur between the number of cycles until failure versus the number of full cycles until failure, the data for a lithium iron phosphate ($LiFePO_4$) battery [50] was used. Table 2.1 shows the DoD, the number of cycles at the given DoD, and the number of full cycles.

As shown in Table 2.1, the 10% DoD has the most cycles until failure, but 20% DoD has the most full cycles until failure. Therefore, a consistent 20% DoD would result in a longer lifetime. This is further exemplified in Figures 2.1 and 2.2, where the number of cycles and the number of full cycles until failure versus the DoD is shown respectively.

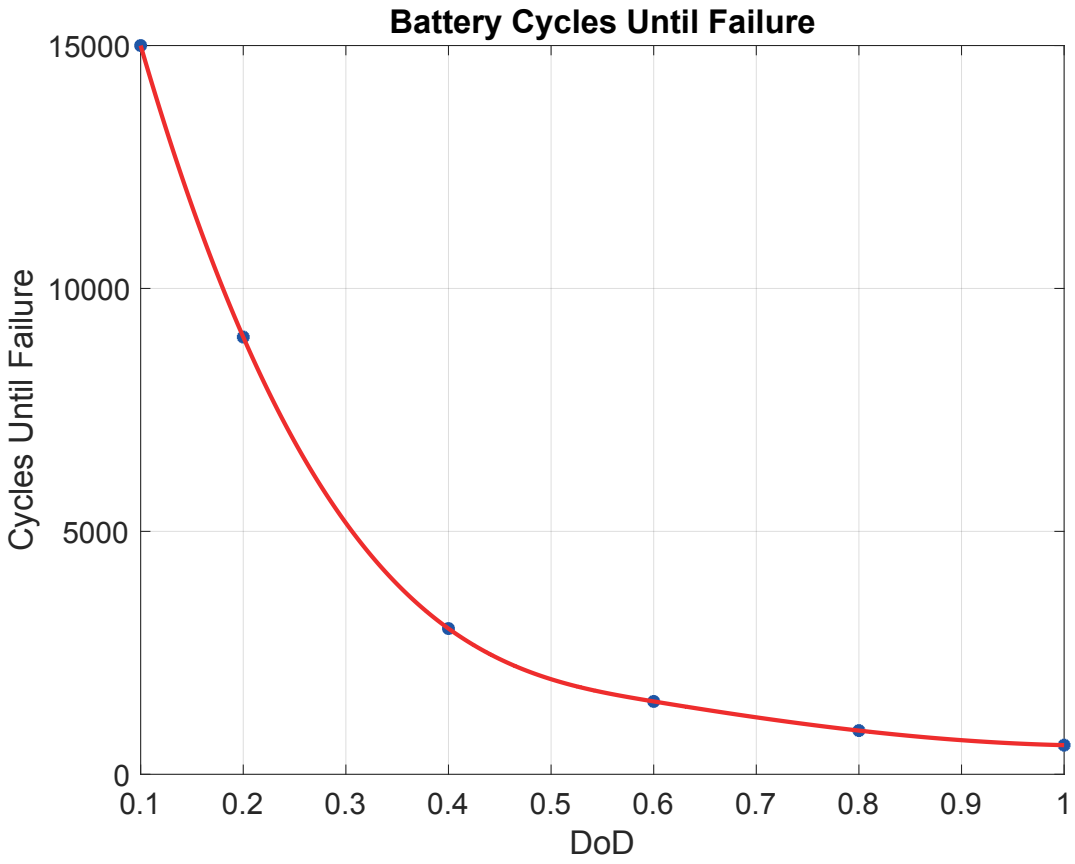

Figure 2.1: The cycles until failure versus the DoD for a $LiFePO_4$ battery [50]

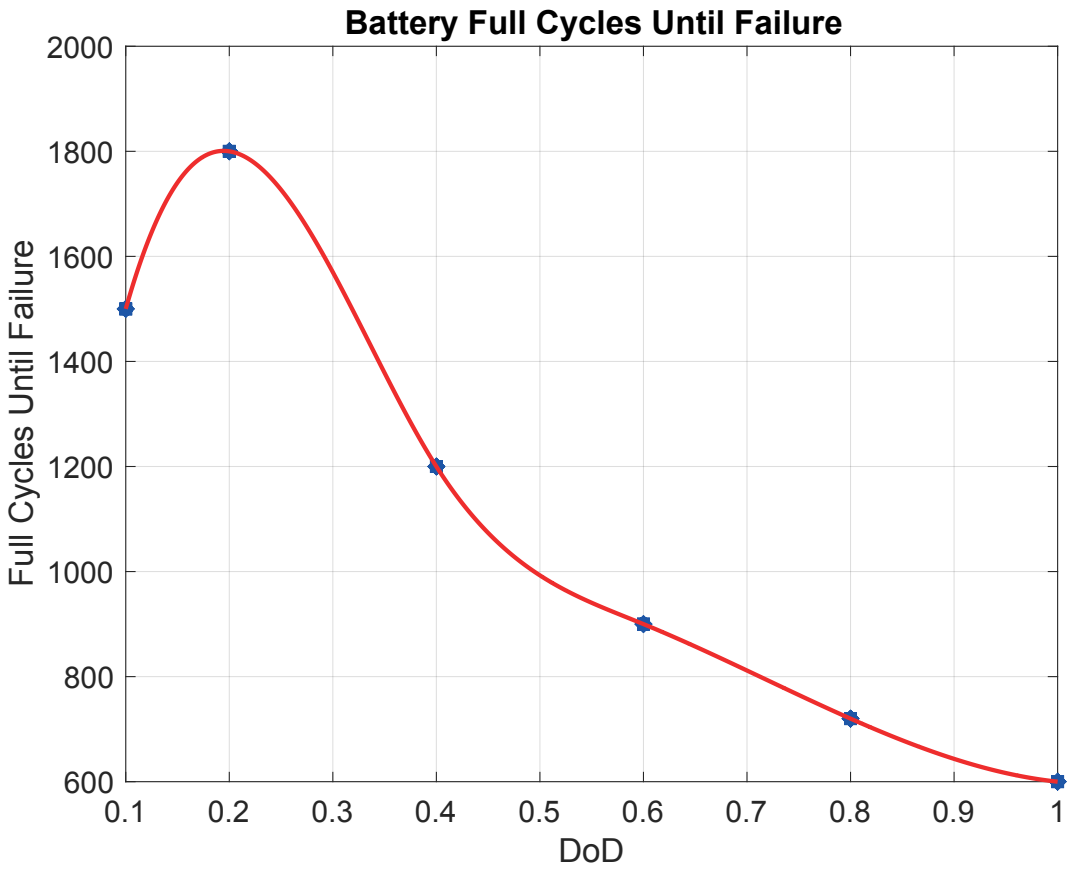

Figure 2.2: The full cycles until failure versus the DoD for a $LiFePO_4$ battery [50]

Table 2.1: Data for a $LiFePO_4$ battery displaying the DoD, cycles until failure, and full cycles until failure [50]

DoD (%)	$LiFePO_4$ Cycles	$LiFePO_4$ Full Cycles
100	600	600
80	900	720
60	1500	900
40	3000	1200
20	9000	1800
10	15000	1500

As shown in Figure 2.2 the number of full cycles, displays a non-monotonic function. Ideally, the battery should be encouraged to discharge to a 20% DoD then discouraged from discharging further. This will be used in the economic droop control to compare with the generator IC.

2.2.3 Battery Incremental Cost

The definition of the IC, in the case of economic droop control with the use of the Lagrangian relaxation technique, is the cost to produce one more unit of power. Since the battery does not fit into a quadratic cost function well, instead a linear cost function was used to compare with the generator's IC. As shown above, for the battery sample given the ideal discharge depth was found to be 20% and any further discharge would reduce the lifetime of the battery. Therefore, the cost to discharge the battery further would therefore be an equivalent comparison to the cost to produce one more unit of power from the generator IC. Therefore, an IC equation for the battery was developed to compare with the traditional generators.

The comparison between the battery and generators must be performed using the energy output of the battery. This is due to the battery operating differently than the generators.

The generators assume that there is enough fuel available to output the power requested, but the battery does not assume that there is sufficient charge. The lifetime energy output of the battery can first be calculated using the number of full cycles until failure as follows.

$$LOE = (FC(DoD)) * (E_{cap}) \tag{2.30}$$

where LOE is the lifetime energy output of the battery and E_{cap} is the energy capacity of the battery. Next, the individual discharge of the battery was calculated based on the DoD and energy capacity.

$$E_{batt} = (DoD) * (E_{cap}) \tag{2.31}$$

where E_{batt} is the energy output by the battery. To associate a cost to the battery, a set replacement cost was used, R, which was then used to price the cost per full cycle of the battery, C_{actual}.

$$C_{actual} = \frac{R}{LOE} \tag{2.32}$$

The number was full cycles until failure was a non-monotonic function, but the IC of the generators were a linear function. Therefore, the function for the battery must also be formulated as a linear function. To capture the features of the non-monotonic function, a multi-linear normalization approach was taken. The number of pieces included in the normalization would be dependent on the accuracy required for the application. For example, for the data given in Figure 2.2, three pieces could be considered from 10% to 20%, 20% to 40%, and 40% to 100%. However, the number of pieces could be adjusted. The pieces calculated using the following normalization term.

$$\alpha_l = \frac{FC(DoD) - FC_{max,l}}{FC_{min,l} - FC_{max,l}}, l = 1, 2, ..., n \tag{2.33}$$

where l indicates the linear piece up to n pieces, $FC_{max,l}$ is the maximum number of full cycles within piece l, and $FC_{min,l}$ is the minimum number of full cycles within piece l. As calculated earlier, the normalization term can also be determined based on the energy output using E_{batt} rather than the DoD, which will give equivalent results. The cost function can then be applied using the cost to replace to the battery as follows.

$$C_l(\alpha_l) = (1 - \alpha_l)C_{actual,min,l} + \alpha_l C_{actual,max,l} \tag{2.34}$$

where $C_{actual,min,l}$ is the minimum cost per full cycle in piece l and $C_{actual,max,l}$ is the maximum cost per full cycle in piece l. Therefore, the piece-wise linear cost function, $C_l(\alpha_l)$, can be used to compare with the IC of the generator.

Using this formulation, the IC of the generators and batteries can be compared. The piece-wise linear droop control scheme has been studied previously on [51] and will operate similarly with the changing droop control curve. The IC of the units can be minimized to ensure that the next unit of power is used to the least costly as possible. Therefore, the battery's age, cost of the unit, and the meeting the demand was considered in one step.

2.2.4 Case Study and Optimization

To develop a case study for this formulation, a generator and battery were considered for the load applied in a single time step. The generator quadratic cost function was as follows [52]:

$$C_l(P_{G1}) = 0.005P_{G1}^2 + 6P_{G1} + 100 \tag{2.35}$$

where $C_1(P_{G1})$ is the cost of the generator at output power P_{G1}. Therefore, the IC function was:

$$IC_1(P_{G1}) = 0.01P_{G1} + 6 \tag{2.36}$$

This source was considered the main unit for this case study with generating limits of 7-28 MW. The battery used was the $LiFePO_4$ battery discussed above with the DoD data shown in 2.1. Within the single time step of 1 hour, it was considered that the battery would only be able to discharge by 40%. Therefore, it would last at least two time steps of maximum discharge would be possible. The total energy capacity of the battery was 20 MWh with a replacement cost of $200,000. The maximum discharge was limited to 40%, therefore, a linear function with two pieces was considered.

$$C_{2,1}(\alpha_1) = (1 - \alpha_1)5.53 + \alpha_1 8.83 \text{ for } DoD \leq 20\% \tag{2.37}$$

$$C_{2,2}(\alpha_2) = (1 - \alpha_2)5.53 + \alpha_2 8.33 \text{ for } DoD > 20\% \tag{2.38}$$

where α_1 is valid from a DoD of 0-20%, which is equivalent to 0 to 4 MW and the α_2 is valid from a DoD of 20% to 40% or 4 to 8 MW. The function in terms of power was:

$$C_2(P_{B1}) = \begin{cases} -0.57P_{B1} + 7.81, & \text{if } P_{B1} \leq 4MW \\ 0.7P_{B1} + 2.73, & \text{if } P_{B1} > 4MW \end{cases} \tag{2.39}$$

Table 2.2: Simulation results displaying the applied load, generator load, P_{G1}, battery load P_{B1}, and the cost, which is the sum of the IC of the generator and the cost of the battery.

Load (MW)	P_{G1} (MW)	P_{B1}	Cost ($)
7	7	0	13.88
8	7	1	12.74
11	7	4	11.60
12	8	4	11.61
15	11	4	11.64
30	26	4	11.79
31	27	4	11.80
33	28	5	12.51
36	28	8	14.61

To simulate this problem the following optimization problem was formulated.

$$\min \quad IC_{total} = IC_1(P_{G1}) + \Delta t * C_2(P_{B1}) \tag{2.40a}$$

$$\text{s.t.} \quad P_{G1} + P_{B1} = P_D \tag{2.40b}$$

$$7MW \leq P_{G1} \leq 28MW \tag{2.40c}$$

$$0MW \leq P_{B1} \leq 8MW \tag{2.40d}$$

Therefore, the IC of the two units were minimized, meet the load demand, and the battery is encouraged to discharge to the ideal 20% DoD and discouraged from charging further. This optimization problem was simulated in Gurobi Python interface with loads ranging from the minimum, 7 MW, to the maximum, 36 MW. The total load, load applied to the generator, P_{G1}, and the battery, P_{B1}, and total cost was recorded in Table 2.2.

As shown in Table 2.2, a load of 7 MW is allocated solely to the generator's minimum operating power. Following with an increase in load is allocated solely to the battery until

it reaches a DoD of 20%, which occurs at a total load of 11 MW or 4 MW, applied to the battery. After this, the remaining load is applied to the generator until the generator's load is maximized at a total load of 33 MW. To fulfill the remaining load demand until 36 MW, the battery is discharged until the full 40% DoD in a single time step at 36 MW. This method determines the most economical way to add another unit of power using the sources IC functions. The battery was encouraged to discharged to the 20% DoD but will discharge further if necessary. The battery supported the system while preventing any unnecessary loss of life and ultimately reducing costs.

2.3 Conclusion

An economic dispatch problem was formulated including a battery and generator. The battery lifetime was determined based on the number of full cycles until failure at various DoD levels. This provided a method that can be easily applied to various batteries based on the manufacturer data from cycling the battery. Furthermore, a piece-wise linear cost function was developed to encourage the battery to discharge to its ideal DoD and discouraged from discharging further. This was simulated using single time step optimization using a battery and generator. This method will be improved by developing a time-horizon problem considering the battery SoC and generator loading.

2.3.1 Summary of Contributions

This chapter focused on applying an economic component to batteries in a way that was compatible with generators' cost functions. In this case, the focus was on the incremental cost of the generators as these both applied as linear cost functions. However, the use of this is not limited to only incremental cost formulations, as will be shown in the following

chapters. The battery cost function considered the number of cycles until failure, which is readily available on most battery data sheets. Therefore, a versatile cost function was developed. Applying this formulation will increase the lifetime of the battery, allow for use of the battery as main power component of the shipboard microgrid, and provide an economic control.

CHAPTER 3

FUEL EFFICIENCY OF DIESEL GENERATORS AND GAS TURBINES

Although the quadratic cost function for the generators provides a basic cost structure for generator's usage, it is limited to what can be captured within the quadratic fit. For example, the quadratic cost function typically considers the fuel cost, heat rate, input and output, and incremental cost [52]. This formulation can be expanded to a cubic cost function by considering other factors such as valve placement. However, this additional factor does not add significance to the results. In terms of a cost function, the quadratic fit is typically the highest order that was considered. This optimizes the load to be split between the units relative to the cost formulated. Therefore, if two identical generators are considered, the load will always be split equally between the units. However, this does not capture the optimal scenario in terms of fuel efficiency.

The fuel efficiency of each unit is an important factor to consider due to the limited reserve of fuel on board a ship. The fuel on board both takes up space and weight. A balance must be made to ensure that the correct amount of fuel, with some margin for error, is onboard without wasting available space. To ensure the most efficient use of space, the same fuel is used for both diesel generators and gas turbines onboard.

3.1 Fuel Efficiency Curve for Diesel Generators

The fuel efficiency curve for a diesel generator provides the gallons per hour (Gal/hr) vs. the load. This was formulated as a function to the fourth power, as shown below. Higher order equations may be available depending on the accuracy required.

$$F = ax^4 + bx^3 + cx^2 + dx + e \tag{3.1}$$

where F is the fuel used per hour and x is the load applied. An example of the fitted curve for a diesel generator is as follows [53]:

$$F_{D1} = 2.314 * 10^{-6} P_{D1}^4 - 3.295 * 10^{-4} P_{D1}^3 + 2.537 P_{D1}^2 + 2.537 P_{D1} + 19.21 \tag{3.2}$$

where F_{D1} is the fuel consumed by the diesel generator and P_{D1} is the load applied. As mentioned above, the load when a quadratic cost function was used, the load is split as a ratio based on this function. In other words, if two identical generator quadratic cost functions were applied, the load would always be split equally between the two units. However, this is not the case when the above formulation was used.

To prove that the unequal split of the generators may be the optimal solution in some cases, two identical diesel generators were considered using the sample curve shown in Equation 3.2.

$$F_{D2} = 2.314 * 10^{-6} P_{D2}^4 - 3.295 * 10^{-4} P_{D2}^3 + 2.537 P_{D2}^2 + 2.537 P_{D2} + 19.21 \tag{3.3}$$

where F_{D2} is the fuel consumed by the second diesel generator for the corresponding load P_{D2}. The following optimization problem was solved:

$$\begin{aligned} \min \quad & F_{D1} + F_{D2} && \text{(3.4a)} \\ \text{s.t.} \quad & P_{D1} + P_{D2} = P_D && \text{(3.4b)} \end{aligned}$$

where P_D was the total demand considered, which was assumed to be 120 MW for the following test. For this example, generation limits were not applied but if limits were to be applied, it can be assumed the values would be adjusted to be within those limits. This assumption will also be proved in the following simulated case study where limits are placed on the units.

The problem was solved using the Lagrangian relaxation technique, which resulted in the following Lagrangian:

$$\begin{aligned}\mathcal{L}\left(P_1, P_2, \lambda, \right) &= f(P_{D1}, P_{D2}) + \lambda g(P_{D1}, P_{D2}) \\ &= 2.314 * 10^{-6} P_{D1}^4 - 3.295 * 10^{-4} P_{D1}^3 + 2.537 P_{D1}^2 \\ &+ 2.537 P_{D1} + 19.21 + 2.314 * 10^{-6} P_{D2}^4 - 3.295 * 10^{-4} P_{D2}^3 \\ &+ 2.537 P_{D2}^2 + 2.537 P_{D2} + 19.21 + \lambda(P_{D1} + P_{D2} - P_D)\end{aligned} \tag{3.5}$$

where λ was the Lagrangian multiplier. Next, the necessary conditions were calculated by taking the derivative with respect to P_{D1}, P_{D2}, and λ.

$$\begin{aligned}L_{P_{D1}}(P_{D1}) =& \frac{\partial \mathcal{L}}{\partial P_{D1}} \\ =& 9.256 * 10^{-6} P_{D1}^3 - 9.885 * 10^{-4} P_{D1}^2 - 0.008 P_{D1} \\ &+ 2.537 + \lambda = 0\end{aligned} \tag{3.6}$$

$$\begin{aligned}L_{P_{D2}}(P_{D2}) =& \frac{\partial \mathcal{L}}{\partial P_{D2}} \\ =& 9.256 * 10^{-6} P_{D2}^3 - 9.885 * 10^{-4} P_{D2}^2 - 0.008 P_{D2} \\ &+ 2.537 + \lambda = 0\end{aligned} \tag{3.7}$$

$$L_\lambda(P_{D1}, P_{D2}, P_D) = \frac{\partial \mathcal{L}}{\partial \lambda} = P_{D1} + P_{D2} - P_D = 0 \tag{3.8}$$

The equations were solved as a system of nonlinear equations which resulted in following values for P_{D1} and P_{D2}.

$$P_{D1} = 113.6434, 6.3566, 60 \tag{3.9}$$

$$P_{D2} = 6.3566, 113.643460 \tag{3.10}$$

Therefore, the possible solutions for (P_{D1}, P_{D2}) are:

$$(P_{D1}, P_{D2}) = (113.6434, 6.3566), (6.3566, 113.6434), (60, 60) \tag{3.11}$$

As shown above, the equal split between the units is still present. Since this solution would be given by the quadratic cost function, the results must be investigated further to prove which combination is the minimizer.

The solutions given above are considered the necessary conditions, but they are not sufficient. Therefore, the second order conditions must be investigated. The second order conditions were calculated using the Bordered Hessian, which has the following form.

$$\nabla^2_{P_{D1},P_{D2}} = \begin{bmatrix} 0 & g_{P_{D1}} & g_{P_{D2}} \\ g_{P_{D1}} & L_{P_{D1},P_{D1}} & L_{P_{D1},P_{D2}} \\ g_{P_{D2}} & L_{P_{D1},P_{D2}} & L_{P_{D2},P_{D2}} \end{bmatrix} \tag{3.12}$$

where $L_{P_{D1},P_{D1}}$ is the second order partial derivative of $L_{P_{D1}}$ with respect to P_{D1}, $L_{P_{D1},PD2}$ is the second order partial derivative of $L_{P_{D1}}$ with respect to P_{D2}, and $L_{P_{D2},P_{D2}}$ is the second order partial derivative of $L_{P_{D2}}$ with respect to P_{D2}. The constraints were represented as $g_{P_{D1}}$ and $g_{P_{D2}}$. Therefore, $L_{P_{D1},P_{D1}}$, $L_{P_{D1},P_{D2}}$, $L_{P_{D2},P_{D1}}$, and $L_{P_{D2},P_{D2}}$ were calculated as:

$$L_{P_{D1},P_{D1}} = 2.776 * 10^{-5} P_{D1}^2 - 0.002 P_{D1} - 0.008 \tag{3.13}$$

$$L_{P1,P2} = 0 \tag{3.14}$$

$$L_{P2,P1} = 0 \tag{3.15}$$

$$L_{P_{D2},P_{D2}} = 2.776 * 10^{-5} P_{D2}^2 - 0.002 P_{D2} - 0.008 \tag{3.16}$$

Each candidate was then considered, and the determinant of the Bordered Hessian was calculated. If the determinant was positive, then this candidate was a maximizer and if the determinant was negative then it was a minimizer. In this case, the minimizers are of interest since the least amount of fuel is of interest. The bordered Hessian that was investigated for each candidate was:

$$\nabla^2_{P_{D1},P_{D2}} = \begin{bmatrix} 0 & 1 & 1 \\ 1 & 2.776 * 10^{-5} P_{D1}^2 - 0.002 P_{D1} - 0.008 & 0 \\ 1 & 0 & 2.776 * 10^{-5} P_{D2}^2 - 0.002 P_{D2} - 0.008 \end{bmatrix} \tag{3.17}$$

The bordered Hessian for each case will have the subscript representing the candidate with respect to P_{D1}, P_{D2}. For example $\nabla^2_{60,60}$ investigates the candidate $P_{D1} = 60, P_{D2} = 60$.

$$\nabla^2_{(60,60)} = \begin{bmatrix} 0 & 1 & 1 \\ 1 & -0.0266 & 0 \\ 1 & 0 & -0.0266 \end{bmatrix} \tag{3.18}$$

$$det(\nabla^2_{(60,60)}) = 0.0533 \tag{3.19}$$

$$\nabla^2_{(6.3566,113.6434))} = \begin{bmatrix} 0 & 1 & 1 \\ 1 & 0.1259 & 0 \\ 1 & 0 & -0.0194 \end{bmatrix} \tag{3.20}$$

$$det(\nabla^2_{(6.3566,113.6434)}) = -1.065 \tag{3.21}$$

$$\nabla^2_{(113.6434,6.3566)} = \begin{bmatrix} 0 & 1 & 1 \\ 1 & -0.0194 & 0 \\ 1 & 0 & 0.1259 \end{bmatrix} \tag{3.22}$$

$$det(\nabla^2_{(113.6434,6.3566)}) = -1.065 \tag{3.23}$$

Therefore, the equal split of 60 MW between the two units (60, 60) is a maximizer. Meanwhile the unequal split between the two units, (6.3566, 113.6434) and (113.6434, 6.3566). The minimizers will consume the least amount of fuel, which proves that unequal split of the load will saves more fuel compared to splitting the load equally between the two identical generators.

This was observed in the fuel efficiency curve and the derivative of the fuel efficiency curve. As noted from the Lagrangian method used above, the derivative plays a vital role in determining the optimal solution. Both the fuel efficiency and derivative curves were

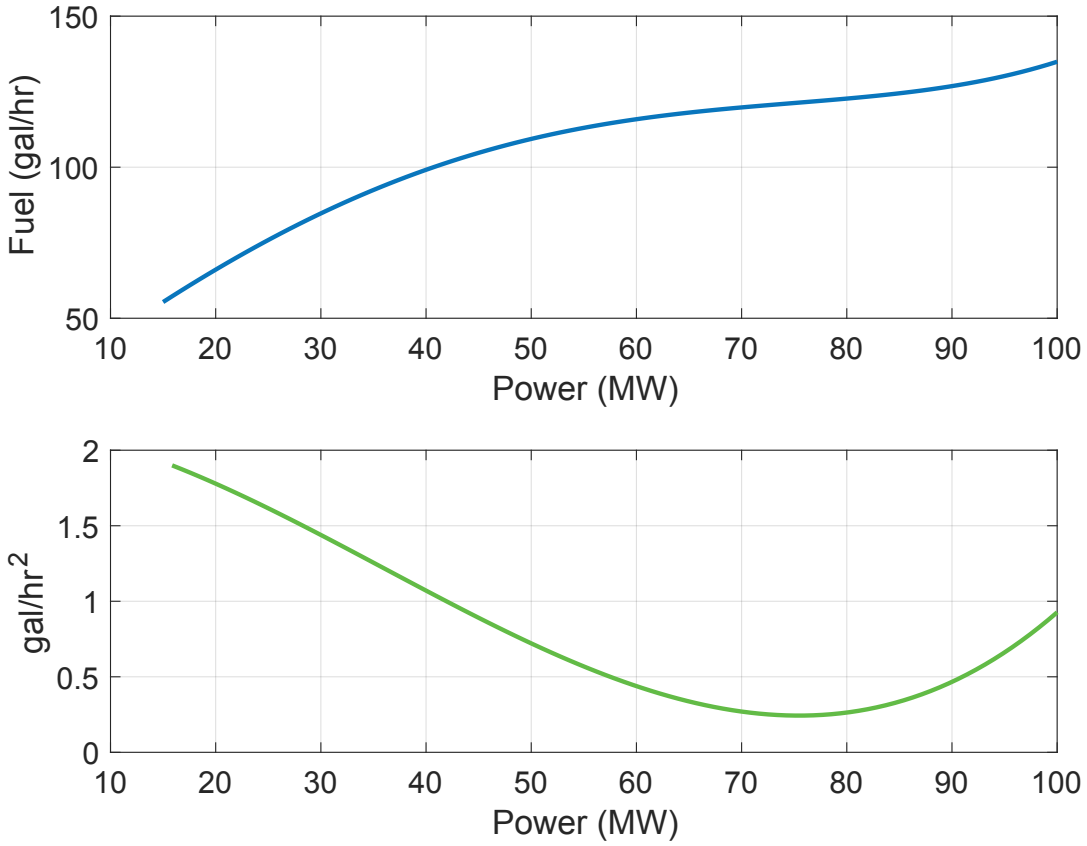

Figure 3.1: The top graph is the fuel usage from 10-100MW using the fuel efficiency curve and the bottom graph is the derivative of the top graph.

plotted in Figure 3.1, which display the increases and decreases that can be taken advantage of depending on the load applied to the unit.

As shown in the curve, the derivative decreases until approximately 75 MW, when the curve increases. This is evident that the unequal split being optimal until at least this point. Following the equal split is expected to be optimal, which is the typical result for the quadratic cost function. Therefore, using this method provides an optimal fuel usage that could be taken advantage of if the load profile is within the applicable range.

3.2 Fuel Efficiency Curve for Gas Turbines

Similarly, the fuel efficiency curve for a gas turbine follows a form with a curve to the fourth power. A sample fuel efficiency curve for a gas turbine is shown below [54].

$$F_{G1} = -3.101 * 10^{-5} P_{G1}^4 + 7.442 * 10^{-3} P_{G1}^3 - 0.6256 P_{G1}^2 + 45.61 P_{G1} + 189.6 \quad (3.24)$$

where F_{G1} is the fuel consumption in gallons per hour for the gas turbine labeled $G1$ with a power output of P_{G1}. If the fuel efficiency curves of gas turbines and diesel generators were compared directly, it would be noted that the gas turbines tend to have a lower fuel efficiency compared to the diesel generators. However, gas turbines have a higher power density and are lighter than diesel generators. Therefore, the gas turbines may consume more fuel, but use less space onboard, which is crucial.

When the gas turbines fuel efficiency curve and derivative were plotted in Figure 3.2, features of local minimums and maximums were noted, which would indicate than an unequal split may also be optimal in some cases. Therefore, a similar sample calculation was followed using the fuel efficiency curve in Equation 3.24. Two identical diesel generators were used where the second diesel generator had the following equation.

$$F_{G2} = -3.101 * 10^{-5} P_{G2}^4 + 7.442 * 10^{-3} P_{G2}^3 - 0.6256 P_{G2}^2 + 45.61 P_{G2} + 189.6 \quad (3.25)$$

where F_{G2} is the fuel consumption for the second gas turbine with the power output of P_{G2}. The optimization problem for the two identical gas turbines was formulated as follows:

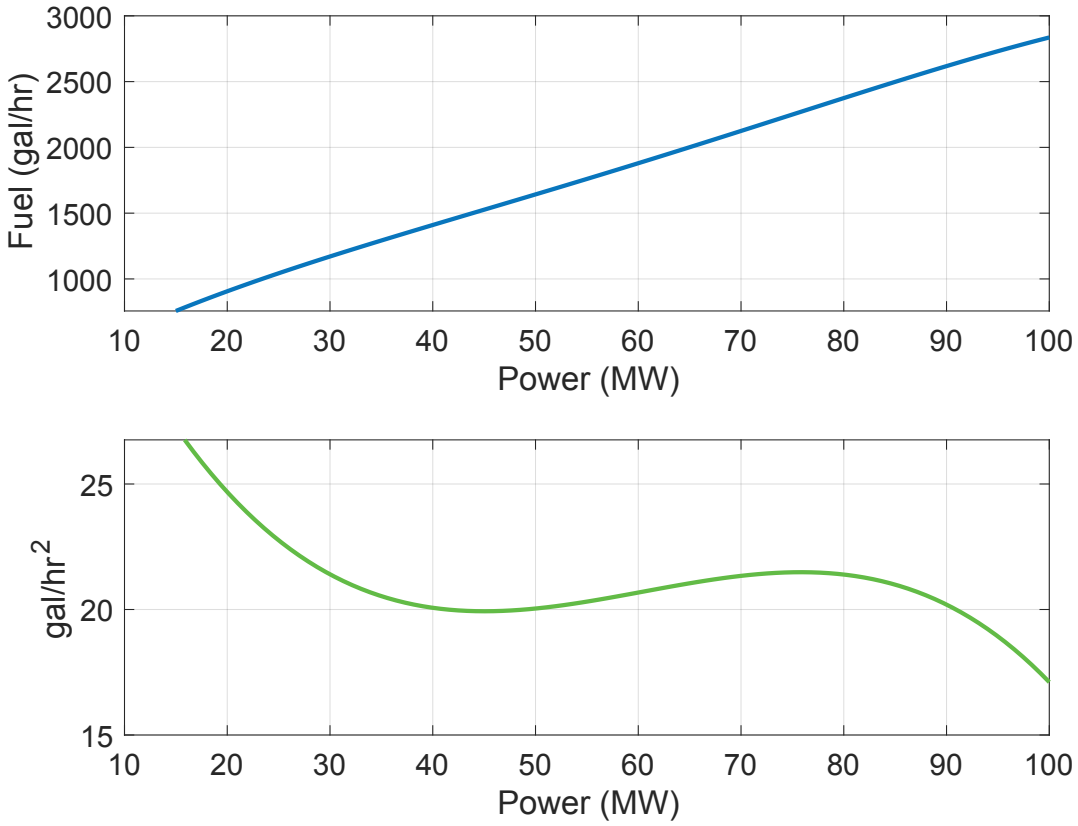

Figure 3.2: The top graph is the fuel usage from 10-100MW of the gas turbine using the fuel efficiency equation and the bottom graph is the derivative of the top graph.

$$\begin{aligned} \min \quad & F_{G1} + F_{G2} && \text{(3.26a)} \\ \text{s.t.} \quad & P_{G1} + P_{G2} = P_D && \text{(3.26b)} \end{aligned}$$

Again, it should be noted that limits were not placed on the generating units for this sample but will be applied later in the case study. The Lagrangian was calculated as:

$$\begin{aligned} \mathcal{L}\left(P_{G1}, P_{G2}, \lambda, \right) =& f(P_{G1}, P_{G2}) + \lambda g(P_{G1}, P_{G2}) \\ =& -3.101 * 10^{-5} P_{G1}^4 + 7.442 * 10^{-3} P_{G1}^3 - 0.6256 P_{G1}^2 \\ & + 45.61 P_{G1} + 189.6 - 3.101 * 10^{-5} P_{G2}^4 + 7.442 * 10^{-3} P_{G2}^3 \\ & - 0.6256 P_{G2}^2 + 45.61 P_{G2} + 189.6 + \lambda(P_{G1} + P_{G2} - P_D) \end{aligned} \tag{3.27}$$

Next, the necessary conditions were calculated by taking the derivative with respect to P_{G1}, P_{G2}, and λ.

$$L_{P_{G1}}(P_{G1}) = \frac{\partial \mathcal{L}}{\partial P_{G1}} = -1.2404 * 10^{-4} P_{G1}^3 - 0.0223 P_{G1}^2 - 1.2512 P_{G1} + 45.61 + \lambda = 0 \tag{3.28}$$

$$L_{P_{G2}}(P_{G2}) = \frac{\partial \mathcal{L}}{\partial P_{G2}} = -1.2404 * 10^{-4} P_{G2}^3 - 0.0223 P_{G2}^2 - 1.2512 P_{G2} + 45.61 + \lambda = 0 \tag{3.29}$$

$$L_{\lambda}(P_{G1}, P_{G2}, P_D) = \frac{\partial \mathcal{L}}{\partial \lambda} = P_{G1} + P_{G2} - P_D = 0 \tag{3.30}$$

If the load, P_D, was again 120 MW, the following load pairs for (P_{G1}, P_{G2}) were calculated to be:

$$(P_{G1}, P_{G2}) = (60, 60), (86.6790, 33.321), (33.321, 86.6790) \tag{3.31}$$

The result of an equal split is again present in the possible optimizers. Therefore, the Bordered Hessian was calculated for this problem to solve for the second order conditions.

$$\nabla^2_{P_{G1},P_{G2}} = \begin{bmatrix} 0 & 1 & 1 \\ 1 & -3.7212 * 10^{-4} P_{G1}^2 + 0.0447 P_{G1} & 0 \\ & -1.2512 & \\ 1 & 0 & -3.7212 * 10^{-4} P_{G2}^2 + 0.0447 P_{G2} \\ & & -1.2512 \end{bmatrix} \tag{3.32}$$

The bordered Hessian for each case will have the subscript representing the candidate with respect to P_{G1}, P_{G2}.

$$\nabla^2_{(60,60)} = \begin{bmatrix} 0 & 1 & 1 \\ 1 & 0.0883 & 0 \\ 1 & 0 & 0.0883 \end{bmatrix} \tag{3.33}$$

$$det(\nabla^2_{(60,60)}) = -0.1766 \tag{3.34}$$

$$\nabla^2_{(86.6790,33.321)} = \begin{bmatrix} 0 & 1 & 1 \\ 1 & -0.1765 & 0 \\ 1 & 0 & -0.1766 \end{bmatrix} \tag{3.35}$$

$$det(\nabla^2_{(86.6790,33.321)}) = 0.3532 \tag{3.36}$$

$$\nabla^2_{(33.321,86.6790)} = \begin{bmatrix} 0 & 1 & 1 \\ 1 & -0.1766 & 0 \\ 1 & 0 & -0.1765 \end{bmatrix} \tag{3.37}$$

$$det(\nabla^2_{(33.321,86.6790)}) = 0.3532 \tag{3.38}$$

As shown above, the equal split proves to be the optimum. This displays that the assumption of the minimum operation constraint and all loading conditions do not produce the unequal split as the optimum case. However, the possibility of the unequal split being optimum is displayed later in the Gurobi simulation. Therefore, this economic split was best considered as a baseline.

3.3 Test Case and Simulation Results

Although each of these optimization problems individually show that an unequal split is optimal, this is not a realistic test case for the shipboard microgrid load allocation. There must be limits placed on the units and although there are typically twins of units onboard to ensure redundancy, it may not only be two diesel or gas turbines. Therefore, an optimization problem was developed to add limits to the generation with two diesel generators and two gas turbines. This was formulated using the following fuel efficiency equations for two diesel generators and two gas turbines.

$$F_{D1} = 2.314 * 10^{-6} P^4_{D1} - 3.295 * 10^{-4} P^3_{D1} + 2.537 P^2_{D1} + 2.537 P_{D1} + 19.21 \tag{3.39}$$

$$F_{D2} = 2.314 * 10^{-6} P_{D2}^4 - 3.295 * 10^{-4} P_{D2}^3 + 2.537 P_{D2}^2 + 2.537 P_{D2} + 19.21 \quad (3.40)$$

$$F_{G1} = -3.101 * 10^{-5} P_{G1}^4 + 7.442 * 10^{-3} P_{G1}^3 - 0.6256 P_{G1}^2 + 45.61 P_{G1} + 189.6 \quad (3.41)$$

$$F_{G2} = -3.101 * 10^{-5} P_{G2}^4 + 7.442 * 10^{-3} P_{G2}^3 - 0.6256 P_{G2}^2 + 45.61 P_{G2} + 189.6 \quad (3.42)$$

where F_{D1} and F_{D2} represent the fuel efficiency equations for the diesel generators with the respective power outputs P_{D1} and P_{D2}. The fuel efficiency for the gas turbines were represented by F_{G1} and F_{G2} with the respective power outputs P_{G1} and P_{G2}. The optimization problem was then formulated as:

$$\begin{aligned}
\min \quad & c_1 F_{D1} + c_2 F_{D2} + c_3 F_{G1} + c_4 F_{G2} && (3.43a)\\
\text{s.t.} \quad & P_{D1} + P_{D2} + P_{G1} + P_{G2} = P_D && (3.43b)\\
& 15 \leq P_{D1} \leq 100 && (3.43c)\\
& 15 \leq P_{D2} \leq 100 && (3.43d)\\
& 15 \leq P_{G1} \leq 100 && (3.43e)\\
& 15 \leq P_{G2} \leq 100 && (3.43f)
\end{aligned}$$

where c_1, c_2, c_3, and c_4 are constants that can be adjusted to differentiate the fuel cost of the units. For the purposes simplicity and direct comparison, all the constants were set to be equal to 1. Finally, the optimization problem was solved using various load demands, as shown in Table 3.1 and plotted in Figure 3.3. For comparison purposes, the the fuel usage for an equal loading condition across the units are shown in Table 3.2.

Table 3.1: Simulation results of the fuel efficiency load distribution for two diesel generators and two gas turbines. The total load, load applied to the two diesel generators, P_{D1} and P_{D2}, and two gas turbines, P_{G1} and P_{G2}, and the total fuel used.

Total Load (MW)	P_{D1} (MW)	P_{D2} (MW)	P_{G1} (MW)	$P_{G2}(MW)$	Total Fuel (gal)
60	15	15	15	15	1623.82
80	35	15	15	15	1660.91
100	55	15	15	15	1681.48
120	75	15	15	15	1689.7
140	95	15	15	15	1698.63
160	100	30	15	15	1732.69
180	78	72	15	15	1755.57
200	85	85	15	15	1762
220	95	95	15	15	1773.45
240	100	100	25	15	2069.37
260	100	100	45	15	2552.56
280	100	100	65	15	3027.66
300	100	100	85	15	3524.42
320	100	100	100	20	4011.55
340	100	100	100	40	4515.36
360	100	100	100	60	4985.04
380	100	100	100	80	5480.11
400	100	100	100	100	5941.02

Table 3.2: Fuel usage of two diesel generators and two gas turbines with equal loading conditions for comparison to unequal split loading. The total load, load applied to the two diesel generators, P_{D1} and P_{D2}, and two gas turbines, P_{G1} and P_{G2}, and the total fuel used.

Total Load (MW)	P_{D1} (MW)	P_{D2} (MW)	P_{G1} (MW)	$P_{G2}(MW)$	Total Fuel (gal)
60	15	15	15	15	1623.82
80	20	20	20	20	1944.45
100	25	25	25	25	2237.83
120	30	30	30	30	2510.77
140	35	35	35	35	2769.19
160	40	40	40	40	3018.17
180	45	45	45	45	3261.92
200	50	50	50	50	3503.80
220	55	55	55	55	3746.28
240	60	60	60	60	3991.01
260	65	65	65	65	4238.75
280	70	70	70	70	4489.41
300	75	75	75	75	4742.04
320	80	80	80	80	4994.81
340	85	85	85	85	5245.06
360	90	90	90	90	5489.26
380	95	95	95	95	5723.00
400	100	100	100	100	5941.02

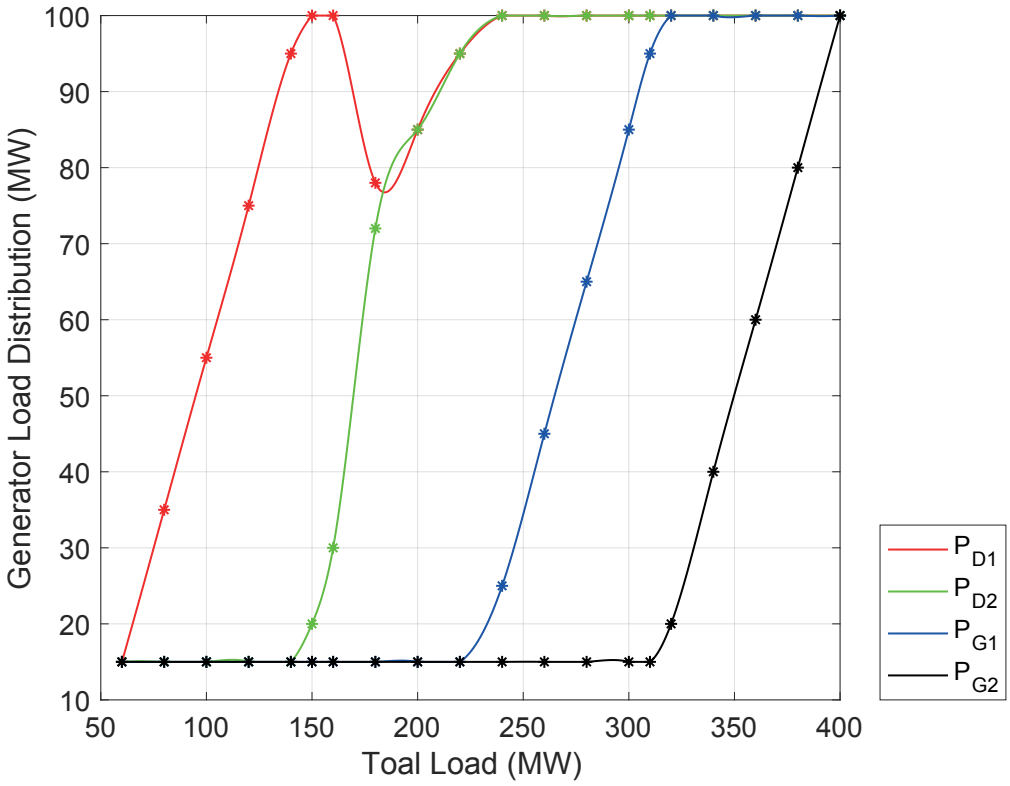

Figure 3.3: The optimization results are displayed for the total load on the shipboard microgrid with the load distribution across the generating units, the two diesel generators, P_{D1} and P_{D2}, and the gas turbines, P_{G1} and P_{G2}, where the y-axis represents the power applied to each unit.

3.4 Time Horizon Optimization

The fuel efficiency optimization was shown above for a single time step, which displayed the fuel saving benefit for the unequal load split between the units. However, the benefit of saving fuel over the course of a single time step may not outweigh the cons, such as the unequal maintenance schedules this causes. Additionally, a single time step does not provide any reserve for changes that may occur within the load. For example, a sample load profile is shown in Figure 3.4 which displays a sample time horizon load profile with a reserve available occur. This sample load profile shows the predicted load as the solid black line with the available power accommodation as the red dotted line. A time horizon formulation will develop a baseline economic function over the predicted load profile for the ship where the benefit of considering the fuel efficiency formulation becomes more evident. Therefore, the single time step formulation was expanded to consider the time horizon problem of the predicted load profile.

As mentioned, the load profile of a ship can be predicted based on similar trips and typical loads. Therefore, a time horizon problem was solved by considering the fuel savings of the generators and batteries onboard the ship. The predicted load profile was distributed across the two diesel generators, two gas turbines, and batteries on board. The batteries provided further efficiency and alleviated the loading required on the generators. The objective function was adjusted to minimize the cost per MW, rather than the fuel, due to the batteries included. The fuel that is universal for both diesel generators and gas turbines is the distillate fuel F76, which the standard fuel price is $4.15 per gallon [55]. Therefore, multiplying the standard fuel price by the fuel efficiency equations gives dollars per MW, which can be compared with the cost of using the battery. Using the fuel efficiency curves, the cost functions for the diesel generator and gas turbine are shown respectively.

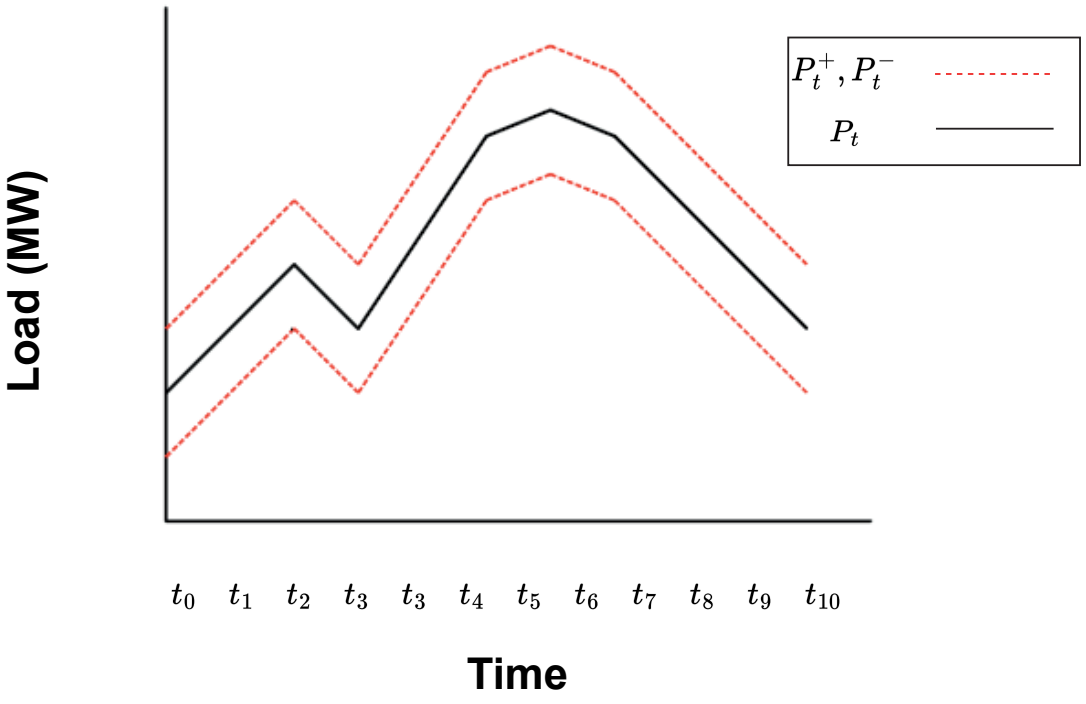

Figure 3.4: Sample load profile with the predicted load profile, P_t, the load change accommodation, P_t^+, P_t^- shown to develop the economic baseline load distribution.

$$\begin{aligned} C_{G1}(P_{G1}) =& 9.603 * 10^{-6} P_{G1}^4 - 1.367 * 10^{-3} P_{G1}^3 \\ &+ 1.656 * 10^{-2} P_{G1}^2 + 10.529 P_{G1} + 79.722 \end{aligned} \tag{3.44}$$

$$\begin{aligned} C_{D1}(P_{D1}) =& - 1.287 * 10^{-4} P_{D1}^4 + 3.09 * 10^{-2} P_{D1}^3 \\ &- 2.596 P_{D1}^2 + 189.282 P_{D1} + 786.84 \end{aligned} \tag{3.45}$$

For the cost of the battery, the formulation developed in Chapter 2 was used, which considered the cycle life of a Li-ion battery. The cycle life was optimal when the battery discharged to a 20% depth of discharge (DOD), which had the highest cycle life, and encourages the battery to discharge to this DOD and discourages the battery from discharging further using a piece-wise linear cost function as listed in Equation 2.39, which is rewritten below.

$$C_{Bj}(P_{Bj}) = \begin{cases} -0.57 P_{Bj} + 7.81, & \text{if } P_{Bj} \leq 4MW \\ 0.7 P_{Bj} + 2.73, & \text{if } P_{Bj} > 4MW \end{cases}$$

where C_{Bj} is the cost and P_{Bj} is the power output of battery Bj and where j is the index for the number of batteries onboard. In this case, 20 MW batteries were considered, therefore, the ideal 20% DOD was 4 MW, and two pieces were used. Next, the formulation for the time horizon used the new cost objective and added constraints for the batteries' charge, discharge, and state of charge (SOC). Therefore, the time horizon objective was set for the cost of both traditional generators and batteries.

The time horizon problem considered a predicted load applied to the shipboard microgrid and minimize the cost of handling the load across the diesel generators, gas

turbines, and batteries. To further increase the resiliency, a percentage above the predicted load was included to account for a margin of error in the prediction. This margin only considered the generators available power rather than the batteries. The batteries may be used elsewhere in real-time due to their quick response time. If the batteries were to be included in the reserve, the SOC would be required to stay at the specified level to ensure the allocated reserve was available. However, this may not be the best use of the resource during the real-time adjustment. The time horizon optimization was developed as follows:

$$\min \quad \sum_{t=1}^{T}\left[\sum_{n=1}^{N} C_{Dn,t}(P_{Dn,t}) + \sum_{m=1}^{M} C_{Gm,t}(P_{Gm,t}) + \sum_{j=1}^{J} \Delta t * C_{Bj,t}(P_{Bj,t})\right] \tag{3.46a}$$

$$\text{s.t.} \quad \sum_{n=1}^{N} P_{Dn,t} + \sum_{m=1}^{M} P_{Gm,t} + \sum_{j=1}^{J} P^{d}_{Bj,t} = P_{D,t} + \sum_{j=1}^{J} P^{c}_{Bj,t} \tag{3.46b}$$

$$P_{Dn,t} - P_{Dn,t-1} \leq RU_{Dn} \tag{3.46c}$$

$$P_{Gm,t} - P_{Gm,t-1} \leq RU_{Gm} \tag{3.46d}$$

$$P_{Dn,t} - P_{Dn,t-1} \leq RD_{Dn} \tag{3.46e}$$

$$P_{Gm,t} - P_{Gm,t-1} \leq RD_{Gm} \tag{3.46f}$$

$$\delta P_{D,t} \leq P_{t}^{\text{available}} \tag{3.46g}$$

$$\text{SOC}_{Bj,t} = P^{cap}_{Bj} * \text{SOC}_{Bj,t-1} + P^{c}_{Bj,t}\eta_c - P^{d}_{Bj,t}/\eta_d \tag{3.46h}$$

$$\text{SOC}_{\min} \leq \text{SOC}_{Bj,t} \leq \text{SOC}_{\max} \tag{3.46i}$$

$$P^{d}_{Bj,t} * P^{c}_{Bj,t} = 0 \tag{3.46j}$$

$$P^{c}_{\min} \leq P^{c}_{Bj,t} \leq P^{c}_{\max} \tag{3.46k}$$

$$P^{d}_{\min} \leq P^{d}_{Bj,t} \leq P^{d}_{\max} \tag{3.46l}$$

$$P_{Dn,min} \leq P_{Dn} \leq P_{Dn,max} \tag{3.46m}$$

$$P_{Gm,min} \leq P_{Gm} \leq P_{Gm,max} \tag{3.46n}$$

where minimizing the total fuel across the units over the time horizon was the objective. The constraints were reestablished to meet the load demand at each time step, $P_{D,t}$. Next the ramp up, RU_i and ramp down RD_i for each unit must be followed, which using the counter i in P_i and $P_{i,t-1}$ including P_{D1}, P_{D2}, P_{G1}, and P_{G2}. The most important part of this function is that the load demand must have an accommodation for any changes in load.

This is accomplished by setting a percentage, δ that the available power capacity of the online units must be able to handle over the predicted load $P_{D,t}$.

The optimization minimized the objective, which was the total cost of using the diesel generators, gas turbines, and batteries across the time horizon. In other words, the total cost of supplying the predicted load across the period was minimized. The total of the generators output and batteries' discharging power must be equal the load demand and the batteries' charging power, as shown in constraint 3.47b. Generators have a ramp up and ramp down requirement, which stipulates how much the load applied can be increased or decreased from the previous time-step. Constraints 3.47c and 3.47d ensure that the ramp up requirement was met and 3.47e and 3.57f set the ramp down requirement for the diesel generators and gas turbines respectively. The next constraint added a power reserve based on the available remaining generation power, $P_t^{available}$, using a δ percentage above and below the predicted load. In 3.47h, the SOC was calculated based on the previous time step's SOC, charging, and discharging power, and ensured the SOC is within the minimum and maximum SOC limits, as shown in 3.47i. The battery was not allowed to charge and discharge at the time, as shown in constraint 3.47j. Finally, the power limits for the batteries' charging and discharging power were set in 3.47k and 3.47l and the generators' limits were set in 3.47m and 3.47n.

3.5 Simulation Results

As mentioned, the load profile of a ship can be predicted based on similar trips and typical loads. Therefore, a time horizon problem was solved by considering the fuel savings of the generators and the cycling life of the batteries onboard the ship. The predicted load profile was distributed across the two diesel generators, two gas turbines, and batteries on

board. The batteries provided further efficiency and alleviated the loading required on the generators.

To test the formulation, predicted load profiles were developed and used with two diesel generators, two gas turbines, and two batteries. The values chosen for the preset values listed in the nomenclature section are shown in Table 3.5. Using these values and optimization, four simulations were performed to test the control system. The load profile of a ship can multiple profiles including a parabola, trapezoid, or various peaks throughout [56, 57]. Therefore, a total of four load profiles were run to represent multiple possibilities and show the resiliency of the simulation.

The first simulation was a short load profile with a simple increase and decrease to prove the economic component of the battery. Typically, batteries are not considered as a main contributor to the power system. Instead, they are primarily used for reserve, peak shaving, or quick response instances. However, with the cycle life formulation developed in Chapter 2, the batteries can be used without unnecessary aging and provide a more economic result. Next, the 24-hour load profiles are considered with two diesel generators, two gas turbines, and two batteries. Three differing load profiles were used where the first load profile peaks at approximately the middle of the time horizon, the second peaks early in the time horizon, and the final load profile has two peaks.

3.5.1 Battery Price Reduction with Short Load Profile

This formulation uses both generators and batteries as main power sources within the shipboard microgrid. This is unique to this formulation as batteries are typically used as supplementary sources and often do not include an economic consideration. However, the economic battery formulation given in Chapter 2 provided a method to implement batteries

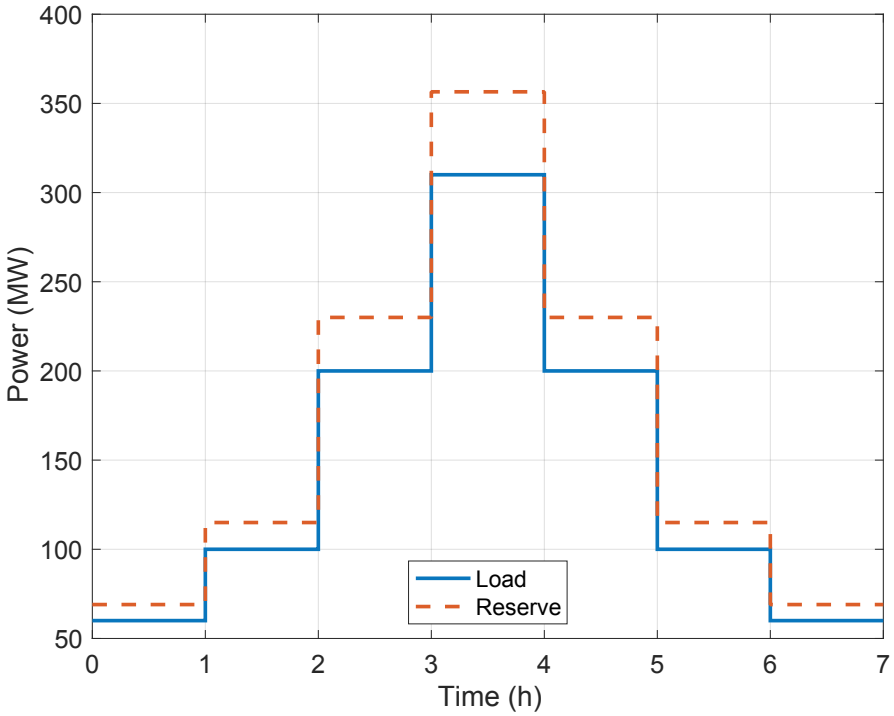

Figure 3.5: Load profile with 7 time steps to test cost difference between using only traditional generators and implementing a battery.

as a main component in the power system. To prove that this is economically beneficial, a profile with 7-time steps was used to calculate the total cost with and without a battery implemented.

The load profile shown in Figure 3.5 was developed to provide a baseline load to compare between the system with and without a battery. To perform the simulation, the values shown in Table 3.5 were used. First, the simulation was performed using two diesel generators and two gas turbines. The load distribution across the generators are shown in Figure 3.6 and the cost breakdown is shown in Table 3.3.

Next, the simulation was run with a battery implemented. To further prove the benefit of the battery implementation, it was assumed that the battery started discharged to the

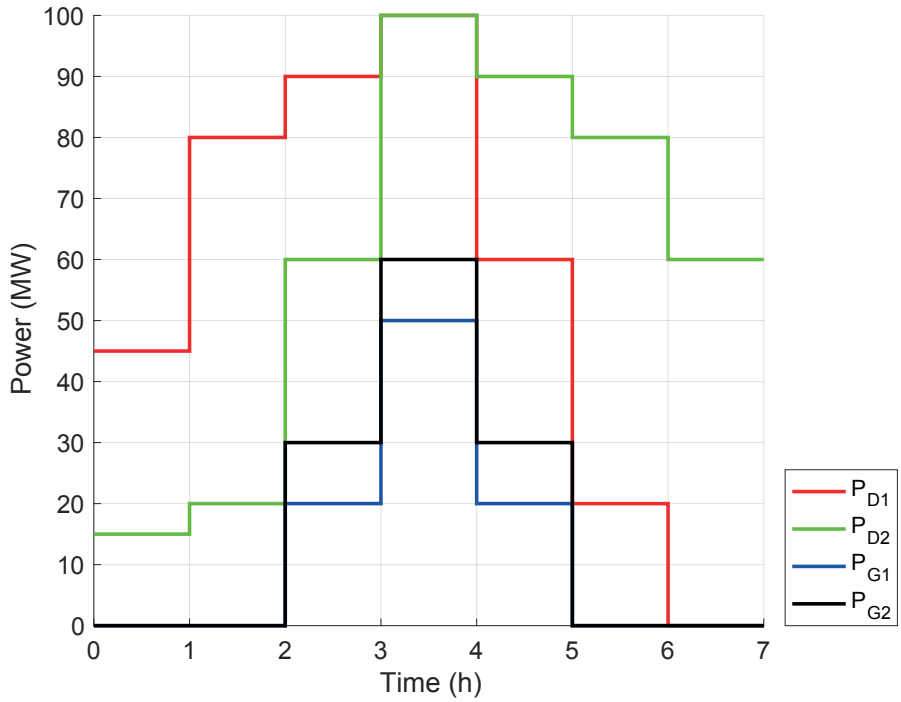

Figure 3.6: Generator distribution for load profile shown in Figure 3.5 without a battery implemented.

Table 3.3: Cost breakdown of load profile shown in Figure 3.5 without a battery implemented.

t	C_{D1} (\$)	C_{D2} (\$)	C_{G1} (\$)	C_{G2} (\$)	Startup (\$)
1	434	229	786	786	0
2	509	274	786	786	0
3	526	480	3761*	4858*	4000
4	559	559	6829	7800	0
5	480	526	3761	4858	0
6	274	509	786	786	0
7	79	480	786	786	0
Total Cost: \$48089.71					

minimum SOC of 20%. The distribution across the generators and battery are shown in Figures 3.7a and 3.7b respectively. The cost breakdown is shown in Table 3.4.

The total cost without the battery comes out to be $48,089.71 and the total cost with the battery is $45,545.52, which results in a cost savings of $2,544.19. This is with the battery requiring to be charged at the beginning of the time horizon. Therefore, over a longer period and with an initial full charge, the cost savings would be significant. The implementation of the battery not only provides a cost savings by using the economic function, but the formulation also helps prevents the premature replacement of the battery. This proves that the implementation of the battery provides an economic benefit in addition to the other benefits of using a battery.

3.5.2 Load Profile 1 - Center Load Peak

The first load profile, shown in Figure 3.8 follows an off-center parabolic shape with small peaks throughout. The peak toward the center of the time horizon is similar to the typical voyage pattern shown in [56]. However, the peaks were added, in comparison to the smooth curve, to challenge the system to meet the ramp up and ramp down requirements while leveraging the battery charging and discharging. This will challenge the economic benefits of when to turn on additional generators. For example, the peaks shown in the first 7-time steps are relatively small and may only require two generators. However, by time step 11, the load requires three generators without a reserve allocation. Therefore, the generators must be managed appropriately to ensure that the four generators are turned on by this time step.

The plot of the four generators' outputs are shown in Figure 3.9 and the two batteries' outputs are shown in Figure 3.10.

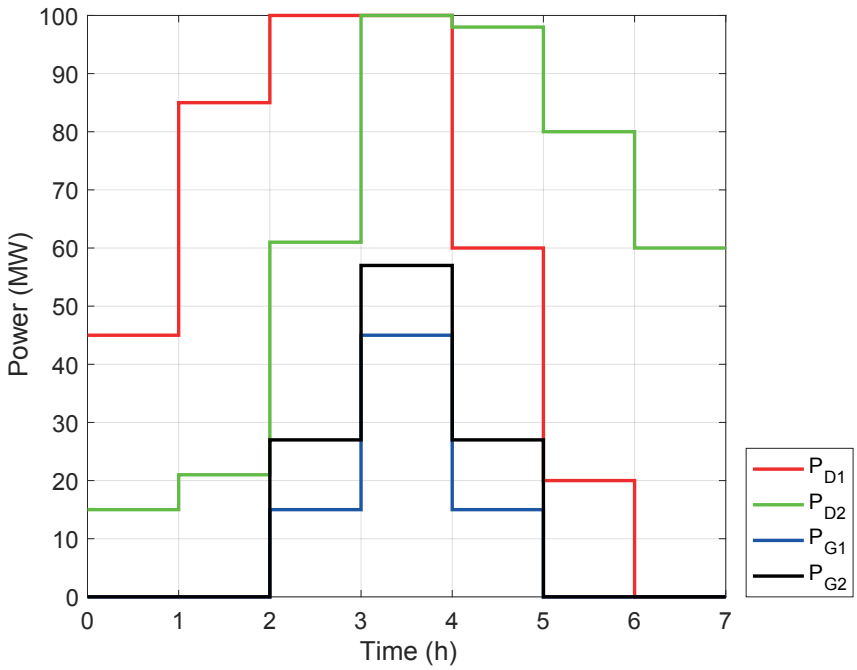

(a) Generator distribution for load profile shown in Figure 3.5 with a battery implemented.

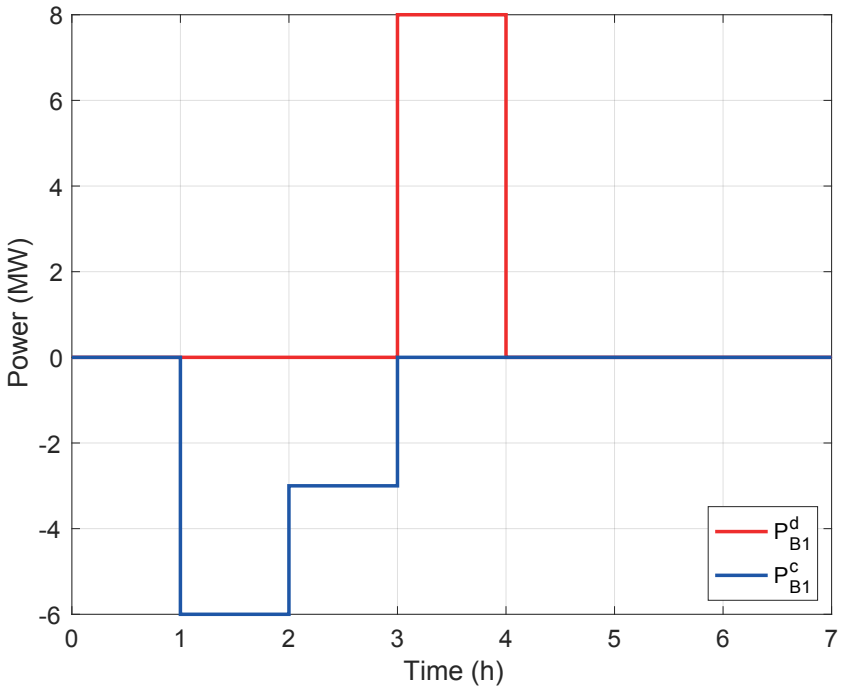

(b) Battery charge and discharge power for load profile shown in Figure 3.5.

Figure 3.7: Load distribution across diesel generators, gas turbines, and battery for load profile shown in Figure 3.5.

Table 3.4: Cost breakdown of load shown in Figure 3.5 with a battery implemented.

t	C_{D1} (\$)	C_{D2} (\$)	C_{G1} (\$)	C_{G2} (\$)	Startup (\$)	C_{B1} (\$)
1	434	229	786	786	0	0
2	516	284	786	786	0	0
3	559	483	3139*	4544*	4000	0
4	559	559	6343	7501	0	8.33
5	480	551	3139	4544	0	0
6	274	509	786	786	0	0
7	79	480	786	786	0	0
Total Cost: \$45545.52						

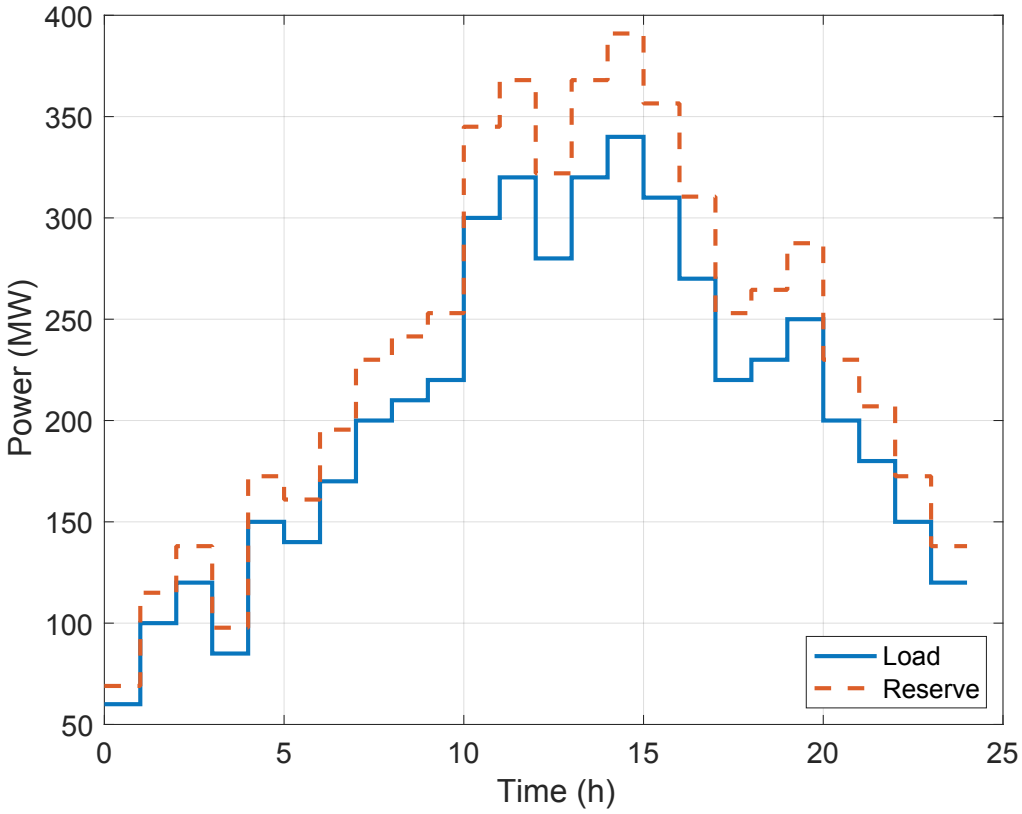

Figure 3.8: A sample predicted 24 hour load profile with the reserve requirement.

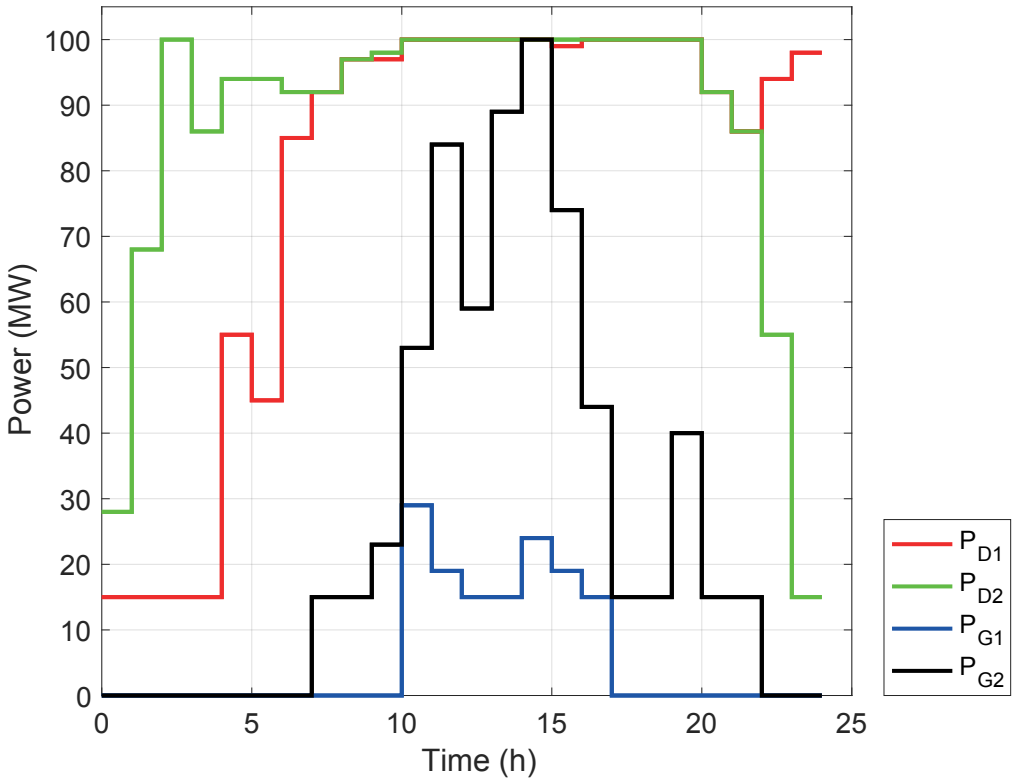

Figure 3.9: Load distribution across the two diesel generators and two gas turbines for the load profile shown in Figure 3.8.

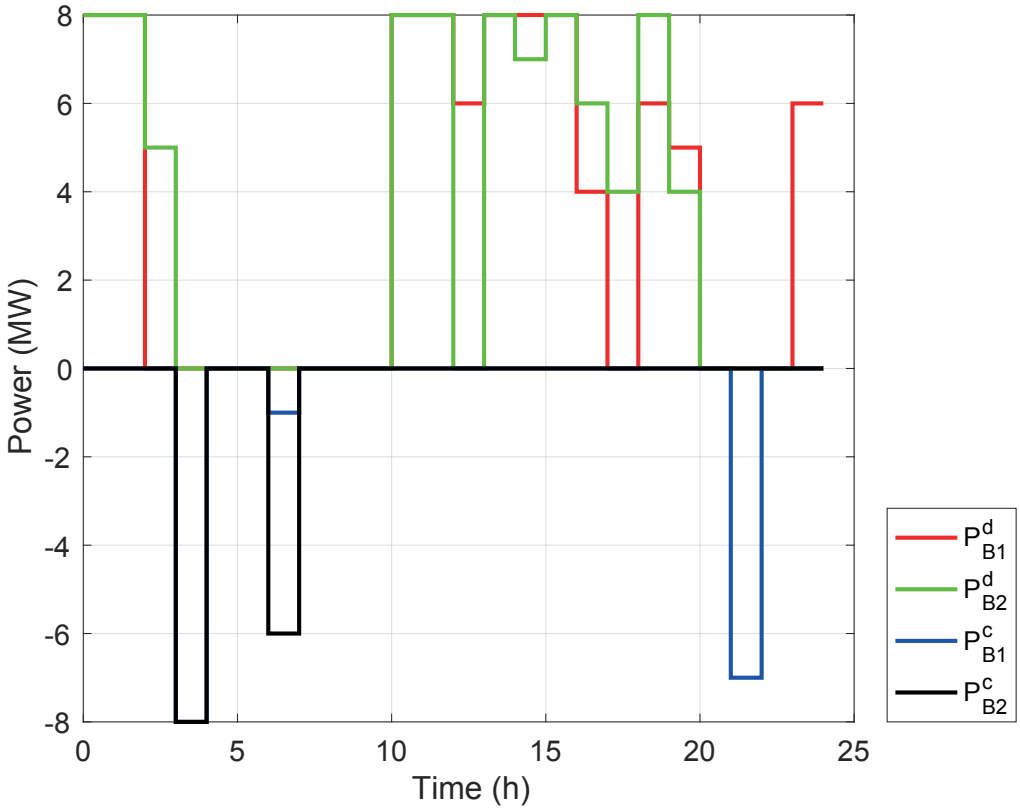

Figure 3.10: Charging and Discharging power of the two batteries across the load profile shown in Figure 3.8.

Table 3.5: Preset values for the time horizon optimization of the control of shipboard microgrid resources.

Variable	Value	Variable	Value
$P_{Dn,min}$	15 MW	$\text{SOC}_{Bj,min}$	20%
$P_{Dn,max}$	100 MW	$\text{SOC}_{Bj,max}$	90%
$P_{Gm,min}$	15 MW	$P^{c}_{Bj,min}$	0 MW
$P_{Gm,max}$	100 MW	$P^{c}_{Bj,max}$	8 MW
δ	15%	$P^{d}_{Bj,min}$	0 MW
$P_{D,t}$	See Fig. 3.8	$P^{c}_{Bj,max}$	8 MW
η_c	95%	η_d	90%

As noted, the main objective of this function is to minimize the cost throughout the time horizon while meeting the load demand. Therefore, the cost breakdown of each unit, the total cost per time step, and the reserve allowance is shown in Table 3.6.

This simulation was able to meet the load demand while minimizing the cost. As expected, the diesel generators were used first since they are more fuel efficient. Each generator has a base cost even when not in use, which is $79.00 for the diesel generators and $786.84 for the gas turbines. Each unit was assigned a $2,000 startup cost and was marked in the table with an asterisk. This amount was included in the total for the time step. The reserve typically outperformed the required 15% reserve allocation, which further increased the resiliency of the system. The cost of the battery relates to the discharging cost of the cycle life lost for the discharge. The charging cost was included in the load distribution across the four generators. This system performed economically and allocated the load in an efficient manner.

3.5.3 Load Profile 2 - Early Load Peak

The previous load profile considered as steady increase and decrease of the load throughout the 24-time step period. For the second load profile, shown in Figure 3.11, the peak

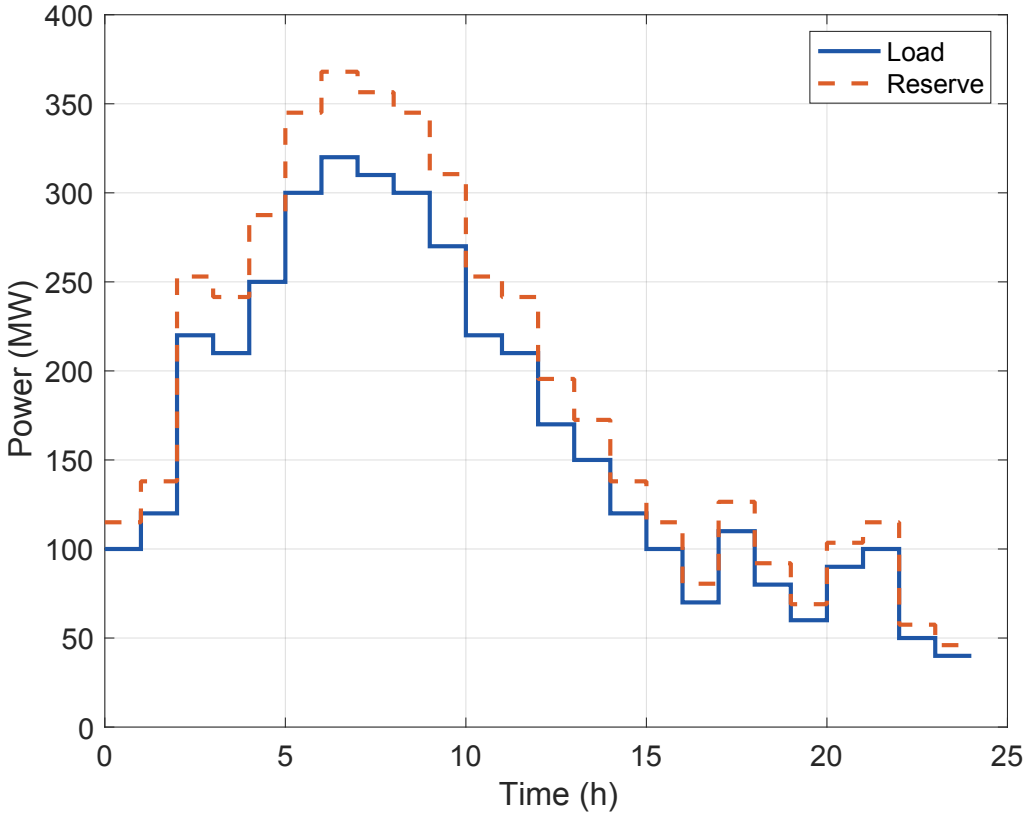

Figure 3.11: The second sample predicted 24 hour load profile with the reserve requirement. This profile peaks early in the time horizon.

load occurred early in the profile with a relatively low load throughout the remainder of the period. This again further stresses the ramp up and ramp down requirements of the generators.

The allocation of the four generators was shown in Figure 3.12 and the batteries' charging and discharging power was shown in Figure 3.13.

The cost breakdown for each unit at each time step with the reserve allocation listed is shown in Table 3.7.

In this simulation, two generators were set to be on for the first time step. By time step 3, three generators were turned on to accommodate the load and the reserve requirement. At

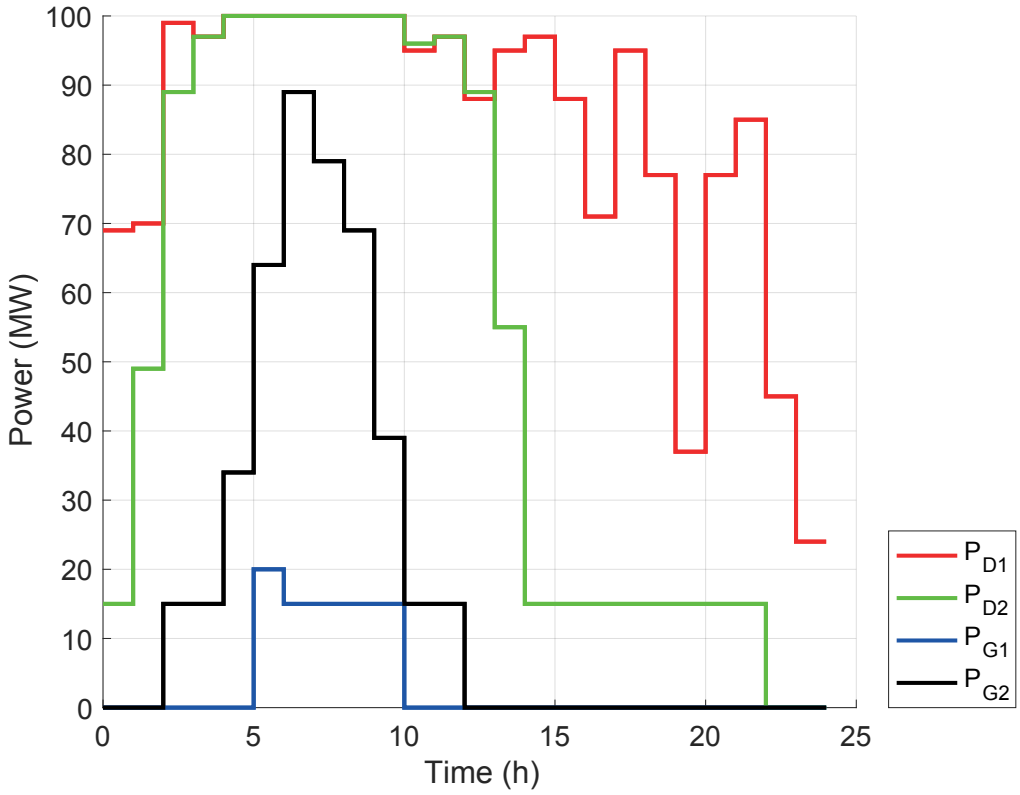

Figure 3.12: Load distribution across two diesel generators and two gas turbines for the predicted load profile shown in Figure 3.11.

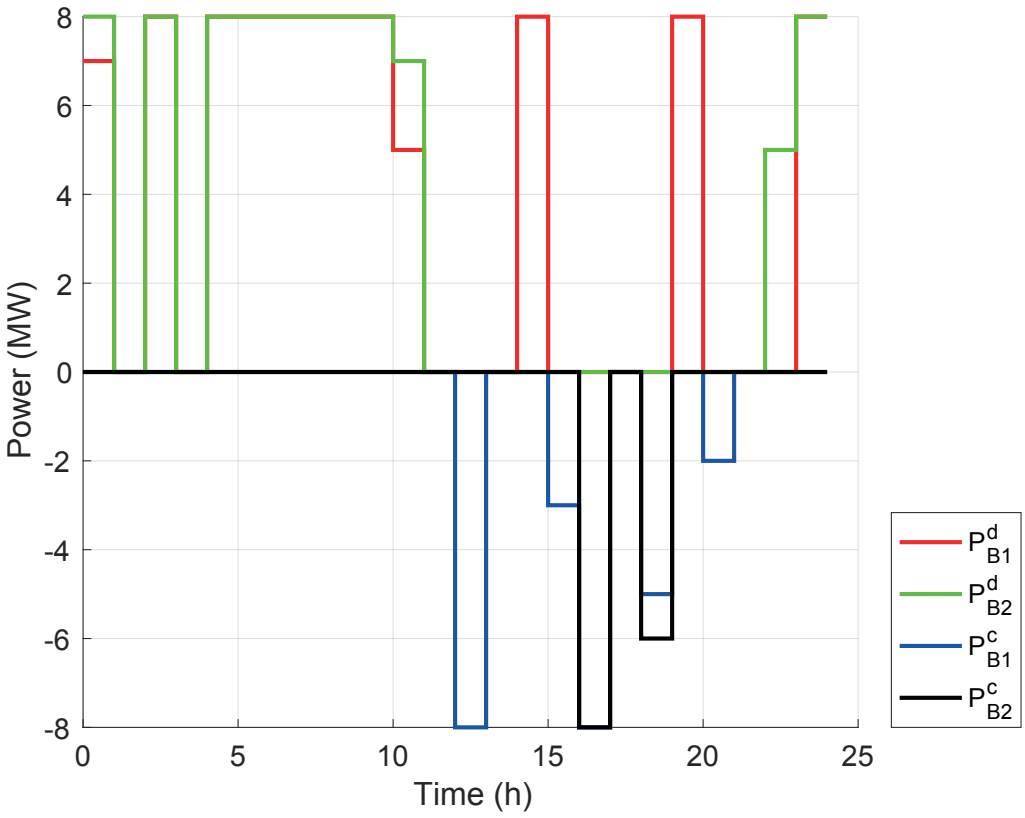

Figure 3.13: Charging and discharging power of the two batteries for the predicted load profile shown in Figure 3.11.

least three generators were on until the time step 12, at which point two generators were on until the final two time steps when only one diesel generators is on. This simulation showed the possibilities from one to four generators being turned on throughout the time horizon. Additionally, the battery was used heavily during the load peak then was recharged to be used again toward the end of the period. This simulation further exemplified the efficiency of the simulation to allocate the number of units on based on the load applied.

3.5.4 Load Profile 3 - Two Load Peaks

For the final predicted load profile, two peaks were used to represent the load profiles shown in [57]. Some speed profiles shown have various peaks throughout the cycle, which lead to the load profile shown in Figure 3.14, which has two peaks throughout the time horizon. This will again further test the system's efficiency and ensuring enough generators are on to accommodate the reserve requirement. Additionally, it was noted that the batteries were used at the peak load times previously. Since there are now two peaks, the charging of the batteries must be strategic to ensure they can be used during each.

The distribution of load across to generators is shown in Figure 3.12 and the charging and discharging power of the batteries is shown in Figure 3.13.

The cost breakdown at each time step with the load reserve at each time is shown in Table 3.8.

The reserve allocation for each time step across the three load profiles are shown in Table 3.9.

This simulation best represents the adaptability of the distribution across the two peaks. As shown in the cost breakdown in Table 3.8, there are multiple occurrences of shutdowns, which later incurs startup costs. However, the optimization determined that this was more

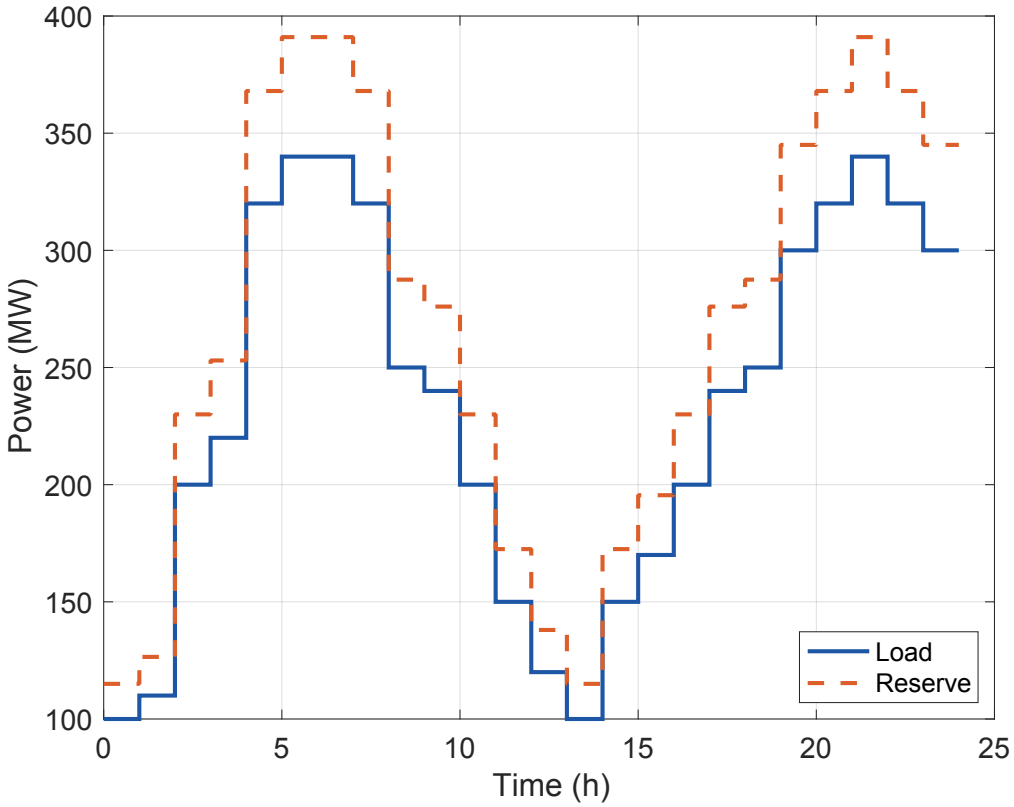

Figure 3.14: The third sample predicted 24 hour load profile with the reserve requirement. This profile has two peaks within the time horizon.

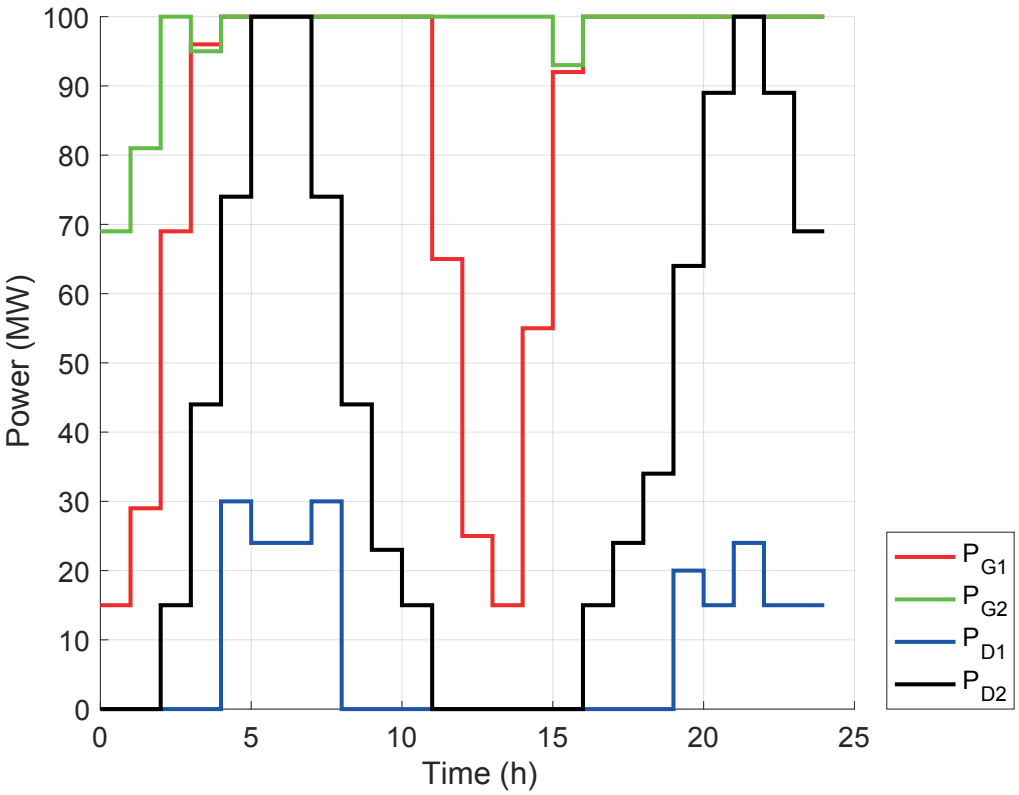

Figure 3.15: Load distribution across two diesel generators and two gas turbines for the predicted load profile shown in Figure 3.14.

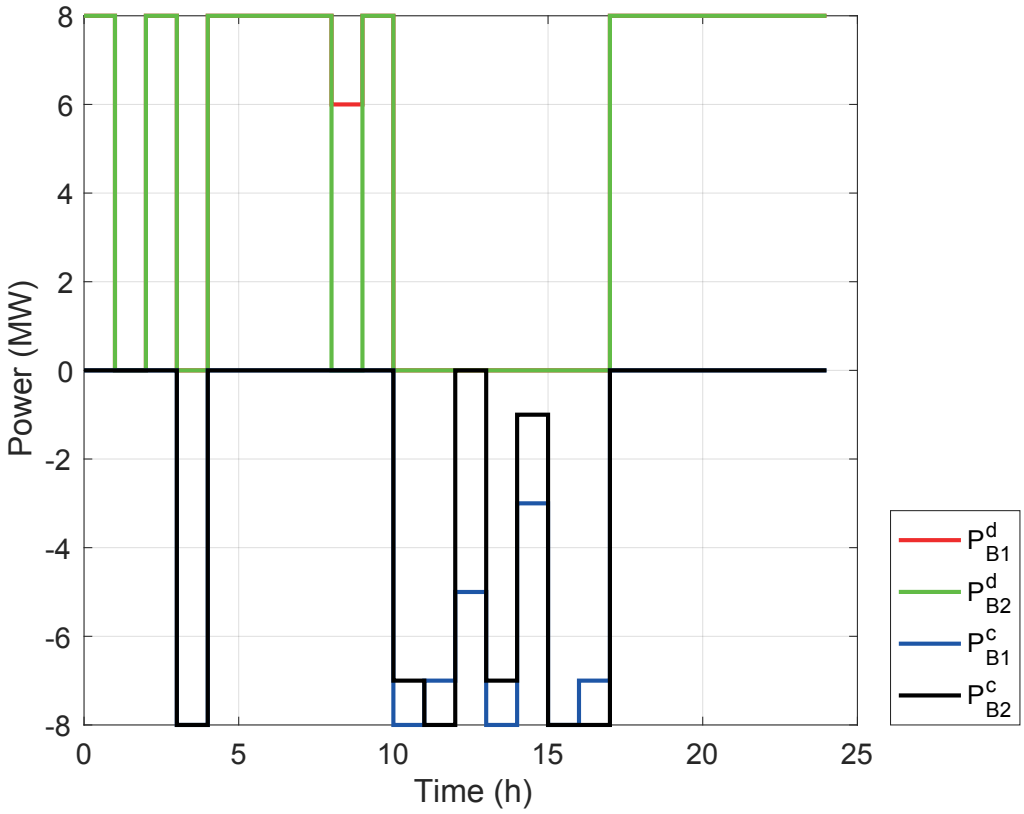

Figure 3.16: Charging and discharging power of the two batteries for the predicted load profile shown in Figure 3.14.

economic rather than having them remain on and have the minimum of 15 MW applied. The percentage reserve requirement ensures that these shutdowns will still have flexibility for load changes. Additionally, the batteries were recharged when the load decreased to anticipate the second peak in the latter part of the time horizon. Therefore, this simulation showed the ability to allocate the batteries for use during peak times and weighing incurring the startup costs versus leaving the generators on.

3.6 Summary of Contributions

This optimization problem developed a time horizon problem to minimize the cost across two generators, two gas turbines, and two batteries. In addition to the cost the generators' minimum and maximum loading, ramp up, and ramp down requirements were considered. The minimum loading was only applied if the generators were turned on; however, if the generators were turned off and a turned on later, a startup cost was applied. Therefore, the optimization had to weigh the cost of applying the minimum load to possibly incurring startup cost later. Additionally, the batteries had a cost applied to them in a unique matter by considering the cycling life costs. In addition to the costs, the batteries had to meet the maximum charging and discharging power requirements and the SOC requirements. The SOC was calculated using the charging and discharging efficiency to ensure that the SOC was not over or underestimated.

The performance of the control system was validated in the form of four load profiles. First a short load profile was used to prove that the cost of implementing a battery was more economic than only using generators to meet the same load demand. Next, to prove that the control was able to efficiently allocate the resources, three 24 hours load profiles were developed based on typical ship speed load profiles. These results proved that the

battery was charged and discharged in a timely manner and the generators were turned on and off in the most economic manner. Furthermore, the distribution was made to be more resilient based on the load reserve percentage applied. This chapter developed an optimization problem, which was able to develop an efficient and resilient control system for the load allocation for a predicted load profile while considering the economic costs incurred resulting in the distribution.

Table 3.6: Cost of each diesel generator, gas turbine, and battery, the total cost, and the reserve power allocation at each time step for 24 Load Profile shown in Figure 3.8.

t	C_{G1} (\$)	C_{G2} (\$)	C_{G1} (\$)	C_{G2} (\$)	C_{B1} (\$)	C_{B2} (\$)	C_{total} (\$)
1	229.78	344.55	786.84	786.84	8.33	8.33	2164.67
2	229.78	495.82	786.84	786.84	8.33	8.33	2315.94
3	229.78	559.88	786.84	786.84	0.00	6.23	2369.57
4	229.78	518.26	786.84	786.84	0.00	0.00	2321.72
5	469.06	540.29	786.84	786.84	0.00	0.00	2583.03
6	437.25	538.33	786.84	786.84	0.00	0.00	2549.26
7	517.56	533.18	786.84	786.84	0.00	0.00	2624.42
8	533.18	533.07	786.84	3139.40*	0.00	0.00	6992.50
9	550.69	547.87	786.84	3139.40	0.00	0.00	5024.80
10	550.69	551.82	786.84	4218.28	0.00	0.00	6107.63
11	559.88	559.88	4861.10*	7206.30	8.33	8.33	15203.81
12	559.88	559.88	3761.20	10265.42	8.33	8.33	15163.02
13	559.88	559.88	3140.00	7700.53	6.93	0.00	11967.22
14	559.88	559.88	3140.00	10766.04	8.33	8.33	15042.46
15	559.88	559.88	4219.76	11767.69	8.33	8.33	17123.86
16	559.88	559.88	3641.57	9336.52	8.33	8.33	14114.50
17	559.88	559.88	3140.00	6333.74	5.53	6.93	10605.95
18	559.88	559.88	786.84	3139.40	0.00	6.23	5052.23
19	559.88	559.88	786.84	3139.40	7.63	8.33	5061.96
20	559.88	559.88	786.84	5851.25	6.93	5.53	7770.30
21	533.18	532.28	786.84	3139.40	0.00	0.00	4977.49
22	518.97	519.34	786.84	3139.40	0.00	0.00	4964.55
23	540.29	469.06	786.84	786.84	0.00	0.00	2583.03
24	551.91	229.78	786.84	786.84	7.52	0.00	2362.90

* indicates a \$2,000 startup cost was applied

Table 3.7: Cost of each diesel generator, gas turbine, and battery, the total cost, and the reserve power allocation at each time step for 24 hour load profile 2.

t	C_{G1} (\$)	C_{G2} (\$)	C_{G1} (\$)	C_{G2} (\$)	C_{B1} (\$)	C_{B2} (\$)	C_{total} (\$)
1	495	229	786	786	8	8	2312
2	497	452	786	786	0	0	2521
3	557	525	786	3139	8	8	7023
4	548	549	786	3139	0	0	5022
5	559	559	786	5263	8	8	7183
6	559	559	3761	8203	8	8	15098
7	559	559	3140	10766	8	8	15040
8	559	559	3140	9751	8	8	14025
9	559	559	3140	8715	8	8	12989
10	559	559	3140	5754	8	8	10028
11	542	545	786	3139	6	7	5025
12	549	548	786	3139	0	0	5022
13	523	525	786	786	0	0	2620
14	540	469	786	786	0	0	2581
15	547	469	786	786	8	0	2596
16	523	229	786	786	0	0	2324
17	498	229	786	786	0	0	2299
18	540	229	786	786	0	0	2341
19	505	229	786	786	0	0	2306
20	395	229	786	786	8	0	2204
21	505	229	786	786	0	0	2306
22	516	229	786	786	0	0	2317
23	434	79	786	786	0	6	2091
24	307	79	786	786	8	8	1974

Table 3.8: Cost of each diesel generator, gas turbine, and battery, the total cost, and the reserve power allocation at each time step for the 24 hour load profile 3 shown in Figure 3.14.

t	C_{G1} (\$)	C_{G2} (\$)	C_{G1} (\$)	C_{G2} (\$)	C_{B1} (\$)	C_{B2} (\$)	C_{total} (\$)
1	229	495	786	786	8.33	8.33	2312
2	344	510	786	786	0	0	2426
3	495	559	786	3139*	8.33	8.33	6995
4	544	542	786	6237	0	0	8109
5	559	559	4861*	9232	8.33	8	17227
6	559	559	4219	11767	8.33	8.33	17120
7	559	559	4219	11767	8.33	8.33	17120
8	559	559	4861	9232	8.33	8.33	15227
9	559	559	786	6237	6	0	8147
10	559	559	786	4218	8.33	8.33	6138
11	559	559	786	3139	0	0	5043
12	490	559	786	786	0	0	2621
13	318	559	786	786	0	0	2449
14	229	559	786	786	0	0	2360
15	469	559	786	786	0	0	2600
16	533	534	786	786	0	0	2639
17	559	559	786	3139*	0	0	7043
18	559	559	786	4218	8.33	8.33	6138
19	559	559	786	5263	8.33	8.33	7183
20	559	559	3761*	8203	8.33	8.33	15098
21	559	559	3140	10766	8.33	8.33	15040
22	559	559	4219	11767	8.33	8.33	17120
23	559	559	3140	10766	8.33	8.33	15040
24	559	559	3140	8715	8.33	8.33	12989

Table 3.9: Available power based on the number of units turned on at each time step for Load Profiles 1, 2, and 3.

	Load Profile 1	Load Profile 2	Load Profile 3
t	$P_t^{available}$ (MW)	$P_t^{available}$ (MW)	$P_t^{available}$ (MW)
1	200	200	200
2	200	200	200
3	200	300	300
4	200	300	300
5	200	300	400
6	200	400	400
7	200	400	400
8	300	400	400
9	300	400	300
10	300	400	300
11	400	300	300
12	400	300	200
13	400	200	200
14	400	200	200
15	400	200	200
16	400	200	200
17	400	200	300
18	300	200	300
19	300	200	300
20	300	200	400
21	300	200	400
22	300	200	400
23	200	100	400
24	200	100	400

CHAPTER 4

SOURCE REDISPATCH WITH CONTROL EFFORT REDUCTION

The previous chapter developed a baseline distribution, which minimized the cost over a time horizon based on a ship's load profile. However, this load profile was predicted and may not follow this baseline during the actual trip. The economic priorities considered in this are not the main concern for distribution when the ship is at sea. Rather, the control effort is of interest. The control effort in this case would be to change the demand on each unit as minimally as possible. This would both keep the distribution as close to the baseline as possible, prevent unnecessary extreme changes in the output of each unit, and keep the applied load as consistent as possible. Therefore, this is achieved by minimizing the change in the load.

As mentioned in the introduction, a zonal control is currently the state of practice for shipboard microgrids, as shown in Figure 1.2. This model allows for a distributed system to be implemented, which prevents a single point of failure. If faults were to occur, load shedding is typically the solution with the critical loads being supported. The zonal control increases reliability by providing the ability to isolate sections if faults were to occur and to transfer power between the zones. The power transfer between the zones must be considered to ensure that the sources and connections are not stressed. When changes from the predicted load occur, remaining as close to the predicted load distribution as possible would prevent transfer issues between the zones. Therefore, when the units are redispatched to accommodate the change in load demand, the change between the units should be minimized.

The discrepancy in change in load is similar to the discrepancy caused by renewable resources, such as solar panels. To handle the discrepancy between the difference between the expected and actual load, an optimization problem was developed in [58] using an affine policy. An affine policy restricts the possible changes to be within an affine function. In other words, the constraint is set to be affine with limited boundaries, which handles the uncertainty. The affine policy typically only works well with one uncertain parameter; therefore, only the source or load could have discrepancies [54]. The optimization problem considered the change in generation change.

4.1 Optimization Formulation

This redispatch method handles the uncertainty if there is only one uncertain parameter. In this case, the generation sources were handled to consider the most economic load distribution while also ensuring there is ample room for load discrepancies. Therefore, this method fit into an affine policy. The objective reduced the change in load distribution to each unit while considering the units' maximum power output and the power output originally expected. The change in load should not be expected to change for only a single time step. Therefore, the redispatch will consider a look-ahead method, which will consider a change in load for a period. For example, the control system detects a change in load, which would occur at $t = 0$. The system would then consider that the expected load will not occur for a portion of the predicted, up to time T, between when a load change is detected to when it matches again. This was formulated as an optimization problem as shown below.

$$\min \quad \sum_{t=1}^{T}\left[\sum_{i=1}^{N}\left(\left(\frac{\Delta P_{i,t}^{+}}{P_i^{\max}}\right)^2+\left(\frac{\Delta P_{i,t}^{-}}{P_i^{\max}}\right)^2\right)+\sum_{Bm=1}^{B} M\left(\left(\frac{\Delta P_{Bm,t}^{d+}}{P_B^{\max} m}\right)^2+\left(\frac{\Delta P_{Bm,t}^{d-}}{P_{Bm}^{\max}}\right)^2+\left(\frac{\Delta P_{Bm,t}^{c+}}{P_{Bm}^{\max}}\right)^2+\left(\frac{\Delta P_{Bm,t}^{c-}}{P_{Bm}^{\max}}\right)^2\right)\right] \tag{4.1a}$$

s.t.

$$\Delta P_{i,t}^{+} \cdot \Delta P_{i,t}^{-}=0 \tag{4.1b}$$

$$\Delta P_{Bm,t}^{d+} \cdot \Delta P_{Bm,t}^{d-}=0 \tag{4.1c}$$

$$\Delta P_{Bm,t}^{c+} \cdot \Delta P_{Bm,t}^{c-}=0 \tag{4.1d}$$

$$\Delta P_{i,t}^{+} \geq 0, \Delta P_{i,t}^{-} \geq 0 \tag{4.1e}$$

$$\Delta P_{Bm,t}^{d+} \geq 0, \Delta P_{Bm,t}^{d-} \geq 0 \tag{4.1f}$$

$$\Delta P_{Bm,t}^{c+} \geq 0, \Delta P_{Bm,t}^{c-} \geq 0 \tag{4.1g}$$

$$\sum_i \Delta P_{i,t}^{+}-\sum_i \Delta P_{i,t}^{-}+\sum_m \Delta P_{Bm,t}^{d+}-\sum_{Bm} \Delta P_{Bm,t}^{d-}-\sum_{Bm} \Delta P_{Bm,t}^{c+}+\sum_{Bm} \Delta P_{Bm,t}^{c-}=\Delta P_{D,t} \tag{4.1h}$$

$$\mathrm{SOC}_{Bm,t}^{redis}=P_{Bm}^{cap} * \mathrm{SOC}_{m,t-1}^{redis}+P_{Bm,t}^{c} \eta_c-P_{Bm,t}^{d} / \eta_d \tag{4.1i}$$

$$1.\delta P_{D,t} \leq P_t^{\text{available}} \tag{4.1j}$$

$$P_i^{\min} \leq P_{i,t}^{\text{redis}} \leq P_{i,t}^{\max} \tag{4.1k}$$

$$P_{Bm}^{d,\min} \leq P_{Bm,t}^{d,\text{redis}} \leq P_{Bm,t}^{d,\max} \tag{4.1l}$$

$$P_{Bm}^{c,\min} \leq P_{Bm,t}^{d,\text{redis}} \leq P_{Bm,t}^{c,\max} \tag{4.1m}$$

$$P_{i,t}-P_{i,t-1} \leq RU_i \tag{4.1n}$$

$$P_{i,t}-P_{i,t-1} \leq RD_i \tag{4.1o}$$

$$\mathrm{SOC}_{Bm}^{\min} \leq \mathrm{SOC}_{Bm,t}^{redis} \leq \mathrm{SOC}_{Bm}^{\max} \tag{4.1p}$$

where $\Delta P_{i,t}^{+}$ and $\Delta P_{i,t}^{-}$ are the positive and negative change in load applied to the diesel generators ($D1, D2$) and gas turbines ($G1, G2$) respectively, P_i^{max} is the maximum power for unit i, $\Delta P_{Bm,t}^{d+}$ and $\Delta P_{Bm,t}^{d-}$ are the positive and negative change in discharge power of the battery, $\Delta P_{Bm,t}^{c+}$ and $\Delta P_{Bm,t}^{c-}$ are the positive and negative charge power of the battery, P_{Bm}^{max} is the maximum power for battery Bm, $P^{available}$ is the total available power across all units, δ is the required percentage discrepancy in expected load, ΔP_D is the difference in load demand between the predicted and actual load, $P_{i,t}^{redis}$ is the redispatched power for the generators, $P_{Bm,t}^{d,redis}$ is the redispatched discharge power of the battery, $P_{Bm,t}^{c,redis}$ is the redispatched charging power of the battery, RU_i is the ramp up power limit for unit i, and RD_i is the ramp down power limit for unit i.

As mentioned, the objective function, reduces the change in load, $\Delta P_{i,t}^{+}$, $\Delta P_{i,t}^{-}$, $\Delta P_{Bm,t}^{d,t}$, $P_{Bm,t}^{c,t}$, where the positive superscript indicates an increase in load and the negative superscript indicates a decrease in load. This difference is calculated by subtracting the predicted output power of each unit, $P_{i,t}$, $P_{Bm,t}^{d}$, and $P_{Bm,t}^{c}$, from the redispatched power, $P_{i,t}^{\text{redis}}$, $P_{Bm,t}^{d,\text{redis}}$, and $P_{Bm,t}^{c,\text{redis}}$. However, the size of the unit must be considered since a small change for one unit may be a large change for another. Therefore, the change in load is divided by the maximum power output. Each of these fractions are squared to ensure they are positive and do not cancel. This total considered load change is summed for all units at every time step within the considered period.

The constraints ensure that the objective functions consider the limitations of the units and load discrepancy. The first constraint, 4.1b, ensures that the discrepancy is either positive or negative at each time step. The total of each of these positive and discrepancies must be equal to the total change in dispatch power, as shown in constraint 4.1c. Although this optimization uses the look-ahead method to ensure that the future

discrepancies are caught, there may be other unexpected changes in load. Therefore, the percentage requirement for load change must also be adhered to, which is represented in 4.1d. The remaining constraints ensure that the generating units are operating within the maximum and minimum power limits, 4.1e, and the changes in load are within the unit ramp up, 4.1f, and ramp down, 4.1g, ability.

To better understand the look-ahead function of the control, the power in the objective function can be rewritten as:

$$P_{i,t} = P_{i,0} + \sum_{t'=1}^{t} \Delta P_{i,t'} \tag{4.2}$$

where $P_{i,0}$ is the power output for unit i at time step 0 and $P_{i,t'}$ is the new power output at the following time steps within the look-ahead period. This objective function exemplifies that the look-ahead function has a rolling effect. In that the previous time step affects the following time step. By using the rolling effect, the generators are ensured to be within the ramp up and ramp down limits. By limiting the allowed discrepancy and minimizing the change in output load, the control ensures that the generating units address the applied load while limiting the change applied to the generator.

In the previous section, a baseline profile with an accommodation was developed with a sample shown in Figure 3.4. This method would operate as shown in Figure 4.1, which considers the actual load profile. As shown, there are sections where the load profile follows the predicted load profile and others where it does not. The sections where the load profile does not follow the predicted load was where the above redispatch function was used. The redispatch function notes the change in load at the first time step and uses a look-ahead function to develop a rolling load accommodation. Therefore, this section improves on the baseline function to consider the change in load and source redistribution.

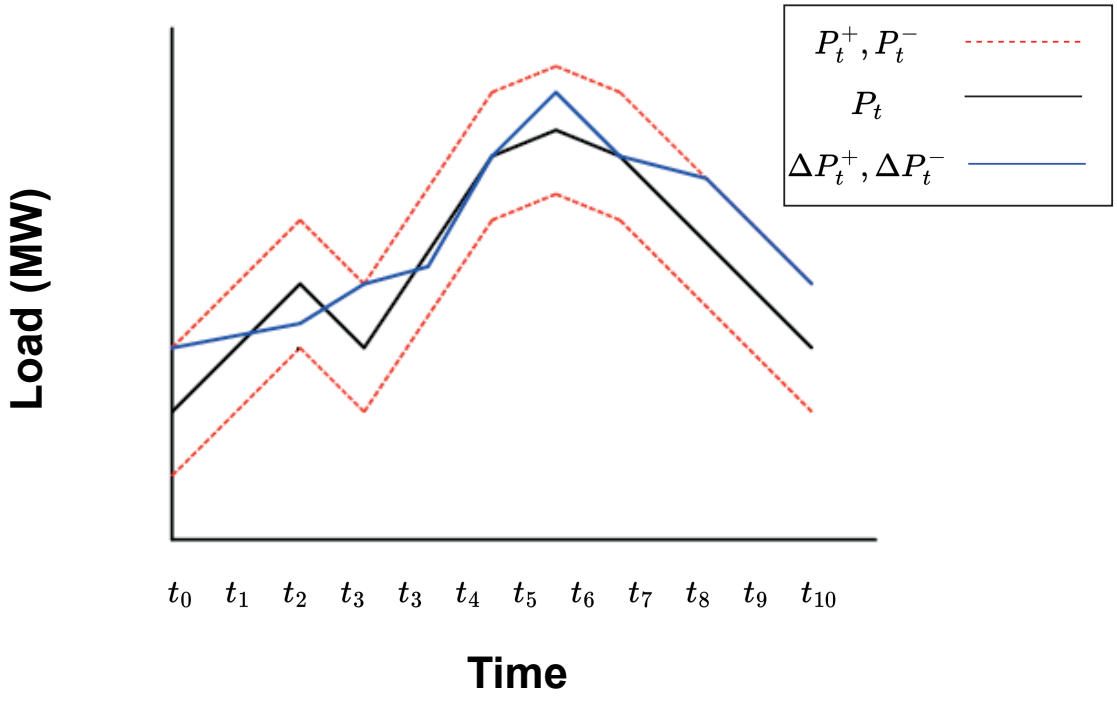

Figure 4.1: Redispatch load profile with the predicted load profile, P_t, the load change accommodation, P_t^+, P_t^-, and the actual load profile $\Delta P_t^+, \Delta P_t^-$ shown.

4.1.1 Modes of Operations

Although this problem redispatches the load in real time, the varying ship types and route requirements may have differing requirements, reliability concerns, and remainder of the trip may constitute a different strategy. Therefore, this method will also implement adjustments via modes. The modes may adjust the δ percentage applied, which considers how much reserve power should always be available. This percentage can be increased to make a conservative consideration or reduced for a more relaxed technique. This would be additional protection as the baseline profile also had a reserve consideration, which allowed the use of the affine policy. However, depending on the change in load and reliability requirements, a set reserve may be required as the load increases.

The second control consideration would deemphasize the role of the reserve percentage and instead set a minimum number of units that must be operational. For example, if there are 4 traditional generating units onboard, a more conservative mode would require that at least 3 units be always on. Therefore, the percentage requirement would only come into play when the load is approaching the limit of the three always on generators. Another mode may set a requirement for a minimum available SOC of the batteries to ensure that fast response resources are always available. This would accommodate a ship with critical loads that would be detrimental to consider a load shedding event and requires a fast response. Therefore, these two considerations would provide flexible requirements that could be applied across various types of hybrid-electric shipboard microgrids.

4.2 Case Study

The redispatch feature requires a predicted load profile with the load distribution across the available units. For the purposes of this case study, the results from Chapter 3 will be used. This shipboard microgrid included two diesel generators, two gas turbines, and two batteries. The preset values associated with these units, including the maximum and minimum limits of the generators and batteries, were set to be the same as the previous simulations, which are shown in Table 3.5. The following predicted load profile used the predicted load profile as shown in Figure 3.8. Based on this predicted load profile, the control system distributed the load across the generators as shown in Figure 3.9 and across the batteries in Figure 3.10.

Based on the predicted load profiles shown in Chapter 3, actual load profiles were developed. These profiles deviated from the previous predicted load profiles within the reserve allocation and the ramp down of the on-line units. The redispatch control was tested using the actual load profiles and changing the modes of operation. For example, in Table 3.5, the reserve allocation was set to a 15% reserve. However, if during the operation, a larger reserve should be considered, this percentage may be increased. The flexibility of the redispatch method was tested by considering a few cases.

4.3 Simulation Results

As mentioned previously, this method requires a predicted load profile and an actual load profile. The redispatch may operate throughout the entire time horizon or for a look-ahead period. To simplify the following two cases, a single 24-hour actual load profile was developed, where one case will section off a portion of it to demonstrate the look-ahead

method and another will use the entire period. The flexibility of this method came from two main types of changes that can be made, which were adjusting the reserve allocation and requiring a set number of units to always be on-line. First, a consideration was made that the predicted load may be seen to be deviating farther than expected from the predicted load. Therefore, an increase in the load reserve allocation was required, which was performed by increasing the δ percentage. Next, a consideration was made where a specific number of units may be required to be on-line whether acting as a type of spinning reserve, further assurance of reliability, or to alleviate any start-up costs or time constraints.

In the previous chapter three 24-hour load profiles were developed considering the typical load profiles of ships. This redispatch optimization will use each of these three predicted load profiles and distributions. As mentioned, this redispatch has two options to remain flexible and increase resiliency, the reserve increase, and the operation mode change. To show the capabilities of the optimizations, each load profile will be redispatched twice, first with the reserve increase and second with the mode change.

4.3.1 Redispatch of Load Profile 1 - Center Load Peak

The first load profile developed followed the traditional center peak, similar to the tall trapezoidal or parabolic curves found on ships. Various peaks were added throughout the curve to test the resiliency of the system in terms of ramp up, ramp down, and when to charge and discharge the batteries. The actual load profile remained within the reserve requirement with two sections deviating from the prediction. The first section was lower than predicted profile, while the second section was higher. The first section was used to test the reserve increase, to anticipate a rising load later, and the second was used to exhibit the operation mode change to ensure an essential generator does not turn off.

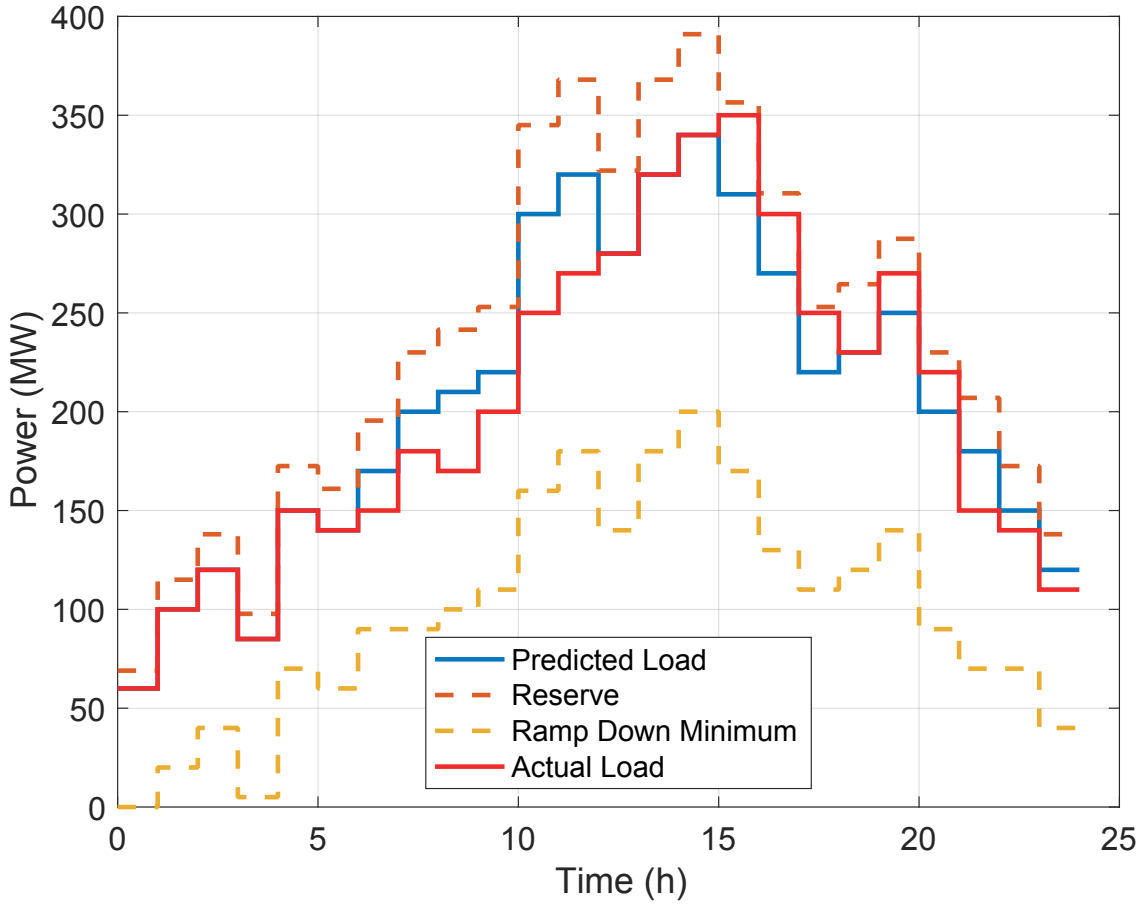

Figure 4.2: The predicted load profile and reserve requirement from Figure 3.8 with the actual load and minimum allowable load based on ramp-down of the units at each time step.

Reserve Allocation Increase

If the reserve allocation appears to be insufficient, the percentage can be increased to redispatch the load and ensure a higher margin is available for future time periods. In the predicted load profile in this case, a 15% margin was applied. Therefore, to show the reserve increase, the percentage, δ, was set to 20% instead. This was applied for the actual load profile shown in Figure 4.2.

For this case, a look-ahead approach was taken. As shown in the actual load profile, there is a period where the load matches the predicted load at time periods 6 and 13 but deviates in between. Therefore, this case will look at this period where the load deviates between and assume the periods before 6 and after 13 matched the predicted load profile. The generator and battery redistribution results with the increased δ percentage across this period are shown in Figure 4.3a and Figure 4.3b respectively. The solid line shows the redistributed power, where the variables are denoted with the superscript $redis$, and the predicted load applied are shown in dotted lines. The specific differences for each unit are shown in Table 4.1.

As shown in the simulation results, the control method was able to redistribute the load based on the actual load throughout the selected period. The change applied to each of the units was minimized without regard for the cost of the units since in a redispatch control, the cost is no longer the main issue. Therefore, this method was proven to work for a short period of time when a load change was detected.

Operation Mode Change

The typical operation mode does not specify the number of units which must be on-line at a given period. The number of units on-line are determined based on the constraints of the predicted load control systems' formulation, which was determined based on cost and the given constraints. However, there may be times when the units should deviate from the predicted plan and remain on during the selected period.

For this test, the case was set to be the load increase shown in Figure 4.2 from time step 16 throughout the remainder of the period. The requirement was changed such that at least three units always remain on. In the case of this load prediction, it was concluded that the

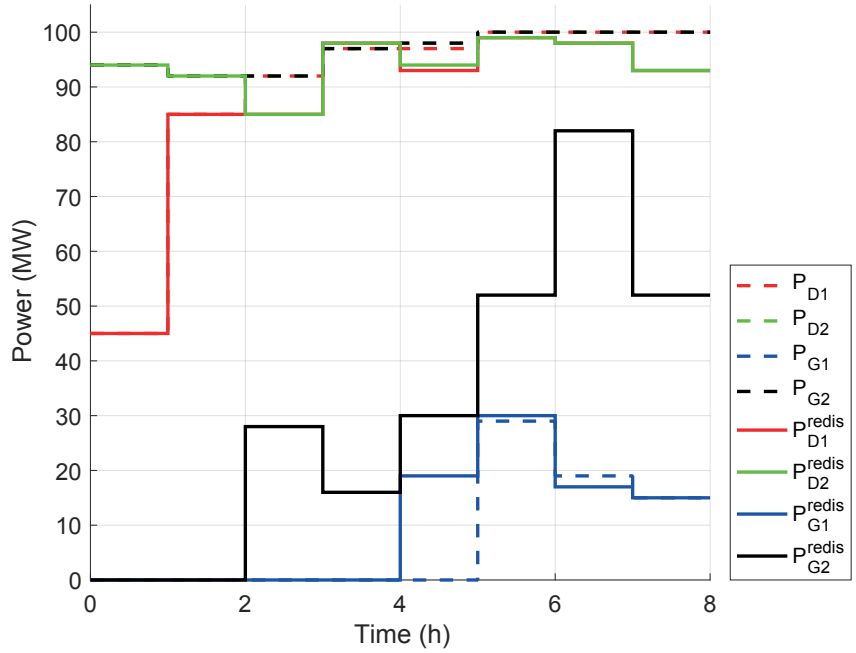

(a) Redispatched load distribution across the two diesel generators and two gas turbines for the load profile shown in Figure 4.2.

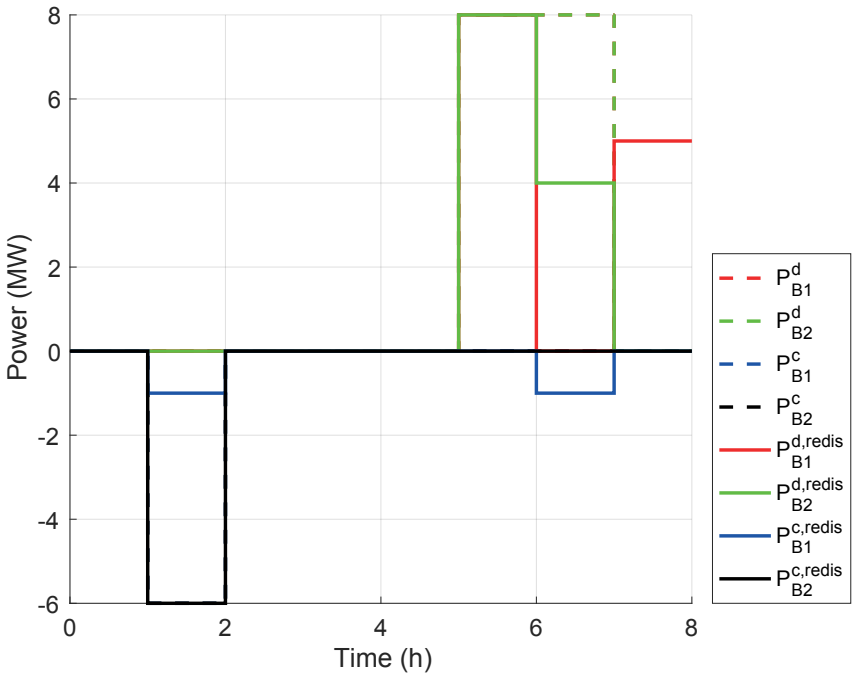

(b) Redispatched Charging and Discharging power of the two batteries across the load profile shown in Figure 4.2.

Figure 4.3: Load distribution across diesel generators, gas turbines, and batteries.

Table 4.1: Change in load applied to each unit including the two diesel generators, two gas turbines, and change in charge and discharge power of the batteries. These results were obtained from the redispatch optimization of Load Profile 1, shown in Figure 4.2 for the reserve increase section.

t	1	2	3	4	5	6	7	8
$\Delta P^{+}_{D1,t}$ (MW)	0	0	0	0	0	0	0	0
$\Delta P^{-}_{D1,t}$ (MW)	0	10	10	20	7	11	14	0
$\Delta P^{+}_{D2,t}$ (MW)	0	0	0	0	0	0	0	0
$\Delta P^{-}_{D2,t}$ (MW)	0	10	10	20	7	11	14	0
$\Delta P^{+}_{G1,t}$ (MW)	0	0	0	0	0	0	0	1
$\Delta P^{-}_{G1,t}$ (MW)	0	0	0	0	0	12	4	0
$\Delta P^{+}_{G2,t}$ (MW)	0	0	0	0	0	0	0	2
$\Delta P^{-}_{G2,t}$ (MW)	0	0	0	0	6	12	14	0
$\Delta P^{d+}_{B1,t}$ (MW)	0	0	0	0	0	0	0	0
$\Delta P^{d-}_{B1,t}$ (MW)	0	0	0	0	0	3	3	3
$\Delta P^{c+}_{B1,t}$ (MW)	0	0	0	0	0	0	0	0
$\Delta P^{c-}_{B1,t}$ (MW)	0	0	0	0	0	0	0	0
$\Delta P^{d+}_{B2,t}$ (MW)	0	0	0	0	0	0	0	0
$\Delta P^{d-}_{B2,t}$ (MW)	0	0	0	0	0	1	1	0
$\Delta P^{c+}_{B2,t}$ (MW)	0	0	0	0	0	0	0	0
$\Delta P^{c-}_{B2,t}$ (MW)	0	0	0	0	0	0	0	0
Total	0	-20	-20	-40	-20	-50	-50	0
Load Difference	0	-20	-20	-40	-20	-50	-50	0

two diesel generators, $G1$ and $G2$, and the gas turbine $G2$ should remain on since these units are on the most throughout the period. This was set by adjusting a binary variable in front of each of the power output constraints to be set to 1 throughout the period. Therefore, the three units will always have at least 15 MW applied to them throughout the period. The results of this simulation are shown in Figure 4.4a and 4.4b for the generator and battery distribution respectively. The differences between the predicted and reidspatched load for each unit is shown in Table 4.2.

As shown in this simulation result, the units have at least 15 MW applied to them throughout the period. The gas turbine's' power, labeled P_{G2} in Figure 4.4a, had only 15 MW applied when the unit had been predicted to be turned off. This proves the minimization strategy of this control, which applies the least possible deviation from the predicted load profile. Therefore, this flexible control can be applied using a look-ahead approach or for a total deviation based on the mission needs.

4.3.2 Redispatch of Load Profile 2 - Early Load Peak

The second load profile had an early peak in the load profile of the ship. The predicted load profile, actual load profile, the previous reserve allocation, and the ramp down minimum at each time step is shown in Figure 4.5. The minimum ramp down is based on the number of on-line units at that time step. In this case, the actual load profile remained within the reserve allocated in the predicted load profile. There are two sections of the load where it deviates from the predicted, which will be used the redispatch the sources using the two options.

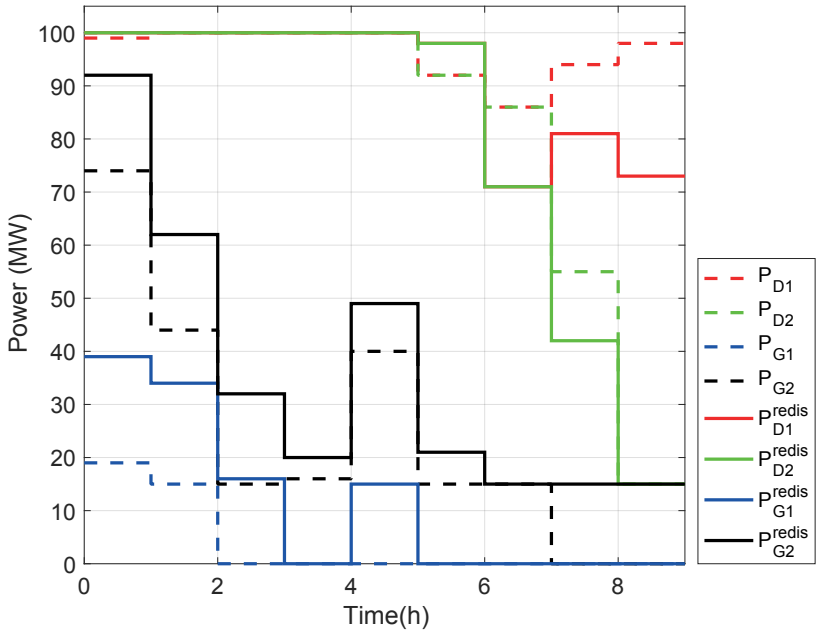

(a) Load distribution across the two diesel generators and two gas turbines for the load profile shown in Figure 4.2.

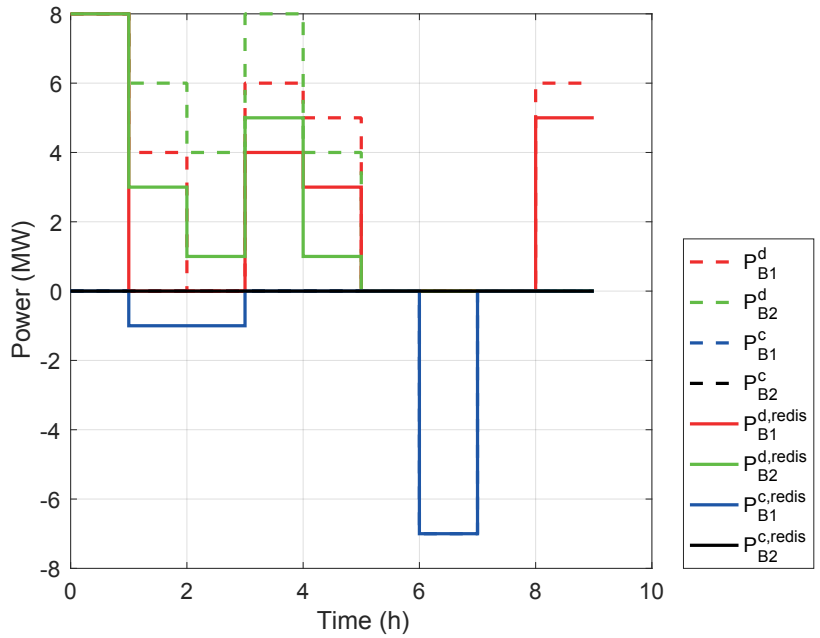

(b) Charging and Discharging power of the two batteries across the load profile shown in Figure 4.2.

Figure 4.4: Load distribution across diesel generators, gas turbines, and batteries.

Table 4.2: Change in load applied to each unit including the two diesel generators, two gas turbines, and change in charge and discharge power of the batteries. These results were obtained from the redispatch optimization of Load Profile 1, shown in Figure 4.2 for the operation mode change section.

t	1	2	3	4	5	6	7	8	9
$\Delta P^{+}_{D1,t}$ (MW)	2	0	0	0	0	7	0	0	0
$\Delta P^{-}_{D1,t}$ (MW)	0	0	0	0	0	0	15	13	25
$\Delta P^{+}_{D2,t}$ (MW)	0	0	0	0	0	7	0	0	0
$\Delta P^{-}_{D2,t}$ (MW)	0	0	0	0	0	0	15	12	0
$\Delta P^{+}_{G1,t}$ (MW)	20	19	16	0	15	0	0	0	0
$\Delta P^{-}_{G1,t}$ (MW)	0	0	0	0	0	0	0	0	0
$\Delta P^{+}_{G2,t}$ (MW)	18	18	17	4	9	6	0	15	15
$\Delta P^{-}_{G2,t}$ (MW)	0	0	0	0	0	0	0	0	0
$\Delta P^{d+}_{B1,t}$ (MW)	0	0	0	0	0	0	0	0	0
$\Delta P^{d-}_{B1,t}$ (MW)	0	4	0	2	2	0	0	0	0
$\Delta P^{c+}_{B1,t}$ (MW)	0	1	1	0	0	0	0	0	0
$\Delta P^{c-}_{B1,t}$ (MW)	0	0	0	0	0	0	0	0	0
$\Delta P^{d+}_{B2,t}$ (MW)	0	0	0	0	0	0	0	0	0
$\Delta P^{d-}_{B2,t}$ (MW)	0	2	2	2	2	0	0	0	0
$\Delta P^{c+}_{B2,t}$ (MW)	0	0	0	0	0	0	0	0	0
$\Delta P^{c-}_{B2,t}$ (MW)	0	0	0	0	0	0	0	0	0
Total	40	30	30	0	20	20	-30	-10	-10
Load Difference	40	30	30	0	20	20	-30	-10	-10

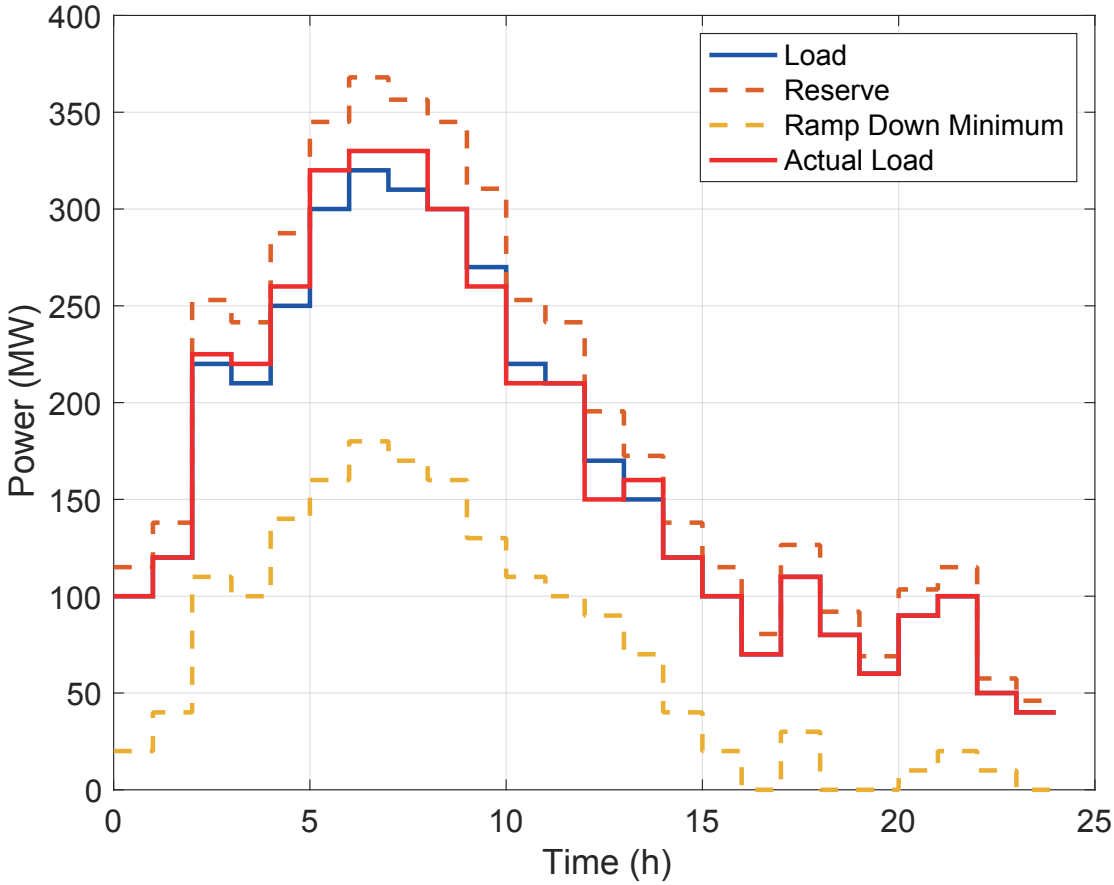

Figure 4.5: The predicted load profile and reserve requirement from Figure 3.11 with the actual load and minimum allowable load based on ramp-down of the units at each time step.

Redispatch of Load Profile 2

The first section of the load where it deviates is shown in Figure 4.5 from time step 3-8, for a total of 6 time steps were required to be redispatch. To consider the ramp up and down of the generators and SOC of the batteries, time step 2 was included in the redispatch. Time step 9 was also included to represent the detection of no change in load. Therefore, a total of 7 time steps were included in the first dispatch to consider the load reserve increase. The redistribution results for the generators are shown in Figure 4.6a and the batteries are shown in Figure 4.6b. The specific numerical results are shown in Table 4.4.

As shown in the load redispatch, the first and last time steps match the load distribution in time step 2 shown in the load distribution in Figure 3.12 for the generators and 3.13. The specific differences at each time step are shown in Table 4.3. The previous load distribution is also represented by the dotted lines corresponding to the same color of each source. As mentioned, the objective of this simulation was to minimize the change in load from the predicted result. However, the load at time step 9 did deviate although the load applied remained the same. This was due to the change in the battery distribution across the load. Although this was the case, the control as still successful in meeting the load demands presented.

Operation Mode Change

The second deviated load section in Figure 4.5 is shown from time steps 10-14. Again, time steps 9 and 15 were included to mark the beginning and the end of the change in load. This section was considered for the change of mode operation in terms of keeping a minimum number of generators turned on. Therefore, the load redistribution will be evident based on three the generators having a minimum of 15 MW always applied throughout the time

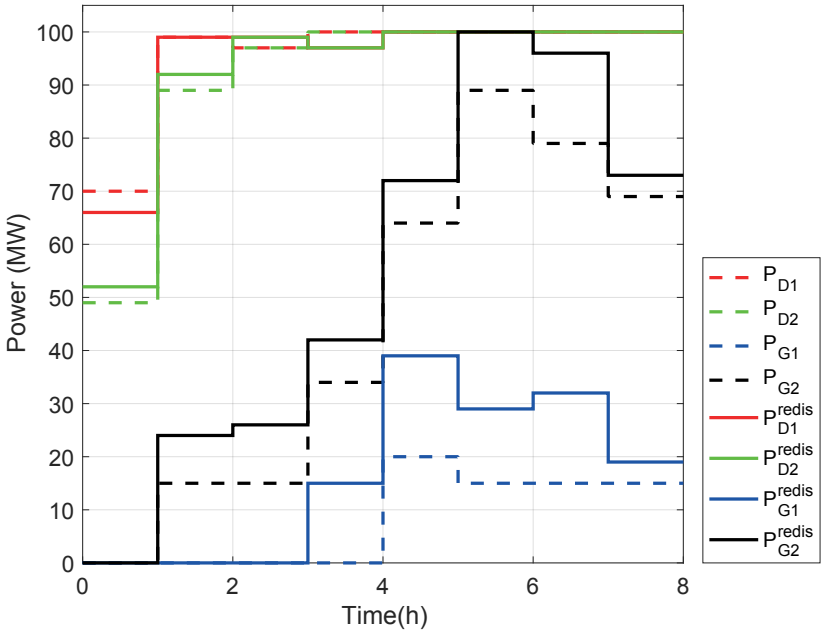

(a) Load distribution across the two diesel generators and two gas turbines for the load profile shown in Figure 4.5.

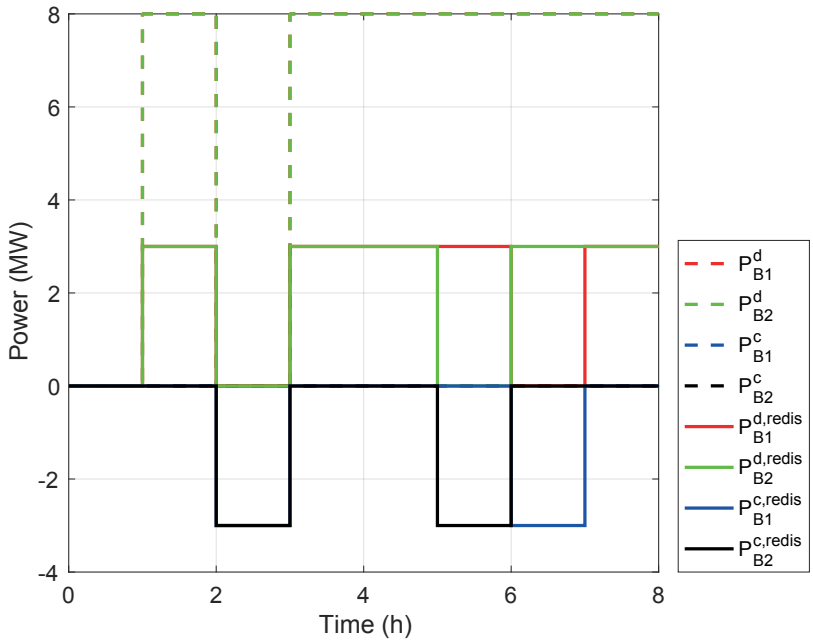

(b) Charging and Discharging power of the two batteries across the load profile shown in Figure 4.5.

Figure 4.6: Load distribution across diesel generators, gas turbines, and batteries for load profile shown in Figure 4.5.

Table 4.3: Change in load applied to each unit including the two diesel generators, two gas turbines, and change in charge and discharge power of the batteries. These results were obtained from the redispatch optimization of Load Profile 1, shown in Figure 4.5 for the reserve increase section.

t	1	2	3	4	5	6	7	8
$\Delta P^{+}_{D1,t}$ (MW)	0	0	2	0	0	0	0	0
$\Delta P^{-}_{D1,t}$ (MW)	3	0	0	3	0	0	0	0
$\Delta P^{+}_{D2,t}$ (MW)	3	4	3	0	0	0	0	0
$\Delta P^{-}_{D2,t}$ (MW)	0	0	0	2	0	0	0	0
$\Delta P^{+}_{G1,t}$ (MW)	0	0	0	15	19	14	18	4
$\Delta P^{-}_{G1,t}$ (MW)	0	0	0	0	0	0	0	0
$\Delta P^{+}_{G2,t}$ (MW)	0	9	11	8	9	11	17	4
$\Delta P^{-}_{G2,t}$ (MW)	0	0	0	0	0	0	0	0
$\Delta P^{d+}_{B1,t}$ (MW)	0	0	0	0	0	0	0	0
$\Delta P^{d-}_{B1,t}$ (MW)	0	4	0	4	4	4	8	4
$\Delta P^{c+}_{B1,t}$ (MW)	0	0	3	0	0	0	3	0
$\Delta P^{c-}_{B1,t}$ (MW)	0	0	0	0	0	0	0	0
$\Delta P^{d+}_{B2,t}$ (MW)	0	0	0	0	0	0	0	0
$\Delta P^{d-}_{B2,t}$ (MW)	0	4	0	4	4	8	4	4
$\Delta P^{c+}_{B2,t}$ (MW)	0	0	3	0	0	3	0	0
$\Delta P^{c-}_{B2,t}$ (MW)	0	0	0	0	0	0	0	0
Total	0	5	10	10	20	10	20	0
Load Difference	0	5	10	10	20	10	20	0

horizon. It was set that three of the generators must remain on-line. Based on the predicted load distribution, the two diesel generators, $D1$ and $D2$, and one gas turbines, $G1$, was set to remain on. The new load distribution across the generators is shown in Figure 4.7a and the batteries in Figure 4.7b. The differences applied to each unit are shown in Table 4.4.

As shown in Figure 4.7a, the requirement for three generators to remain on is evident from time steps 5-7 where the gas turbine, $G1$, has previously been slated to turn off. However, based on the operation mode change, the generator now has 15 MW applied. The load increase on this generator was made up by reducing the load applied to the other generators and using the batteries.

These two operation mode changes on two sections of the load profile show evidence that the redispatch was able to remain flexible by redistributing the load across the sources. This was done while minimizing the load change applied to each of the units, which reduced the control effort. Additionally, the control remained resilient by either increasing the reserve allocation or requiring a specific number of units to remain on throughout the time horizon.

4.3.3 Redispatch of Load Profile 3 - Two Load Peaks

The final load profile best exemplified the capabilities of the previous optimization problem with the multitude of turning on and off the units and strategic battery usage. Therefore, this simulation will also further test the resiliency of the redispatch control. The predicted load profile with the corresponding reserve, and the actual load profile used for the redispatch is shown in Figure 4.8. The two sections where the load deviates are from time steps 1-8 and 14-20. The first load deviation is beyond the reserve requirement set by the predicted load. Therefore, the simulation was tested to ensure that it can handle further stress in

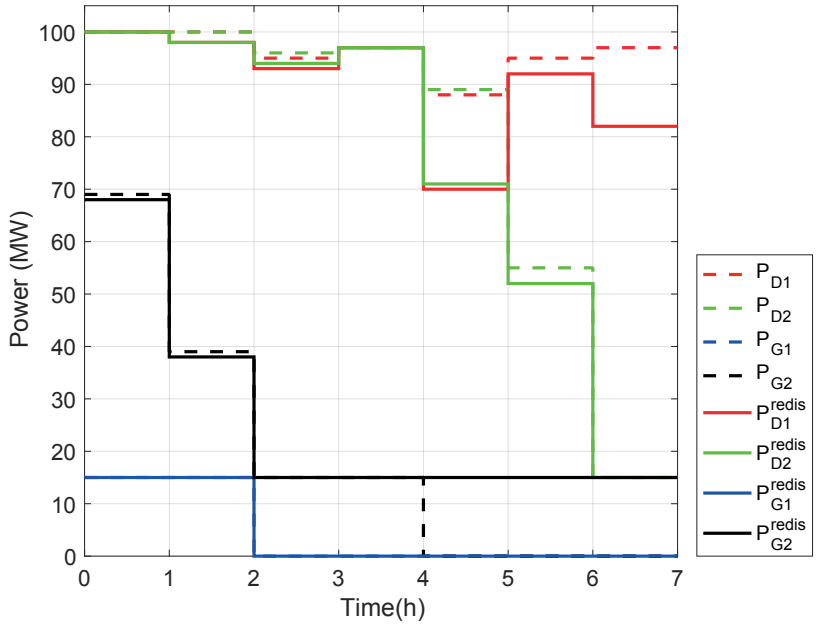

(a) Load distribution across the two diesel generators and two gas turbines for the load profile shown in Figure 4.5.

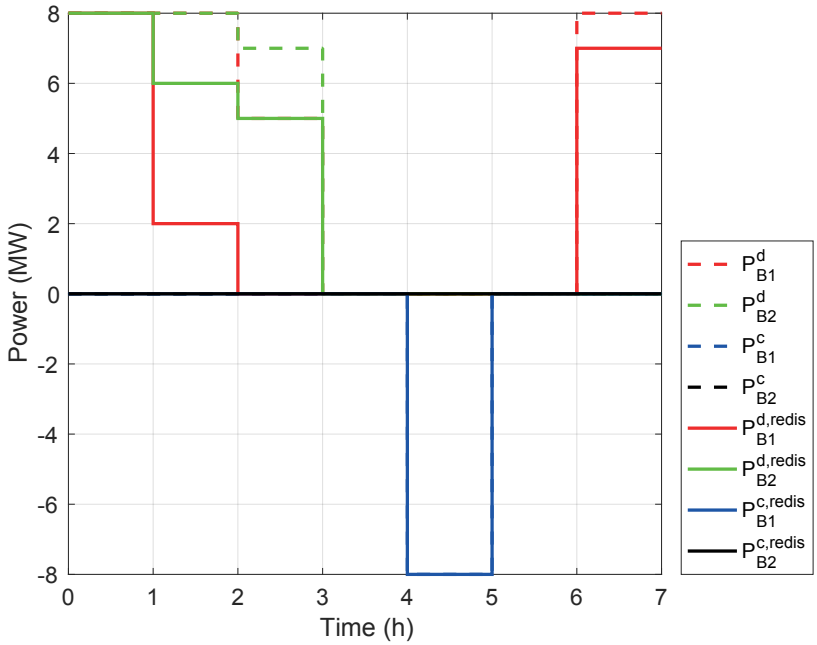

(b) Charging and Discharging power of the two batteries across the load profile shown in Figure 4.5.

Figure 4.7: Load distribution across diesel generators, gas turbines, and batteries for load profile shown in Figure 4.5.

Table 4.4: Change in load applied to each unit including the two diesel generators, two gas turbines, and change in charge and discharge power of the batteries. These results were obtained from the redispatch optimization of Load Profile 1, shown in Figure 4.5 for the operation mode change section.

t	1	2	3	4	5	6	7
$\Delta P^{+}_{D1,t}$ (MW)	0	0	0	0	0	0	0
$\Delta P^{-}_{D1,t}$ (MW)	0	2	2	0	18	3	15
$\Delta P^{+}_{D2,t}$ (MW)	0	0	0	0	0	0	0
$\Delta P^{-}_{D2,t}$ (MW)	0	2	2	0	17	2	0
$\Delta P^{+}_{G1,t}$ (MW)	0	0	0	0	0	0	0
$\Delta P^{-}_{G1,t}$ (MW)	0	0	0	0	0	0	0
$\Delta P^{+}_{G2,t}$ (MW)	0	0	0	0	15	15	15
$\Delta P^{-}_{G2,t}$ (MW)	0	0	0	0	0	0	0
$\Delta P^{d+}_{B1,t}$ (MW)	0	0	0	0	0	0	0
$\Delta P^{d-}_{B1,t}$ (MW)	0	5	5	0	0	0	0
$\Delta P^{c+}_{B1,t}$ (MW)	0	0	0	0	0	0	0
$\Delta P^{c-}_{B1,t}$ (MW)	0	1	1	0	0	0	0
$\Delta P^{d+}_{B2,t}$ (MW)	0	0	0	0	0	0	0
$\Delta P^{d-}_{B2,t}$ (MW)	0	1	1	0	0	0	0
$\Delta P^{c+}_{B2,t}$ (MW)	0	0	0	0	0	0	0
$\Delta P^{c-}_{B2,t}$ (MW)	0	0	0	0	0	0	0
Total	0	-10	-10	0	-20	10	0
Load Difference	0	-10	-10	0	-20	10	0

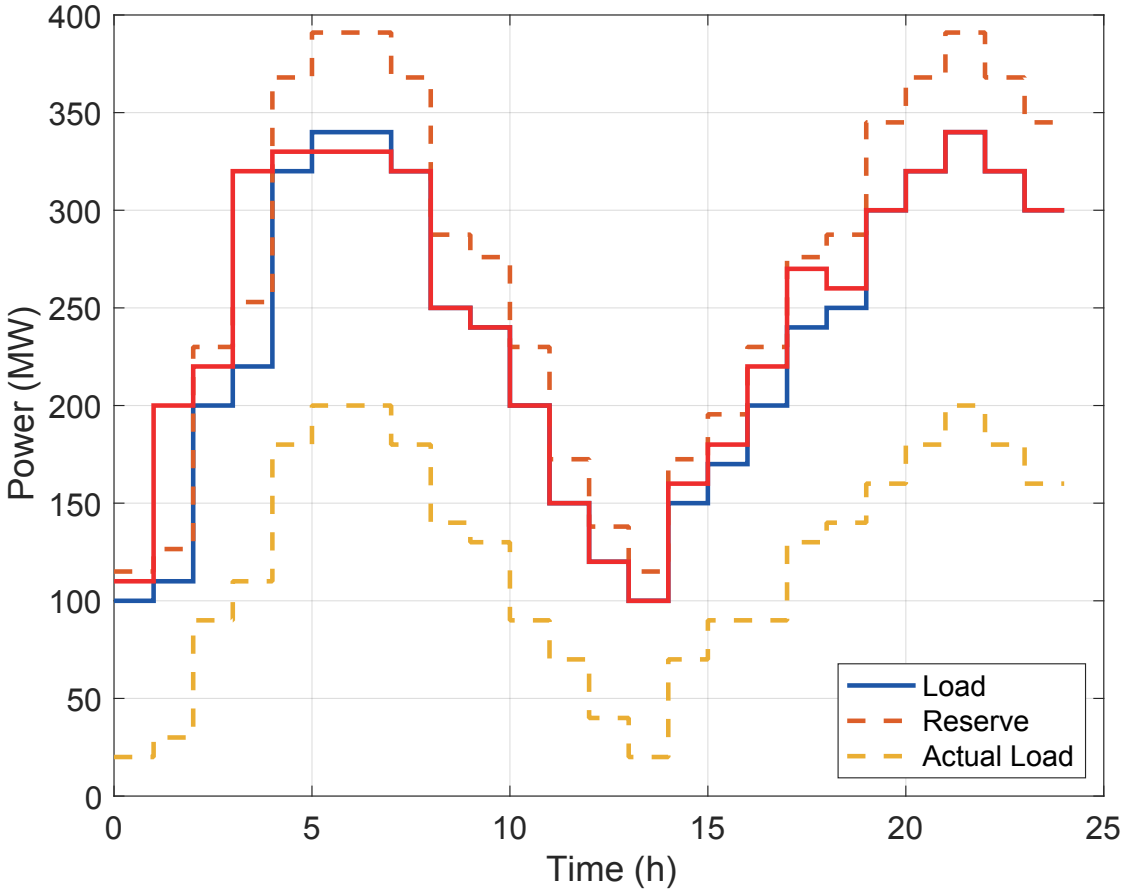

Figure 4.8: The predicted load profile and reserve requirement from Figure 3.14 with the actual load and minimum allowable load based on ramp-down of the units at each time step.

addition to increasing the load reserve. The second load deviation remained within the reserve requirements and was therefore used to test the operation mode change.

Reserve Increase

As mentioned, the load deviates from the time step 1 until it matches the predicted load at time step 8. The actual load remains beyond the reserve, but the load can handle the more than expected load increase by leveraging the on units' ramp up and discharging

the batteries. The new load distributions across the generators and batteries are shown in Figures 4.9a and 4.9b respectively. The differences applied to each unit are shown in Table 4.5.

The load was increased during the beginning of the period, from time steps 0 through 5. This is evident in the increase in load distribution across the generators during these time steps. However, after this point, the actual load is lower than the predicted load distribution. Therefore, the load distribution across the generators remains approximately the same, but the batteries show a reduction in the predicted discharge.

Therefore, this optimization was able to redispatch the load outside of the predicted reserve requirement and provide an additional reserve percentage on top of the increased load. This displays the resilient and flexible nature of the control that can perform beyond the set requirements in this case.

Operation Mode Change

The next change that was performed on this load profile was the operation mode change during the second deviation from the predicted load. The second deviation occurred from time steps 15 through 19, where 14 and 20 were included for matching the predicted load. Therefore, the simulation was a total of 7 time steps. The operation mode change was tested on this section by again requiring three of the generators to always be on. Based on the predicted distribution, the two diesel generators and the gas turbine $G2$ was selected to remain on throughout. The distribution across the generators for the second section Load Profile 3 is shown in Figure 4.10a. The new battery distribution was shown in Figure 4.10b.

As shown in the figure, the gas turbine labeled $G2$ remains on throughout the period with at least 15 MW applied throughout. This load change requirement was adjusted by

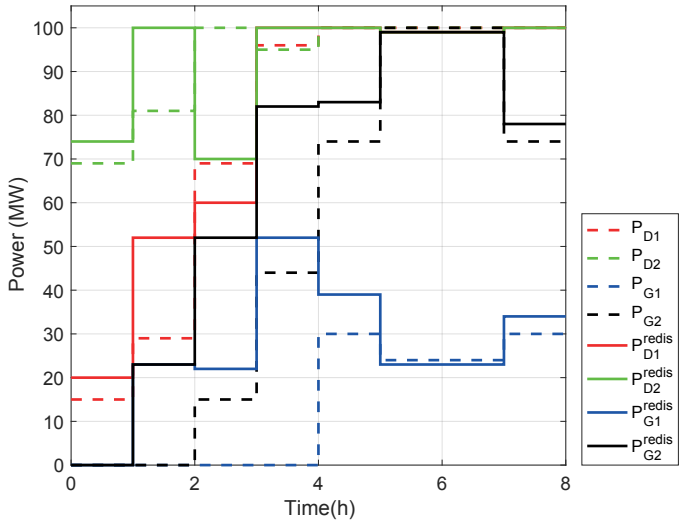

(a) Load distribution across the two diesel generators and two gas turbines for the load profile shown in Figure 4.8. The dotted line shows the predicted load distribution and the solid line shows the redispatched load distribution with an increased reserve requirement.

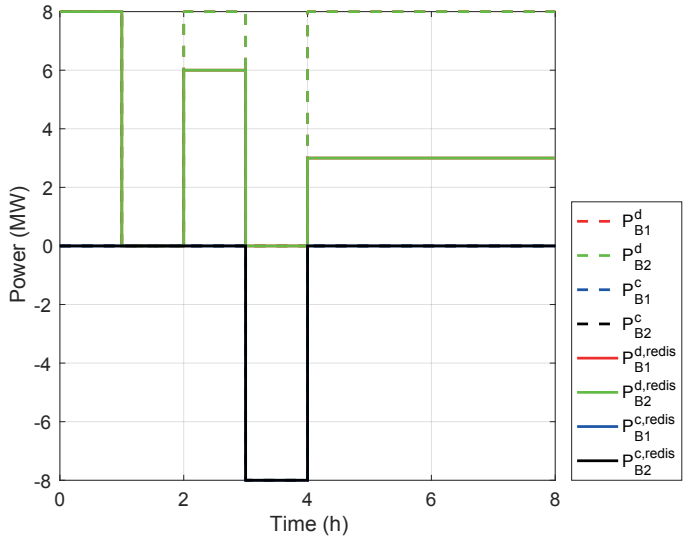

(b) Charging and Discharging power of the two batteries across the load profile shown in Figure 4.8. The dotted line shows the predicted charge and discharge power and the solid line shows the redispatched battery power with an increased reserve requirement.

Figure 4.9: Load distribution across diesel generators, gas turbines, and batteries for load profile shown in Figure 4.8.

Table 4.5: Change in load applied to each unit including the two diesel generators, two gas turbines, and change in charge and discharge power of the batteries. These results were obtained from the redispatch optimization of Load Profile 3, shown in Figure 4.8 for the reserve increase section.

t	1	2	3	4	5	6	7	8
$\Delta P^{+}_{D1,t}$ (MW)	5	24	0	4	0	0	0	0
$\Delta P^{-}_{D1,t}$ (MW)	0	0	8	0	0	0	0	0
$\Delta P^{+}_{D2,t}$ (MW)	5	20	0	4	0	0	0	0
$\Delta P^{-}_{D2,t}$ (MW)	0	0	29	0	0	0	0	0
$\Delta P^{+}_{G1,t}$ (MW)	0	24	22	53	9	0	0	4
$\Delta P^{-}_{G1,t}$ (MW)	0	0	0	0	0	0	0	0
$\Delta P^{+}_{G2,t}$ (MW)	0	24	37	39	9	0	0	4
$\Delta P^{-}_{G2,t}$ (MW)	0	0	0	0	0	0	0	0
$\Delta P^{d+}_{B1,t}$ (MW)	0	0	0	0	0	0	0	0
$\Delta P^{d-}_{B1,t}$ (MW)	0	0	1	0	6	6	4	4
$\Delta P^{c+}_{B1,t}$ (MW)	0	0	0	0	0	0	0	0
$\Delta P^{c-}_{B1,t}$ (MW)	0	0	0	0	0	0	0	0
$\Delta P^{d+}_{B2,t}$ (MW)	0	0	0	0	0	0	0	0
$\Delta P^{d-}_{B2,t}$ (MW)	0	0	1	0	6	6	4	4
$\Delta P^{c+}_{B2,t}$ (MW)	0	0	0	0	0	0	0	0
$\Delta P^{c-}_{B2,t}$ (MW)	0	0	0	0	0	0	0	0
Total	10	90	20	100	10	-10	-10	0
Load Difference	10	90	20	100	10	-10	-10	0

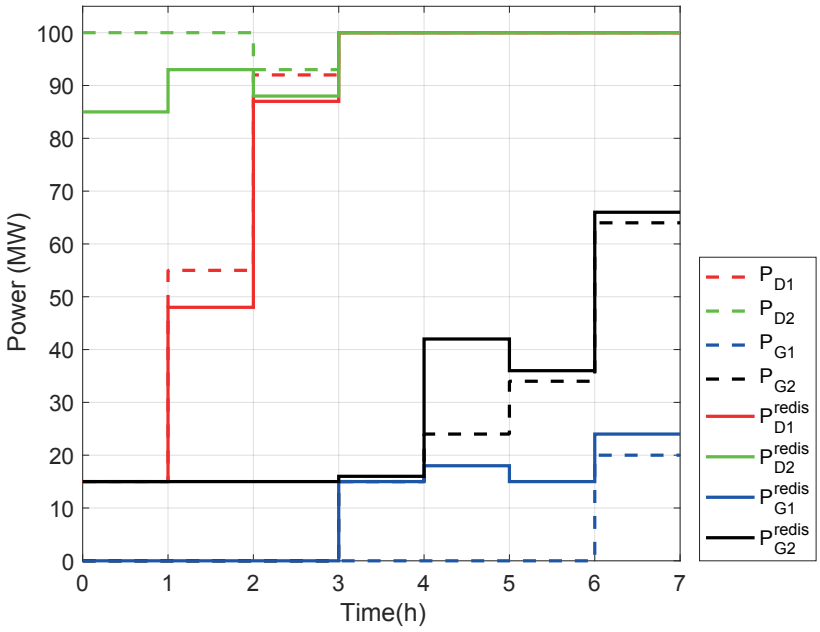

(a) Load distribution across the two diesel generators and two gas turbines for the load profile shown in Figure 4.8.

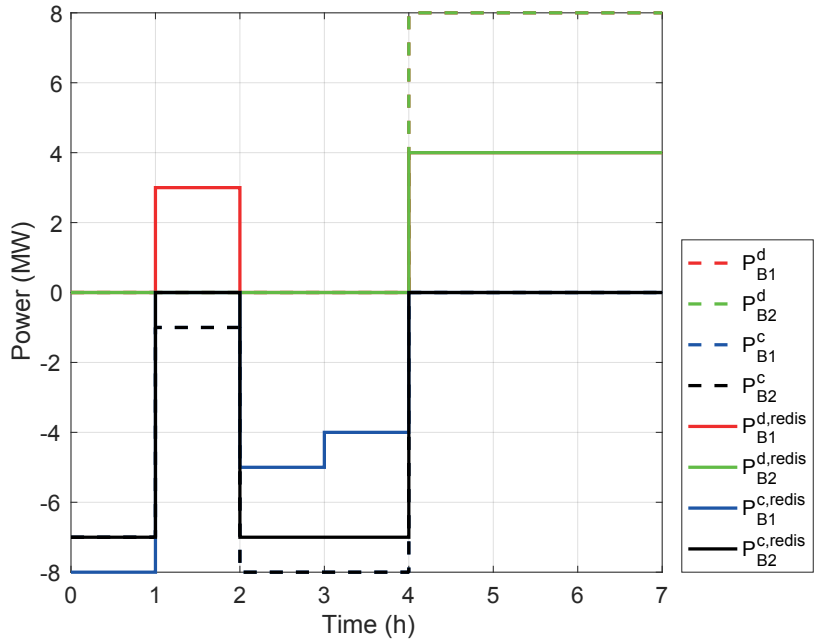

(b) Charging and Discharging power of the two batteries across the load profile shown in Figure 4.8.

Figure 4.10: Load distribution across diesel generators, gas turbines, and batteries for load profile shown in Figure 4.8.

reducing the load across the other generators and batteries to have the minimum change applied to each unit. A breakdown of the exact change in load at each time step is shown in Table 4.6.

This proved that the system was able to redispatch the load across the generators and batteries while meeting the load actual load demand. The operation mode change required a change in either the positive or negative power change even if the load demand remained the same. However, the control optimized the distribution to have minimal impact on the other units. Therefore, the simulation was successful in redistributing the load while keeping the required number of units on and accommodating the change in load.

4.4 Conclusion

The proposed redispatch optimization problem reduced the control effort by minimizing the change in load realized by each unit. A baseline formulation was assumed with a reserve allocation already considered. However, additional modes were applied to develop a flexible control that considers the needs and requirements of the ship. This was performed both by adjusting the reserve based on the newly applied load and considering the units onboard such as the number of units that must always remain on. The simulation proved the validity of the control and showed the control effort reduction via the minimized change seen by each unit. This allows for easy implementation into a zonal control and reduces the impacts on transfer between the zones as the adjustments are minimized. Therefore, this redispatch control had available adjustments that developed a reliable, flexible control.

Table 4.6: Change in load applied to each unit including the two diesel generators, two gas turbines, and change in charge and discharge power of the batteries. These results were obtained from the redispatch optimization of Load Profile 1, shown in Figure 4.8 for the operation mode change section.

t	1	2	3	4	5	6	7
$\Delta P^{+}_{D1,t}$ (MW)	0	1	0	0	0	0	0
$\Delta P^{-}_{D1,t}$ (MW)	0	3	5	0	0	0	0
$\Delta P^{+}_{D2,t}$ (MW)	0	0	0	0	0	0	0
$\Delta P^{-}_{D2,t}$ (MW)	15	7	5	0	0	0	0
$\Delta P^{+}_{G1,t}$ (MW)	0	0	0	15	18	15	4
$\Delta P^{-}_{G1,t}$ (MW)	0	0	0	0	0	0	0
$\Delta P^{+}_{G2,t}$ (MW)	15	15	15	1	18	1	2
$\Delta P^{-}_{G2,t}$ (MW)	0	0	0	0	0	0	0
$\Delta P^{d+}_{B1,t}$ (MW)	0	3	0	0	0	0	0
$\Delta P^{d-}_{B1,t}$ (MW)	0	0	0	0	3	3	3
$\Delta P^{c+}_{B1,t}$ (MW)	0	1	3	3	0	0	0
$\Delta P^{c-}_{B1,t}$ (MW)	0	0	0	0	0	0	0
$\Delta P^{d+}_{B2,t}$ (MW)	0	0	0	0	0	0	0
$\Delta P^{d-}_{B2,t}$ (MW)	0	0	0	0	3	3	3
$\Delta P^{c+}_{B2,t}$ (MW)	0	1	3	3	0	0	0
$\Delta P^{c-}_{B2,t}$ (MW)	0	0	0	0	0	0	0
Total	0	10	10	20	30	10	0
Load Difference	0	10	10	20	30	10	0

4.5 Summary of Contributions

This chapter established a redispatch control scheme for hybrid electric ships. This control required a baseline distribution and load with a new load curve featuring load points that differed from the predicted load and remained the same. The predicted load profiles and distributions were collected from the Chapter 3 load distributions. The actual load profiles each featured two sections that deviated from the predicted load. One of the sections were used to feature the option to have a reserve increase and the other featured the operation mode change in which a required number of units to remain on. The optimization problem was designed to accommodate a zonal control scheme. Within a zonal control there are constraints on the power that can be transferred between each zone. Therefore, a minimal impact as a result as a change in load would prevent issues from occurring by overloading the exchange between the zones. Therefore, this control operated by minimizing the change on each unit, which also reduced the control effort.

These three load profiles each had unique challenges and stresses to the control. Load profile 1 had an actual load profile which featured a mix of increases and decreases. This stressed the optimal use of the battery and generators while maintaining the SOC and ramp up and ramp down requirements. Load Profile 2 further stressed the ramp up and ramp down requirements by peaking earlier and faster in the time horizon compared to Load Profile 1. Meanwhile, Load Profile 3 provided additional stress to the system by featuring an actual load which deviated beyond the allotted reserve requirement set during the predicted load. However, the system was able to manage this load change and redispatch the sources appropriately. There was also a larger stress on the batteries due to the two load peaks. This required strategic use of discharging the battery with the change in load being accommodated. Therefore, a flexible, resilient control was developed to

accommodate a change in load and compliment the predicted load control developed in Chapter 3.

CHAPTER 5

SUMMARY OF CONTRIBUTIONS

This work fills a gap in the control of microgrids where the economic considerations of the units and control efforts are balanced. Large scale power systems consider the economics to remain competitive on the market and may be performed selfishly or holistically. Although this dynamic of being selfish in terms of a market does not exist on a shipboard microgrid, the operation of the units still involves the economics of operation. Therefore, this was investigated two-fold within the control scheme.

Although within ships the economics of the units were not relevant in terms of outperforming competitors, the sources onboard can be better distributed considering the costs of using each unit. Traditionally, the ships only used generators, such as diesel generators and gas turbines. However, as ships are becoming electric, the use of batteries onboard are becoming more common. If the economics are considered, the use of batteries onboard hybrid ships has been generally limited to supplementary roles rather than main power sources. The batteries within this scheme were to operate as a main power sources; however, since the economics of generators were considered, a method to apply a cost to the battery had to be developed.

There are works that provide a cost as result of aging the batteries, they require specific knowledge and extensive testing of each battery. Therefore, this is not conducive to application on any Li-ion battery being implemented. However, a majority of manufacturers' data sheet reports the cycling life of batteries in terms of cycles until failure. Therefore, this information as used to develop an economic scheme for the battery. Based

on the cycling life, an optimal number of cycles was calculated using the number of full cycles until failure to normalize the power output across the tested DoD levels. A cost was applied to each cycle based on the replacement cost of the battery. Furthermore, a piece-wise linear function was calculated to encourage the battery to discharge to the ideal level and discouraged from discharging further.

Once an economic function for the battery was developed, an efficient method to consider the cost of using each type of generator was investigated. Previously, the main function used to add an economic consideration to the generators was through a quadratic cost function. This method provided results without much computation power and was typically used with a variety of generator sizes. Due to the nature of the shipboard microgrid system requirements, redundancy is required. Therefore, it is common to have two of each of the traditional prime movers, such as multiple of the same diesel generators and gas turbines. This posed a flaw within the quadratic function, which was addressed by considering the fuel efficiency of the generators.

The fuel efficiency of generators is typically represented by at least a fourth order equation. In contrast to the quadratic cost functions, this allowed for more pairs of optimizers to be found. When the redundant generators were calculated using the quadratic cost function, this left one pair which was always an equal split between the two identical generators. However, when the fuel efficiency was used, the equal split appeared but it was not the optimal solution. Instead, depending on the loading conditions, an unequal split was found to be optimal. Therefore, this allowed to save on fuel costs for the generators and provide a more efficient solution. The same fuel is used for both diesel generators and gas turbines are used onboard ships; therefore, a standard cost per gallon of fuel was used to develop an economic function out of the fuel efficiency equation.

Using the economic functions of both the battery and generators developed an optimization problem to provide a control scheme for the shipboard microgrid. The optimization determined the load distribution across the generators and batteries by minimizing the cost. A predicted load profile was developed based on the ships' typical load curves. Constraints were set that included operational conditions as well as control requirements. Specifically, a constraint was set to provide a reserve requirement for when the load deviates from the predicted load. This developed a resilient and efficient control while considering the economics of the load distribution in the form of a time horizon optimization.

Although the economics provided an efficient control scheme, the cost of using the units are not the main concern when the load deviates from the prediction. When the load deviates from the prediction, redispatching the units to accommodate the new load value while reducing the control effort was of the most importance. This control was developed in the form of an optimization problem. The objective used an affine function to minimize the change in load applied to each of the units. The change was divided by the maximum allowable load applied such that the change was weighted based on the size of the generating source. Each of the positive and negative fractions were squared to ensure that they were not cancelled. The time horizon problem considered a rolling method to ensure that the ramp up, ramp down, SOC, and other time dependent requirements were met while ensuring that each time step met the new loading criteria. The control was able to remain flexible based on the changing conditions by adjusting the reserve percentage and the mode of operation.

The reserve percentage was originally used as an insurance during the predicted load distribution based on the real time distribution. However, since this method is to handle

the load changes as they differ from the prediction, a reassessment of the reserve that may be required. For example, if the load is lower than expected, it may cause the peak that later the peak to be higher than predicted. Therefore, increasing the reserve requirement will ensure that the load availability is there as well as preventing issues with the ramp up requirements. The mode of operation was a new development unique to the redispatch criteria. The mode of operation sets a required number of generators to be on at all time steps to develop a further ensured resiliency. Although hidden from the formulation for clarity, binary values to determine the on and off generators are used throughout the code, which is shown in the appendix. For the mode of operation, these variables are set to be 1 for the time horizon being redispatched. This will ensure that the generators do not turn off as predicted and provides a large reserve as a result. The optimization handles the new minimum loading requirement and minimizes the change in load distribution across the other sources. By using these two options to adjust the control scheme as the load changes, this provides flexibility and further resiliency to ensure that the system can handle the change in load applied.

This dissertation focused on the control of hybrid electric microgrids while focusing on improving the efficiency, flexibility, and resiliency of the system. For the hybrid system, the batteries required an economic function that was versatile across Li-ion batteries, which was developed using the cycling life. Next, the efficiency of the traditional prime mover was improved by considering the fuel efficiency and apply a cost to develop a more in-depth economic function. The economic function developed were then used to create an economic control which optimized the cost across a predicted load profile. Within the time horizon optimization, a reserve was added to ensure that any fluctuation from the predicted was handled by the units. Furthermore, when the fluctuations did occur, a redispatch

optimization was developed, which focused on reducing the control effort in terms of the change applied to each of the sources. The resiliency and flexibility of the system was then increased by allowing for a change in the reserve requirement and an operation mode change. Therefore, the control efforts will be reduced and prevent issues across the zones of the microgrid. The control developed for the hybrid-electric shipboard microgrid was optimized to be efficient, flexible, and resilient.

5.1 Publications

The publications that were obtained while completing this degree are listed below, which includes the work discussed within this dissertation are listed below.

1. **K. Sitch** and L. Du, "Flexible Load Uncertainty Management on Shipboard Microgrids Through Redispatch with Control Effort Reduction," 2023 IEEE Transportation Electrification Conf. & Expo., Detroit, MI

2. **K. Sitch** and L. Du, "Efficient, Resilient Control of Hybrid Shipboard Microgrids Considering Fuel Efficiency and Battery Cycle Life," 2023 IEEE Transportation Electrification Conf. & Expo., Detroit, MI

3. **K. Sitch** and L. Du, "Economic Control for Hybrid-Electric Shipboard Microgrids Considering Battery Degradation and Cycling Life Costs," 2022 IEEE Transportation Electrification Conference & Expo (ITEC), 2022, pp. 647-651, doi: 10.1109/ITEC53557.2022.9813757 [33].

4. **K. Sitch**, D. Sun, L. Du and H. Yang, "Pulsed Electric Bus Charging Management Considering Charge Redistribution Effect," 2020 IEEE Transportation

Electrification Conference & Expo (ITEC), 2020, pp. 1088-1092, doi: 10.1109/ITEC48692.2020.9161717 [36].

5. **K. Sitch**, D. Sun and L. Du, ”Integration of Pulsed Electric Bus Fleet Charging Profiles Through Coordinated Control of Hybrid Microgrids,” 2019 IEEE Transportation Electrification Conference and Expo (ITEC), 2019, pp. 1-6, doi: 10.1109/ITEC.2019.8790513 [59].

CHAPTER 6

FUTURE WORK

The proposed control system developed a methodology that handled a predicted load while considering both control constraints and economic conditions. Following this a redispatch optimization was developed, which did not focus on economics but rather on the control effort. This methodology was designed with a zonal control in mind as this is common among shipboard microgrids; however, the zonal configurations constraints were not specifically addressed within the optimization. Therefore, the future of further implementation and versatility of this control will be related to the implementation within a zonal control.

The zonal control has been popular due to the increased resiliency, grouping and isolation of loads and faults, and allowing power sharing among the units. However, to model this system, more constraints must be added to represent the power transfers. For the predicted control, configurations will be made based on the loads and the time step to ensure the supply of power across the zones is sufficient. Specifically, this may include adding additional paths between the zones to ensure that the power transfer between the zones do not overload the lines. In terms of the connections between the zones, the loads can also be dedicated as critical and non-critical with differing requirements for each. This will be used to ensure that there are multiple sources supplying the critical loads in cases of faults, equipment malfunctions, or isolation conditions. Therefore, this will provide an initial zonal configuration based on the predicted loads and a baseline, adjustable system.

Based on this initial baseline, the redispatch will operate similarly by remaining dependent on the predicted load control and focus on the control effort reduction. The control effort reduction will be expanded to include the zonal configuration parameters. The current formulation was designed to prevent issues with the zonal control by reducing the impact seen by each unit. However, additional constraints will be added to ensure that the transfer between the zones using the predicted zonal configuration will not cause issues. If the current formulation causes violations between the zonal transfer, first the optimization will check if there is another distribution that will prevent reconfiguring the zones. If this is not possible, the next priority will be to minimize the amount of switching to reconfigure the zones. This will continue with the goal of reducing the control effort while meeting the new load demand.

The previous improvements will allow the work presented in this dissertation to align with both state of practice and the current research efforts that are present particularly in shipboard microgrids, but also land-based microgrids. The zonal configurations provide more challenges for the optimization, but also presents further benefits in terms of the efficiency and resiliency. The zonal control will also allow for further cases to be considered in the simulation including faults. The faults particularly require the critical loads to be protected and supplied despite the issues occurring. Limited equipment malfunctions can be simulated in the current formulation, such as generators only being able to output a certain value across all or a portion of the time horizon. However, the types of malfunctions that occur on ships can be further explored with the classification of critical and non-critical loads and the zonal configuration. Therefore, this future work will provide a methodology that can be tested and expanded to further prove its resiliency, efficiency, and flexibility.

BIBLIOGRAPHY

[1] N. Zhi, K. Ding, L. Du, and H. Zhang, "An soc-based virtual dc machine control for distributed storage systems in dc microgrids," *IEEE Transactions on Energy Conversion*, vol. 35, no. 3, pp. 1411–1420, 2020.

[2] Y. Li and L. Du, "Transient stability assessment of islanded microgrids through quantum machine learning," in *2023 IEEE Transportation Electrification Conference & Expo (ITEC), Detroit, MI*, 2023.

[3] D. Sun, L. Du, X. Lu, and L. He, "An energy-stored quasi-z source converter based interlinking converter for hybrid ac/dc microgrids," in *IECON 2018 - 44th Annual Conference of the IEEE Industrial Electronics Society*, 2018, pp. 3821–3826.

[4] N. Zhi, Y. Ding, and L. Du, "Virtual dc generator control strategy based on differential compensation," in *2019 IEEE Energy Conversion Congress and Exposition (ECCE)*, 2019, pp. 1454–1458.

[5] Q. Xu, J. Xiao, P. Wang, and C. Wen, "A decentralized control strategy for economic operation of autonomous AC, DC, and hybrid AC/DC microgrids," *IEEE Transactions on Energy Conversion*, vol. 32, no. 4, pp. 1345–1355, 2017.

[6] N. Zhi, X. Ming, Y. Ding, L. Du, and H. Zhang, "Power-loop-free virtual dc machine control with differential compensation," *IEEE Transactions on Industry Applications*, vol. 58, no. 1, pp. 413–422, 2022.

[7] J. M. Szatkowski, Y. Li, and L. Du, "Enabling reconfigurable naval scada network through software-defined networking," in *2022 IEEE Transportation Electrification Conference & Expo (ITEC)*, 2022, pp. 214–218.

[8] M.-H. Khooban, T. Dragicevic, F. Blaabjerg, and M. Delimar, "Shipboard microgrids: A novel approach to load frequency control," *IEEE Transactions on Sustainable Energy*, vol. 9, no. 2, pp. 843–852, 2017.

[9] S. Fang, Y. Wang, B. Gou, and Y. Xu, "Toward future green maritime transportation: An overview of seaport microgrids and all-electric ships," *IEEE Transactions on Vehicular Technology*, vol. 69, no. 1, pp. 207–219, 2019.

[10] S. Anwar, M. Y. I. Zia, M. Rashid, G. Z. d. Rubens, and P. Enevoldsen, "Towards ferry electrification in the maritime sector," *Energies*, vol. 13, no. 24, p. 6506, 2020.

[11] *U.S. Navy Mission,* "https://www.navy.mil/About/Mission/", (Last accessed on 11.9.2022).

[12] X. Zhaoxia, Z. Tianli, L. Huaimin, J. M. Guerrero, C.-L. Su, and J. C. Vásquez, "Coordinated control of a hybrid-electric-ferry shipboard microgrid," *IEEE Transactions on Transportation Electrification*, vol. 5, no. 3, pp. 828–839, 2019.

[13] N. Doerry, J. Amy, and C. Krolick, "History and the status of electric ship propulsion, integrated power systems, and future trends in the us navy," *Proceedings of the IEEE*, vol. 103, no. 12, pp. 2243–2251, 2015.

[14] H. Bach, A. Bergek, Ø. Bjørgum, T. Hansen, A. Kenzhegaliyeva, and M. Steen, "Implementing maritime battery-electric and hydrogen solutions: A technological innovation systems analysis," *Transportation Research Part D: Transport and Environment*, vol. 87, p. 102 492, 2020.

[15] J. Hou, Z. Song, H. F. Hofmann, and J. Sun, "Control strategy for battery/flywheel hybrid energy storage in electric shipboard microgrids," *IEEE Transactions on Industrial Informatics*, vol. 17, no. 2, pp. 1089–1099, 2021.

[16] Z. Tu, B. Fan, W. Zhang, J. Peng, and W. Liu, "Optimal state-constrained control of dc shipboard power systems for online pulsed power load accommodation," *IEEE Transactions on Smart Grid*, vol. 13, no. 1, pp. 96–105, 2022.

[17] C. S. Chin, C. Zhang, and Z. Gao, "Deploying battery technology for marine vessel electrification," *IEEE Potentials*, vol. 40, no. 6, pp. 24–33, 2021.

[18] S. Fang, Y. Fang, H. Wang, and S. Zhang, "Adaptive voyage-generation scheduling in shipboard microgrid under time-varied weather conditions," in *2020 IEEE/IAS 56th Industrial and Commercial Power Systems Technical Conference (I&CPS)*, 2020, pp. 1–8.

[19] J. Naughton, H. Wang, M. Cantoni, and P. Mancarella, "Co-optimizing virtual power plant services under uncertainty: A robust scheduling and receding horizon dispatch approach," *IEEE Transactions on Power Systems*, vol. 36, no. 5, pp. 3960–3972, 2021.

[20] D. Park and M. Zadeh, "Modeling and predictive control of shipboard hybrid dc power systems," *IEEE Transactions on Transportation Electrification*, vol. 7, no. 2, pp. 892–904, 2021.

[21] N. K. Dhaliwal, F. Bouffard, and M. J. O'Malley, "A fast flexibility-driven generation portfolio planning method for sustainable power systems," *IEEE Transactions on Sustainable Energy*, vol. 12, no. 1, pp. 368–377, 2021.

[22] M. A. Hassan *et al.*, "Dc shipboard microgrids with constant power loads: A review of advanced nonlinear control strategies and stabilization techniques," *IEEE Transactions on Smart Grid*, vol. 13, no. 5, pp. 3422–3438, 2022.

[23] M. Mahmoodi, P. Shamsi, and B. Fahimi, "Economic dispatch of a hybrid microgrid with distributed energy storage," *IEEE Transactions on Smart Grid*, vol. 6, no. 6, pp. 2607–2614, 2015.

[24] Q. Xu, Y. Xu, Z. Xu, L. Xie, and F. Blaabjerg, "A hierarchically coordinated operation and control scheme for dc microgrid clusters under uncertainty," *IEEE Transactions on Sustainable Energy*, vol. 12, no. 1, pp. 273–283, 2021.

[25] H. Ravindra, J. Langston, and K. Schoder, "Model design document," 2021.

[26] W. Zhu, J. Shi, P. Zhi, L. Fan, and G. J. Lim, "Distributed reconfiguration of a hybrid shipboard power system," *IEEE Trans. Power Sys.*, vol. 36, no. 1, pp. 4–16, 2020.

[27] M. Mosayebi, S. M. Sadeghzadeh, M. Gheisarnejad, and M. H. Khooban, "Intelligent and fast model-free sliding mode control for shipboard dc microgrids," *IEEE Transactions on Transportation Electrification*, 2020.

[28] Z. Jin, L. Meng, J. M. Guerrero, and R. Han, "Hierarchical control design for a shipboard power system with dc distribution and energy storage aboard future more-electric ships," *IEEE Transactions on Industrial Informatics*, vol. 14, no. 2, pp. 703–714, 2018.

[29] K. Butler-Purry, "Multi-agent technology for self-healing shipboard power systems," in *Proceedings of the 13th International Conference on, Intelligent Systems Application to Power Systems*, 2005, 5 pp.-.

[30] L. He *et al.*, "A flexible power control strategy for hybrid ac/dc zones of shipboard power system with distributed energy storages," *IEEE Transactions on Industrial Informatics*, vol. 14, no. 12, pp. 5496–5508, 2018.

[31] S. Kim, J. Kucka, G. Ulissi, S.-N. Kim, and D. Dujic, "Solid-state technologies for flexible and efficient marine dc microgrids," *IEEE Transactions on Smart Grid*, vol. 12, no. 4, pp. 2860–2868, 2021.

[32] J. Zeng, Q. Wang, J. Liu, J. Chen, and H. Chen, "A potential game approach to distributed operational optimization for microgrid energy management with renewable energy and demand response," *IEEE Transactions on Industrial Electronics*, vol. 66, no. 6, pp. 4479–4489, 2019.

[33] K. Sitch and L. Du, "Economic control for hybrid-electric shipboard microgrids considering battery degradation and cycling life costs," in *2022 IEEE Transportation Electrification Conference & Expo (ITEC)*, 2022, pp. 647–651.

[34] K. Sitch and L. Du, "Efficient, resilient control of hybrid shipboard microgrids considering fuel efficiency and battery cycle life," in *2023 IEEE Transportation Electrification Conference & Expo (ITEC), Detroit, MI*, 2023.

[35] K. Sitch and L. Du, "Flexible load uncertainty management on shipboard microgrids through redispatch with control effort reduction," in *2023 IEEE Transportation Electrification Conference & Expo (ITEC), Detroit, MI*, 2023.

[36] K. Sitch, D. Sun, L. Du, and H. Yang, "Pulsed electric bus charging management considering charge redistribution effect," in *2020 IEEE Transportation Electrification Conference & Expo (ITEC)*, 2020, pp. 1088–1092.

[37] J. M. Guerrero, J. C. Vasquez, J. Matas, L. G. de Vicuna, and M. Castilla, "Hierarchical control of droop-controlled ac and dc microgrids—a general approach toward standardization," *IEEE Transactions on Industrial Electronics*, vol. 58, no. 1, pp. 158–172, 2011.

[38] A. K. Sahoo, K. Mahmud, M. Crittenden, J. Ravishankar, S. Padmanaban, and F. Blaabjerg, "Communication-less primary and secondary control in inverter-interfaced ac microgrid: An overview," *IEEE Journal of Emerging and Selected Topics in Power Electronics*, vol. 9, no. 5, pp. 5164–5182, 2021.

[39] P. Lin *et al.*, "A distributed control architecture for global system economic operation in autonomous hybrid AC/DC microgrids," *IEEE Transactions on Smart Grid*, vol. 10, no. 3, pp. 2603–2617, 2019.

[40] F. Chen *et al.*, "Cost-based droop schemes for economic dispatch in islanded microgrids," *IEEE Trans. Smart Grid*, vol. 8, no. 1, pp. 63–74, 2016.

[41] T. M. Masaud and E. F. El-Saadany, "Correlating optimal size, cycle life estimation, and technology selection of batteries: A two-stage approach for microgrid applications," *IEEE Transactions on Sustainable Energy*, vol. 11, no. 3, pp. 1257–1267, 2019.

[42] M. Ross, C. Abbey, F. Bouffard, and G. Joós, "Microgrid economic dispatch with energy storage systems," *IEEE Transactions on Smart Grid*, vol. 9, no. 4, pp. 3039–3047, 2018.

[43] B. Xu, J. Zhao, T. Zheng, E. Litvinov, and D. S. Kirschen, "Factoring the cycle aging cost of batteries participating in electricity markets," *IEEE Trans.Power Sys.*, vol. 33, no. 2, pp. 2248–2259, 2018.

[44] M. Koller, T. Borsche, A. Ulbig, and G. Andersson, "Defining a degradation cost function for optimal control of a battery energy storage system," in *2013 IEEE Grenoble Conference*, IEEE, 2013, pp. 1–6.

[45] S. Jeong, Y. J. Jang, and D. Kum, "Economic analysis of the dynamic charging electric vehicle," *IEEE Transactions on Power Electronics*, vol. 30, no. 11, pp. 6368–6377, 2015.

[46] N. Omar *et al.*, "Lithium iron phosphate based battery – assessment of the aging parameters and development of cycle life model," *Applied Energy*, vol. 113, pp. 1575–1585, 2014.

[47] S. Drouilhet, B. Johnson, S. Drouilhet, and B. Johnson, "A battery life prediction method for hybrid power applications," in *35th Aerospace Sciences Meeting and Exhibit*, 1997, p. 948.

[48] J.-O. Lee, Y.-S. Kim, T.-H. Kim, and S.-I. Moon, "Novel droop control of battery energy storage systems based on battery degradation cost in islanded dc microgrids," *IEEE Access*, vol. 8, pp. 119 337–45, 2020.

[49] C. Ju, P. Wang, L. Goel, and Y. Xu, "A two-layer energy management system for microgrids with hybrid energy storage considering degradation costs," *IEEE Transactions on Smart Grid*, vol. 9, no. 6, pp. 6047–6057, 2018.

[50] Battery University, *How to prolong lithium-based batteries*, (Last accessed on 04.22.2022).

[51] Y. Lin and W. Xiao, "Novel piecewise linear formation of droop strategy for dc microgrid," *IEEE Transactions on Smart Grid*, vol. 10, no. 6, pp. 6747–6755, 2019.

[52] M. Zivic Djurovic, A. Milacic, and M. Krsulja, "A simplified model of quadratic cost function for thermal generators," in *Proceedings of the 23rd International DAAAM Symposium*, vol. 23, 2012, pp. 25–28.

[53] J. Amato, M. DiTaranto, M. Dong Qing, Kevin, and S. John, "Development of a control hardware in the loop (chil) testing for diesel electric propulsion plant control system," in *Advanced Machinery Technology Symposium (AMTS) 2022*, Philadelphia, PA, USA, 2022.

[54] D. Bertsimas and V. Goyal, "On the power and limitations of affine policies in two-stage adaptive optimization," *Mathematical programming*, vol. 134, no. 2, pp. 491–531, 2012.

[55] M. McCord, *Fiscal Year 2023 Standard Fuel Price Change*, 2022.

[56] S. Fang, Y. Xu, Z. Li, T. Zhao, and H. Wang, "Two-step multi-objective management of hybrid energy storage system in all-electric ship microgrids," *IEEE Transactions on Vehicular Technology*, vol. 68, no. 4, pp. 3361–3373, 2019.

[57] S. Surko and M. Osborne, "Operating speed profles and the ship design cycle," *Naval Engineers Journal*, vol. 117, no. 3, pp. 79–85, 2005.

[58] W. Wei, Y. Chen, C. Wang, Q. Wu, and M. Shahidehpour, "Nodal flexibility requirements for tackling renewable power fluctuations," *IEEE Transactions on Power Systems*, vol. 36, no. 4, pp. 3227–3237, 2021.

[59] K. Sitch, D. Sun, and L. Du, "Integration of pulsed electric bus fleet charging profiles through coordinated control of hybrid microgrids," in *2019 IEEE Transportation Electrification Conference and Expo (ITEC)*, 2019, pp. 1–6.

APPENDICES

The code used for the optimization problems were performed using a 2019 MacBook Pro. The code environment used was Spyder within Anaconda with Gurobi Optimizer version 9.5.2 .

CHAPTER 3 CODE

The code used for the simulations shown in Chapter 3 are as follows.

```
import gurobipy as gp
from gurobipy import GRB
import collections.abc
import pandas as pd


# Simulation Parameters
load_count = 24 # number of load values tested
#load_demand = [60, 100, 200, 310, 200, 100, 60] ##( Mw)
#load_demand = [30, 40,50,60,70,80,90]
# 24 load 1
#load_demand = [60, 100, 120, 85, 150, 140, 170, 200, 210, 220, 300,
    320, 280, 320, 340, 310, 270, 220, 230, 250, 200, 180, 150, 120]
# 24 load 2
load_demand = [100, 120, 220, 210, 250, 300, 320, 310, 300, 270, 220,
    210, 170, 150, 120, 100, 70, 110, 80, 60, 90, 100, 50, 40]
# 24 load 3
N_t = 24 # number of time steps
generatorcost = [0]
```

```
18
19 # Generator Parameters
20 units = 4 # the total number of units
21 RU = [40, 40, 30, 30]
22 RD = [40, 40, 30, 30]
23 output_min = [15, 15, 15, 15] ## P_iˆth ,min (MW)
24 output_max = [100, 100, 100, 100] ## P_iˆth ,max (MW)
25
26 # Battery parameters
27 batt = 2 #  total number of batteries
28 Cap = 100
29 SOC_ini = 0.9
30 SOC_exp = 0.8
31 eta_c = 0.95
32 eta_d = 0.9
33
34
35
36 # In [] the cost coef a b c d e of these thermal units
37 #coef_A = [2.314*10**(-6), 2.314*10**(-6), -3.101*10**(-5),
       -3.101*10**(-5)] ## a_i ˆth ($/MW ˆ2)
38 #coef_B = [-3.295*10**(-4), -3.295*10**(-4), 7.442*10**(-3),
       7.442*10**(-3)] ## b_i ˆth ($/MW)
39 #coef_C = [2.537,2.537,-0.6256, -0.6256] ## c_i ˆth ($)
40 #coef_D = [-3.99*10**(-3), -3.99*10**(-3), 45.61, 45.61] ## c_i ˆth ($)
41 #coef_E = [19.21, 19.21, 189.6, 189.6] ## c_i ˆth ($)
42
43 ## Defining the model
44 m = gp. Model (" 2Diesel_2Gas ")
```

```
45
46 m.params.NonConvex = 2
47
48
49 # Generator Variables
50 # power outout of each unit
51 Pi = m.addVars(units , N_t, vtype = GRB . CONTINUOUS, name ='
       Power_Outputs')
52 # cost of each unit
53 ci = m. addVars (units , N_t, vtype = GRB . CONTINUOUS , name ='cost')
54 #totalCost = m.addVar(N_t, vtype = GRB.CONTINUOUS(), name = 'totalCost')
55 # on or off variable for units
56 ofi = m.addVars(units, N_t, vtype = GRB . INTEGER , name ='on_off')
57 # intial on/off state of units
58 #ofi[0,0] = 1
59 #ofi[1,0] = 1
60 # ofi[2,0] = 1
61 # ofi[3,0] = 0
62 #totalcost = m.addVars(N_t, vtype = GRB.CONTINUOUS, name ='totalCost')
63 totalcost = [0]
64
65 # Start-up Cost
66 nstart = m.addVars (units, N_t, vtype = GRB . CONTINUOUS , name ='
       startup')
67 startup_cost = [500, 500, 2000, 2000]
68 # startupcost = m.addVars (units, N_t, vtype = GRB . CONTINUOUS , name
       ='startupcost')
69 # startupcost_obj = [0]
70
```

```
# Battery Variables
SOC = m.addVars (batt, N_t , vtype =GRB. CONTINUOUS , lb =0.2 , ub =0.9
    , name ='SOC')
for b in range(batt):
    SOC[b,0] = SOC_ini
Pc = m.addVars (batt, N_t , vtype =GRB . CONTINUOUS , lb =0, ub =8 ,
    name ='Pc')
Pd = m.addVars (batt, N_t,vtype =GRB . CONTINUOUS , lb =0, ub =8 , name
    ='Pd')
cbi = m. addVars (batt , N_t, vtype = GRB . CONTINUOUS , name ='cost')


## Constranits of the operating
#m.addConstrs (( Pi [i]>= output_min [i] for i in range ( units )),name
    ='Operating_Limits_min')
#m.addConstrs (( Pi [i]<= output_max [i] for i in range ( units )),name
    ='Operating_Limits_max')

for t in range(N_t):



    ## Constranits of the operating
    #m.addConstrs (( ofi[i,t]*Pi [i,t]>= ofi[i,t]*output_min [i] for i
    in range ( units )),name='Operating_Limits_min')
    #m.addConstrs ((ofi[i,t]*Pi[i,t] <= ofi[i,t]*output_max[i] for i in
    range (units)),name='OperatingLimints_max')
    m.addConstrs (( Pi [i,t]>= ofi[i,t]*output_min [i] for i in range (
    units )),name='Operating_Limits_min')
```

```
92      m.addConstrs ((Pi[i,t] <= ofi[i,t]*output_max[i] for i in range (
        units)),name='OperatingLimints_max')
93
94      #ofi must be 0 or 1
95      m.addConstrs(ofi[i,t] <= 1 for i in range(units))
96      m.addConstrs(ofi[i,t] >= 0 for i in range(units))
97
98      # Set Load Demand
99      m.addConstr (ofi[0,t]*Pi[0,t]+ofi[1,t]*Pi[1,t]+ofi[2,t]*Pi[2,t]+ofi
        [3,t]*Pi[3,t]+Pd[0,t]+Pd[1,t] == load_demand[t]+Pc[0,t]+Pc[1,t],
        name ='LoadDemand')
100
101
102     #Fuel Efficiency Constraints
103 # F_d1 = 2.314*10**(-6)*P1^4 + (-3.295*10**(-4))*P1^3 + 2.537*P1^2 -
        3.99*10**(-3)*P1 + 19.21
104     F_d1 = m.addGenConstrPoly(Pi[0,t], ci[0, t], [0.0000096031,
        -0.001367425,-0.0165585, 10.52855,  79.7215])
105 # F_d2 = 2.314*10**(-6)*P2^4 + (-3.295*10**(-4))*P2^3 + 2.537*P2^2 -
        3.99*10**(-3)*P2 + 19.21
106     F_d2 = m.addGenConstrPoly(Pi[1,t], ci[1,t], [0.0000096031,
        -0.001367425,-0.0165585, 10.52855,  79.7215])
107 # F_g1 = -3.101*10**(-5)*P3^4 + 7.442*10**(-3)*P3^3 + -0.6256*P3^2 +
        45.61*P3 + 189.6
108     F_g1 = m.addGenConstrPoly(Pi[2,t], ci[2,t], [-1.29e-04, 0.031,
        -2.59624, 189.2815, 786.84])
109 # F_g1 = -3.101*10**(-5)*P3^4 + 7.442*10**(-3)*P3^3 + -0.6256*P3^2 +
        45.61*P3 + 189.6
```

```
110     F_g2 = m.addGenConstrPoly(Pi[3,t], ci[3,t], [-0.000128692,
        0.0308843, -2.59624, 189.2815, 786.84])
111
112     #Ramp up and Ramp down
113     m. addConstrs (( Pi[i, t+1] - Pi[i, t] <= RU [i] for i in range (
        units ) for t in range(N_t-1)), name =" Ramp_Up")
114     m. addConstrs (( Pi[i, t] - Pi[i, t+1] <= RD [i] for i in range (
        units ) for t in range(N_t-1)), name =" Ramp_Down ")
115
116     # Reserve Power Allowance
117     m.addConstr(1.15*load_demand[t] <= gp.quicksum(output_max[i]*ofi[i,t
        ] for i in range (units)) )
118
119     # start up
120     startup = m.addConstrs((ofi[i,t] <= ofi[i,t-1] + nstart[i,t]) for i
        in range(units) for t in range(1,N_t))
121
122     # Battery Constraints
123     p_batt = [0,2,4,6,8]
124     c_batt = [0, 6.67, 5.53, 6.93, 8.33]
125     cost_batt = m.addGenConstrPWL(Pd[0, t], cbi[0,t], p_batt, c_batt )
126     cost_batt1 = m.addGenConstrPWL(Pd[1, t], cbi[1,t], p_batt, c_batt )
127     m.addConstrs(Pd[b,t]*Pc[b,t] == 0 for b in range(batt))
128
129     m.addConstrs(Cap*SOC[b,t] == Cap*SOC[b,t-1] + Pc[b,t]*eta_c-Pd[b,t]/
        eta_d for b in range(batt) for t in range(1,N_t))
130
131
132     #Setting the objective
```

```
133     m.setObjective (gp.quicksum(gp.quicksum(ci[i,t]+nstart[i,t]*
        startup_cost[i] for i in range(units))+ gp.quicksum(cbi[b,t] for b
        in range(batt)) for t in range (N_t))  , GRB.MINIMIZE)
134
135     #output attributes for troubleshooting
136     for v in m.getVars():
137         print(v.x)
138     #print(m.ObjVal)
139     #totalcost.append(m.ObjVal)
140     # startupcost_obj.append(startup_obj)
141
142 m. optimize ()
143 rows = ["Gen" + str(i) for i in range(units)]
144 gen = pd.DataFrame(columns=range(N_t), index=rows, data=0.0)
145
146 for i in range(units):
147     for p in range(N_t):
148         gen.loc["Gen"+str(i), p] = int(Pi[i,p].x)
149 gen
150
151 rows = ["Gen" + str(i) +" Cost" for i in range(units)]
152 cost = pd.DataFrame(columns=range(N_t), index=rows, data=0.0)
153
154 for i in range(units):
155     for p in range(N_t):
156         cost.loc["Gen"+str(i)+ " Cost", p] = int(ci[i,p].x)
157 cost
158
159 rows = ["Gen" + str(i) + " Startup" for i in range(units)]
```

```
startup_gen = pd.DataFrame(columns=range(N_t), index=rows, data=0.0)

for i in range(units):
     for p in range(N_t):
          startup_gen.loc["Gen"+str(i) + " Startup", p] = (nstart[i,p]*
    startup_cost[i]).getValue()

rows = ["ofi Gen" + str(i) for i in range(units)]
ofi_gen = pd.DataFrame(columns=range(N_t), index=rows, data=0.0)

for i in range(units):
    for p in range(N_t):
        ofi_gen.loc["ofi Gen"+str(i), p] = ofi[i,p].x

rows = ["Batt" + str(i) + " Discharge" for i in range(batt)]
Pd_batt = pd.DataFrame(columns=range(N_t), index=rows, data=0.0)

for i in range(batt):
    for p in range(N_t):
        Pd_batt.loc["Batt"+str(i) + " Discharge", p] = int(Pd[i,p].x)
Pd_batt

rows = ["Batt" + str(i) + " Charge" for i in range(batt)]
Pc_batt = pd.DataFrame(columns=range(N_t), index=rows, data=0.0)

for i in range(batt):
    for p in range(N_t):
        Pc_batt.loc["Batt"+str(i) + " Charge", p] = int(Pc[i,p].x)
Pc_batt
```

```
188
189 rows = ["Batt" + str(i) + " Cost" for i in range(batt)]
190 cost_batt = pd.DataFrame(columns=range(N_t), index=rows, data=0.0)
191
192 for i in range(batt):
193     for p in range(N_t):
194         cost_batt.loc["Batt"+str(i) + " Cost", p] = int(cbi[i,p].x)
195 cost_batt
196
197 rows = ["Batt" + str(i) + " SOC" for i in range(batt)]
198 SOC_batt = pd.DataFrame(columns=range(N_t), index=rows, data=0.0)
199
200 for i in range(batt):
201     for p in range(1,N_t):
202         SOC_batt.loc["Batt"+str(i) + " SOC", p] = int(100*SOC[i,p].x)
203 SOC_batt
204
205
206
207 print(gen)
208 print(cost)
209 print(startup_gen)
210 print(ofi_gen)
211 #print(totalcost)
212 print(Pd_batt)
213 print(Pc_batt)
214 print(cost_batt)
215 print(SOC_batt)
216 print(m.ObjVal)
```

CHAPTER 4 CODE

The code used for the simulations shown in Chapter 4 are as follows.

```
    import gurobipy as gp
from gurobipy import GRB
import collections.abc
import pandas as pd

## Defining the model
m = gp. Model (" 2Diesel_2Gas ")
m.params.NonConvex = 2



# Simulation Parameters
load_count = 9 # number of load values tested
#load_demand = [60, 100, 200, 310, 200, 100, 60] ##( Mw)
#load_demand = [30, 40,50,60,70,80,90]
N_t = 8 # number of time steps
generatorcost = [0]

# Generator Parameters
units = 4 # the total number of units
RU = [40, 40, 30, 30]
RD = [40, 40, 30, 30]
output_min = [15, 15, 15, 15] ## P_iˆth ,min (MW)
output_max = [100, 100, 100, 100] ## P_iˆth ,max (MW)

# Battery parameters
```

```
batt = 2 #  total number of batteries
Cap = 20
#SOC_ini = 0.2
SOC_exp = 0.8
eta_c = 0.95
eta_d = 0.9
Pd_max = 8 # maximum discharge power of battery in a single time step

# Load Differences
#load_p = [60, 100, 120, 85, 150, 140, 170, 200, 210, 220, 300, 320,
    280, 320, 340, 310, 270, 220, 230, 250, 200, 180, 150, 120] #
    predicted load
#load_p = [140, 170,  200,  210,  220,  300,  320,  280]
load_p = [310,  270,  220,  230,  250,  200 ,180, 150,  120]
#load_a = [55, 102, 210, 290, 195, 110, 86] # actual load
#load_a = [60, 100, 120, 90, 170, 140, 150, 180, 170, 200, 250, 270,
    280, 320, 340, 340, 300, 250, 230, 270, 220, 150, 140, 110]
load_a = [340,  300,  250,  230 ,270, 220,  150,  140,  110]
#load_a = [140, 150,  180,  170,  200,  250,  270,  280]
load_dif = [load_a[t]-load_p[t] for t in range(N_t)]

Pi_plus = m. addVars (units , N_t, vtype = GRB . CONTINUOUS , name ='
    PosGenPowerDifference')
Pi_minus = m. addVars (units , N_t, vtype = GRB . CONTINUOUS , name ='
    NegGenPowerDifference')
Pd_plus = m. addVars (batt , N_t, vtype = GRB . CONTINUOUS , name ='
    PosBattPowerDifference')
Pd_minus = m. addVars (batt , N_t, vtype = GRB . CONTINUOUS , name ='
    NegBattPowerDifference')
```

```
Pc_plus = m. addVars (batt , N_t, vtype = GRB . CONTINUOUS , name =’
    PosBattPowerDifference’)
Pc_minus = m. addVars (batt , N_t, vtype = GRB . CONTINUOUS , name =’
    NegBattPowerDifference’)


# Generator Variables
# Predicted power output
# Pi = [ [15, 15, 15, 15, 55, 45, 85, 92, 97, 97, 100, 100, 100, 100,
    100, 99,100,100,100,100,92, 86, 94, 98],
#       [28,68,100,86,94,94,92,92,97, 98, 100, 100, 100,  100, 100, 100,
     100, 100, 100, 100, 92,  86, 55, 15],
#       [0, 0, 0, 0, 0, 0, 0, 0, 0, 0,  29, 19, 15, 15, 24, 19, 15, 0,
    0,  0,  0,  0,  0,  0],
#       [0,0,0,0,0,0,0,15, 15, 23, 53, 84, 59, 89, 100, 74, 44, 15, 15,
    40, 15, 15, 0,  0] ]

# Pi = [[45,  85, 92, 97, 97, 100 ,100, 100],
#       [94,  92, 92, 97, 98, 100,  100 ,100],
#       [0, 0,  0,  0,  0,  29, 19, 15],
#       [0, 0,  15, 15, 23, 53, 84, 59]]
Pi = [[99,  100,  100,  100,  100, 92,  86, 94, 98],
      [100, 100,  100,  100,  100 , 92, 86, 55, 15],
      [19,  15, 0,  0,  0,  0,  0,  0,  0],
      [74,  44, 15, 16, 40, 15, 15, 0,  0]]
# Generator on/off
ofi = m.addVars(units, N_t, vtype = GRB . INTEGER , name =’on_off’)

for t in range(N_t):
```

```
    for i in range (units):
        ofi[i,t] = 1

# Battery Variables
output_max_batt = 8
charge_max_batt = 8

# Predicted battery output/charge
# Pd = [[8, 8, 0, 0,  0,  0,  0,  0,  0,  0,  8,  8,  6,  8,  8,  8,  4,
      0,  6,  5,  0,  0,  0,  6],
#       [8, 8, 5, 0,  0,  0,  0,  0,  0,  0,  8,  8,  0,  8,  7,  8,  6,
      4,  8,  4,  0,  0,  0,  0]]
# Pc = [[0, 0, 0, 8,  0,  0,  1,  0,  0,  0,  0,  0,  0,  0,  0,  0,  0,
      0,  0,  0,  0,  7,  0,  0],
#       [0, 0, 0, 8,  0,  0,  6,  0,  0,  0,  0,  0,  0,  0,  0,  0,  0,
      0,  0,  0,  0,  0,  0,  0]]

Pd = [[8  ,4, 0,  6,  5,  0,  0,  0,  6],
      [8  ,6, 4,  8,  4,  0,  0,  0,  0]]
Pc = [[0  ,0, 0,  0,  0,  0,  7,  0,  0],
      [0  ,0, 0,  0,  0,  0,  0,  0,  0]]
SOC= [[0.38],
      [0.45]]

# Redistributed power variables
Pi_redis = m. addVars (units , N_t, vtype = GRB . CONTINUOUS , name ='
   Gen_Difference')
Pd_redis = m. addVars (batt , N_t, vtype = GRB . CONTINUOUS , name ='
   Batt_Discharge_Difference')
```

```
Pc_redis = m. addVars (batt , N_t, vtype = GRB . CONTINUOUS , name =’
    Batt_Charge_Difference’)
SOC_redis = m.addVars (batt, N_t , vtype =GRB. CONTINUOUS , lb =0.2 , ub
     =0.9 , name =’SOC’)
```

```
for t in range(N_t):

    #ofi must be 0 or 1
    m.addConstrs(ofi[i,t] <= 1 for i in range(units))
    m.addConstrs(ofi[i,t] >= 0 for i in range(units))

    # Set Load Demand
    #m.addConstr (ofi[0,t]*Pi_redis[0,t]+ofi[1,t]*Pi_redis[1,t]+ofi[2,t
    ]*Pi_redis[2,t]+ofi[3,t]*Pi_redis[3,t]+Pd_redis[0,t]+Pd_redis[1,t]
    == load_a[t]+Pc_redis[0,t]+Pc_redis[1,t], name =’LoadDemand’)
    # Total Change in load demand must be equal
    m.addConstr (gp.quicksum(Pi_plus[i,t]-Pi_minus[i,t] for i in range (
    units))+gp.quicksum(Pd_plus[b,t]-Pd_minus[b,t]-Pc_plus[b,t]+Pc_minus
    [b,t] for b in range (batt)) == load_dif[t])

    # All differences must be positive
    # Generator
    m.addConstrs (Pi_plus[i,t] >= 0 for i in range(units))
    m.addConstrs(Pi_minus[i,t] >= 0 for i in range (units))
```

```
118     # Battery
119     m.addConstrs (Pd_plus[b,t] >= 0 for b in range(batt))
120     m.addConstrs(Pd_minus[b,t] >= 0 for b in range (batt))
121     m.addConstrs (Pc_plus[b,t] >= 0 for b in range(batt))
122     m.addConstrs(Pc_minus[b,t] >= 0 for b in range (batt))
123
124
125     # New redispatched load must be equal to the new actual load
126     m.addConstr(gp.quicksum(ofi[i,t]*Pi_redis[i,t]+Pd_redis[b,t] for i
    in range (units) for b in range(batt)) == gp.quicksum(load_a[t]+
    Pc_redis[b,t] for b in range(batt)))
127
128     # Change in load must either be positive or negative, not both
129     # Generators
130     m.addConstrs (Pi_plus[i,t]*Pi_minus[i,t] == 0 for i in range (units)
    )
131     # Battery
132     m.addConstrs (Pd_plus[b,t]*Pd_minus[b,t]==0 for b in range(batt))
133     m.addConstrs (Pc_plus[b,t]*Pc_minus[b,t]==0 for b in range(batt))
134
135
136     # Calculate the chnange in load
137     # Generators
138     for i in range (units):
139         Pi_redis[i,t] = Pi[i][t]+1*Pi_plus[i,t]-1*Pi_minus[i,t]
140     # Battery
141     for b in range (batt):
142         Pd_redis[b,t] = Pd[b][t]+1*Pd_plus[b,t]-1*Pd_minus[b,t]
143         Pc_redis[b,t] = Pc[b][t]+1*Pc_plus[b,t]-1*Pc_minus[b,t]
```

```
144         #SOC_redis[0,0] = SOC[b][0]
145
146     # Battery SOC
147     m.addConstrs(Cap*SOC_redis[b,t] == Cap*SOC_redis[b,t-1] + Pc_redis[b
    ,t]*eta_c-Pd_redis[b,t]/eta_d for b in range(batt) for t in range(1,
    N_t))
148     # Battery cannot charge and discharge
149     m.addConstrs(Pd_redis[b,t]*Pc_redis[b,t] == 0 for b in range(batt))
150
151
152     ## Constranits of the operating
153     m.addConstrs (( Pi_redis [i,t]>= ofi[i,t]*output_min [i] for i in
    range ( units )),name='Operating_Limits_min')
154     m.addConstrs ((Pi_redis[i,t] <= ofi[i,t]*output_max[i] for i in
    range (units)),name='OperatingLimints_max')
155     m.addConstrs (Pd_redis[b,t] <= output_max_batt  for b in range(batt)
    )
156     m.addConstrs (Pd_redis[b,t] >= 0  for b in range(batt))
157     m.addConstrs (Pc_redis[b,t] >= 0  for b in range(batt))
158
159
160     #Ramp up and Ramp down
161     m. addConstrs (( Pi_redis[i,t+1] - Pi_redis[i, t] <= RU [i] for i in
     range ( units ) for t in range(N_t-1)), name =" Ramp_Up")
162     m. addConstrs (( Pi_redis[i, t] - Pi_redis[i, t+1] <= RD [i] for i
    in range ( units ) for t in range(N_t-1)), name =" Ramp_Down ")
163
164     # Reserve Power Allowance
```

```
165     m.addConstr(load_a[t] <= 0.85*gp.quicksum(output_max[i]*ofi[i,t] for
        i in range (units)) )
166
167
168
169
170     #Setting the objective
171     m.setObjective (( gp.quicksum((Pi_plus[i,t] / (output_max[i]))**2 +
        (Pi_minus[i,t]/output_max[i])**2 for i in range (units) for t in
        range (N_t)) +
172                                   gp.quicksum(((Pd_plus[b,t] / (
        output_max_batt)))**2 + ((Pd_minus[b,t]/output_max_batt))**2 +
173                                   ((Pc_minus[b,t] /output_max_batt))**2
        + ((Pc_plus[b,t] / (output_max_batt)))**2
174                                   for b in range (batt) for t in range (
        N_t))), GRB.MINIMIZE  )
175
176
177
178     # for v in m.getVars():
179     #     print(v.x)
180
181
182 m.optimize()
183 rows = ["Gen" + str(i) +" Predicted" for i in range(units)]
184 gen = pd.DataFrame(columns=range(N_t), index=rows, data=0.0000)
185 for i in range(units):
186     for p in range(N_t):
187         gen.loc["Gen"+str(i)+" Predicted", p] = int(Pi[i][p])
```

```
gen


rows = ["Gen" + str(i) + " Redispatched" for i in range(units)]
redis = pd.DataFrame(columns=range(N_t), index=rows, data=0.0000)
for i in range(units):
    for p in range(N_t):
        redis.loc["Gen"+str(i) + " Redispatched", p] = int(Pi_redis[i,p
    ].getValue())
redis

rows = ["Gen" + str(i) +" Pi plus" for i in range(units)]
Pi_increase = pd.DataFrame(columns=range(N_t), index=rows, data=0.0000)
for i in range(units):
    for p in range(N_t):
        Pi_increase.loc["Gen"+str(i)+ " Pi plus", p] = int(Pi_plus[i,p].
    x)
Pi_increase

rows = ["Gen" + str(i) +" Pi minus" for i in range(units)]
Pi_decrease = pd.DataFrame(columns=range(N_t), index=rows, data=0.0000)
for i in range(units):
    for p in range(N_t):
        Pi_decrease.loc["Gen"+str(i)+ " Pi minus", p] = int(Pi_minus[i,p
    ].x)
Pi_decrease

rows = ["Batt" + str(i) + " Predicted Discharge" for i in range(batt)]
Pd_batt = pd.DataFrame(columns=range(N_t), index=rows, data=0.0000)
```

```
for i in range(batt):
    for p in range(N_t):
        Pd_batt.loc["Batt"+str(i) + " Predicted Discharge", p] = int(Pd[
    b][p])
Pd_batt

rows = ["Batt" + str(i) + " Predicted Charge" for i in range(batt)]
Pc_batt = pd.DataFrame(columns=range(N_t), index=rows, data=0.0000)
for i in range(batt):
    for p in range(N_t):
        Pc_batt.loc["Batt"+str(i) + " Predicted Charge", p] = int(Pc[b][
    p])
Pc_batt

rows = ["Batt" + str(i) + " Discharge Redispatched" for i in range(batt)
    ]
Pd_batt_redis = pd.DataFrame(columns=range(N_t), index=rows, data
    =0.0000)
for i in range(batt):
    for p in range(N_t):
        Pd_batt_redis.loc["Batt"+str(i) + " Discharge Redispatched", p]
    = int(Pd_redis[i,p].getValue())
Pd_batt_redis

rows = ["Batt" + str(i) + " Charge Redispatched" for i in range(batt)]
Pc_batt_redis = pd.DataFrame(columns=range(N_t), index=rows, data
    =0.0000)
for i in range(batt):
    for p in range(N_t):
```

```
        Pc_batt_redis.loc["Batt"+str(i) + " Charge Redispatched", p] =
    int(Pc_redis[i,p].getValue())
Pc_batt_redis

rows = ["Batt" + str(i) + " Pd plus" for i in range(batt)]
Pd_increase = pd.DataFrame(columns=range(N_t), index=rows, data=0.0000)
for i in range(batt):
    for p in range(N_t):
        Pd_increase.loc["Batt"+str(i) + " Pd plus", p] = int(Pd_plus[i,p
    ].x)
Pd_increase

rows = ["Batt" + str(i) + " Pd minus" for i in range(batt)]
Pd_decrease = pd.DataFrame(columns=range(N_t), index=rows, data=0.0000)
for i in range(batt):
    for p in range(N_t):
        Pd_decrease.loc["Batt"+str(i) + " Pd minus", p] = int(Pd_minus[i
    ,p].x)
Pd_decrease


rows = ["Batt" + str(i) + " Pc plus" for i in range(batt)]
Pc_increase = pd.DataFrame(columns=range(N_t), index=rows, data=0.0000)
for i in range(batt):
    for p in range(N_t):
        Pc_increase.loc["Batt"+str(i) + " Pc plus", p] = int(Pc_plus[i,p
    ].x)
Pc_increase

```

```
rows = ["Batt" + str(i) + " Pc minus" for i in range(batt)]
Pc_decrease = pd.DataFrame(columns=range(N_t), index=rows, data=0.0000)
for i in range(batt):
    for p in range(N_t):
        Pc_decrease.loc["Batt"+str(i) + " Pc minus", p] = int(Pc_minus[i
   ,p].x)
Pc_decrease



print(gen)
print(redis)
print(Pi_increase)
print(Pi_decrease)
print(Pd_batt)
print(Pc_batt)
print(Pd_batt_redis)
print(Pc_batt_redis)
print(Pd_increase)
print(Pc_decrease)
```